

**Quantification of fungal growth:
models, experiments, and observations**

CENTRALE LANDBOUWCATALOGUS



0000 0920 5754

Promotor: Prof. Dr. M.J. Jeger
Hoogleraar in de Ecologische Fytopathologie

Co-promotoren: Dr. F. van den Bosch
Theoretisch Bioloog (IACR-Rothamsted, Engeland)

Dr. A.J. Termorshuizen
Universitair Docent, leerstoelgroep Biologische Bedrijfssystemen

Promotiecommissie: Prof. R.F. Hoekstra (Wageningen Universiteit)
Dr. T.W. Kuyper (Wageningen Universiteit)
Dr. H.J. Broersma (Universiteit Twente)
Dr. A.M. de Roos (Universiteit van Amsterdam)

no 8201, 3177

Angélique Lamour

**Quantification of fungal growth:
models, experiments, and observations**

Proefschrift

ter verkrijging van de graad van doctor
op gezag van de rector magnificus
van Wageningen Universiteit,
Prof. Dr. Ir. L. Speelman,
in het openbaar te verdedigen
op vrijdag 12 april 2002
des namiddags te 13.30 uur in de Aula.

16a627u

Lamour, A., 2002

Quantification of fungal growth: models, experiments, and observations.

PhD Thesis Wageningen University, Wageningen, The Netherlands.

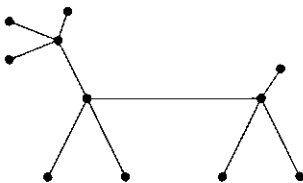
- With ref. - With summary in Dutch.

ISBN 90-5808-623-2

Stellingen

behorende bij het proefschrift van Angélique Lamour,
Quantification of fungal growth: models, experiments, and observations,
 Wageningen Universiteit, 12 april 2002.

1. Een gedetailleerde modellering van koolstof- en stikstofstromen tijdens de afbraak van substraat door schimmels leidt tot een gecompliceerd model, maar kan resultaten geven met een heldere, biologische interpretatie (dit proefschrift).
2. Rhizomorfen van *Armillaria lutea* vormen netwerken om de persistentie te vergroten (dit proefschrift).
3. There is nothing so practical as a good theory (Emanuel Kant, 1724-1804).
4. Het is jammer dat muizen niet graag zwemmen en niet kunnen fietsen:
 Elke dag een stuk hardlopen zorgt ervoor dat muizen slimmer worden doordat ze meer nieuwe hersencellen aanmaken dan niet-rennende soortgenoten (Proceedings of the National Academy of Sciences, 9 november 1999). Aangezien menselijke hersenen ook voortdurend nieuwe cellen aanmaken, wijst dit erop dat hardlopende promovend(ae)(i) de kans op het succesvol afronden van hun proefschrift vergroten. Het zeer voor de hand liggende gunstige effect van triathlon kan door de sportvoorkeur van muizen helaas niet met muizen als proefdier aangetoond worden.
5. Vele promovend(ae)(i) vertonen vergelijking met kabouter Piggelmees (editie *Van het tovervisje*, uitgegeven door Van Nelle): ze willen steeds meer bereiken met hun promotie-onderzoek zonder tevreden te zijn met wat ze hebben en te streven naar geluk.
6. Het huwelijk van Z.K.H. Prins Willem-Alexander en Máxima is niet hét huwelijk van het jaar.
7. This tree* is particularly well-known for its bark:



(*Graph theory says a *tree* is a connected graph with only one path between each pair of vertices.)

8. Zonder *liefde* voor het vak was dit proefschrift van **Lamour** niet tot stand gekomen.

Voor mijn ouders

Abstract

This thesis is concerned with the growth of microscopic mycelial fungi (Section I), and that of macroscopic fungi, which form specialised hyphal structures such as rhizomorphs (Section II). A growth model is developed in Section I in relation to soil organic matter decomposition, dealing with detailed dynamics of carbon and nitrogen. Substrate with a certain carbon:nitrogen ratio is supplied at a constant rate, broken down and then taken up by fungal mycelium. The nutrients are first stored internally in metabolic pools and then incorporated into structural fungal biomass. Analysis of the overall-steady states of the variables (implicitly from a cubic equation) showed that the conditions for existence had a clear biological interpretation. The 'energy' (in terms of carbon) *invested in* breakdown of substrate should be less than the 'energy' *resulting from* breakdown of substrate, leading to a positive carbon balance. For growth the 'energy' necessary for production of structural fungal biomass and for maintenance should be less than this positive carbon balance in the situation where all substrate is colonised. Under the assumption that nutrient dynamics are much faster than the dynamics of fungal biomass and substrate, a quasi-steady analysis was performed. From the resulting simplified model an explicit fungal invasion criterion was derived, which was not possible in the analysis of the original fungal growth model. The fungal invasion criterion takes two forms: one for systems where carbon is limiting, another for systems where nitrogen is limiting. For cases where only carbon is limiting, nitrogen dynamics were excluded from the model, and this further simplification resulted in a model that was fitted to data on growth of the soil-borne plant pathogen *Rhizoctonia solani*. Fungal growth and colonisation of discrete nutrient sites in Petri plates were assessed microscopically for two carbon concentrations of the substrate. Colonisation was faster at the higher carbon concentration. The model predicted a lower asymptote for non-colonised substrate and this value was estimated from the data by non-linear regression for each carbon concentration. A key composite parameter, the positive carbon balance per carbon unit of colonised substrate, was lower for the higher carbon concentration. The carbon decomposition rate was estimated by least squares minimisation, after correction for a lag phase expected after robust handling of the inoculated fungus. The delay in subsequent fungal growth after inoculation was extended when there was less carbon available for physical recovery and physiological adaptation to the new environment. The simplified mean-field model with parameters estimated as described above produced a good fit to the data.

In Section II quantitative studies on the epidemiology of *Armillaria* root rot are reviewed. This fungus is a serious disease in many forests and horticultural tree crops world-wide, and consequently there is much interest in options for avoiding or restricting the spread of disease through growth of the specialised rhizomorphs in soil. Two rhizomorph networks of *A. lutea* growing through a natural soil were observed over areas of 25 m² in *Pinus nigra* and *Picea abies* tree plantations. Both rhizomorph systems had numerous branches and anastomoses resulting in cyclic paths, i.e. regions of the system that start and end at the same point. Each rhizomorph network exhibited both exploitative and explorative characteristics within its overall network structure. One of the observed rhizomorph networks of *A. lutea* was restricted to the cyclic paths only, and the resulting graph was drawn in the plane. The plane graph consisted of 169 rhizomorphs, termed edges, and 107 rhizomorph nodes, termed vertices. The connectivity of the rhizomorph network was explored by focusing on each bridge, i.e. an edge whose removal disconnects the graph into two components. In only two instances was a nutrient source connected to the cycles, and disruption of these two connecting edges would remove the whole network from the sources. A shortest path from a given vertex to a nutrient source was defined in terms of number of edges, and also in terms of length (m). The length of the edges enclosing the faces, i.e. two-dimensional regions defined by the edges in the plane drawing, showed that the fungus exhibited both exploitative and explorative growth, and we speculate about the underlying reasons for these foraging strategies. The introduction of graph-theoretic concepts to fungal growth might lead to an improved ecological understanding of fungal networks in general, provided that relevant biological interpretations can be made.

Contents

1 Introduction	1
SECTION I	
2 Modelling the growth of soil-borne fungi in response to carbon and nitrogen	7
3 Quasi-steady state approximation to a fungal growth model	27
4 A fungal growth model fitted to carbon limited dynamics of <i>Rhizoctonia solani</i>	49
SECTION II	
5 Quantitative aspects of the epidemiology of <i>Armillaria</i> in the field	67
6 Networks formed by rhizomorphs of <i>Armillaria lutea</i>	81
7 Quantification of rhizomorph networks	93
8 General conclusions	111
References	115
Nederlandse samenvatting	129
Curriculum vitae	131

Chapter 1

Introduction

Growth of soil-borne fungi is poorly understood, largely because non-destructive observations on hyphae in natural soil are difficult to make. In simplified laboratory systems, patterns of growth have been observed and analysed (Gilligan & Bailey, 1997; Bolton & Boddy, 1993), but the soil microbial system is complex in terms of number and diversity of organisms, and their interactions (Richards, 1987). Consequently, there are few insights into the growth dynamics of plant pathogens, hyperparasites, and mycorrhizal fungi. Hyphal extension in soil is a means of dispersal for many fungi. These hyphae serve as unique systems for nutrient redistribution to explorative parts of the system after successful colonisation of new sites (Dighton, 1997).

The research presented in this thesis is intended to provide more insight into the allocation of resources by a growing fungus in relation to the availability of substrate (Dighton, 1997; Richards, 1987). There are several alternative or complementary ways for fungi to allocate resources. Although some fungi, for example the yeast *Saccharomyces cerevisiae*, do not form hyphae, most other fungi form microscopic mycelial networks, which results in both an important mechanism for active dispersal and a means of obtaining and allocating food (Mihail et al., 1995; Bending & Read, 1995). A further elaboration for some fungal species, for example *Armillaria spp.*, is the aggregation of hyphal strands into specialised macroscopic structures. The shoestring-like rhizomorphs are 1-3 mm in diameter with a reddish brown to black outer cortex

layer (Cairney et al., 1988), and persist over centuries if there are sufficient nutrient sources for absorption (Rizzo et al., 1992). These two contrasting systems are dealt with in Section I and II respectively, using both modelling and experimental/observational approaches to differing degrees. Section I deals with the fine mycelial hyphae of *microscopic* fungi. In this section, fungal growth models are developed to quantify the dynamics of the fungal biomass in terms of availability and utilisation of carbon and nitrogen. Section II deals with *macroscopic* rhizomorphs of the fungus *Armillaria*, and focuses on direct observations of the network structure, and quantification by means of graph-theoretical concepts (Wilson, 1979).

In Section I, mathematical modelling is presented as a useful complement to experimental research, since it helps to focus attention on the fundamental properties of the system and enables predictions to be made under a wide range of conditions (Bull & Trinci, 1977; Prosser, 1979; Righelato, 1979). Growth models should be based on reasonable biological assumptions regarding growth mechanisms and generate predictions that can be tested experimentally, however, difficulties on hyphal observations in natural soil occur. In Chapter 2, a fungal growth model is introduced in relation to soil organic matter decomposition, along lines previously described (Paustian & Schnürer, 1987a&b), but with detailed attention to carbon and nitrogen dynamics. The model describes the colonisation and decomposition of substrate, subsequent uptake of nutrients, and incorporation into fungal biomass. The overall-steady states of the variables are obtained by standard mathematical procedures, and the conditions for existence of the steady states have a clear biological interpretation. In Chapter 3, this fungal growth model is simplified by assuming that the nutrient dynamics are much faster than the dynamics of fungal growth and substrate, implying that the system will reach a quasi-steady state relatively quickly. A quasi-steady state approximation (Stiefenhofer, 1998) allows the derivation of a fungal invasion criterion, which was not possible for the original model. Importantly, the invasion criterion takes two forms: one for systems where carbon is limiting, another for systems where nitrogen is limiting. Carbon sources are the primary object of competition in soil, and competition for nitrogen may occur in substrates of a high carbon : nitrogen ratio such as woody plant residues (Lockwood, 1981; Lockwood & Filonow, 1981). In Chapter 4 it is assumed that only carbon is limiting fungal growth, and nitrogen dynamics are excluded from the model. The resulting model is then fitted to data on growth of the soil-borne plant pathogen *Rhizoctonia solani* (Sneh et al., 1996), obtained using a model system similar to that described by Bailey et al. (2000). The model produces a good fit to these experimental data.

In Section II, quantification tools other than mathematical modelling are presented. The quantitative epidemiology of the macrofungus *Armillaria* spp. is reviewed in Chapter 5. *Armillaria* root rot is a serious disease in many forests and horticultural tree crops world-wide (Morrison, 1976), and many *Armillaria* species spread largely through rhizomorph growth in soil. Consequently, there is much interest in determining how different silvicultural practices influence disease incidence (Vollbrecht & Agestam, 1995) and options for avoiding or restricting the spread of the disease (Van der Kamp, 1995). A necessary condition for better management of *Armillaria* root rot is an improved understanding of the ecological significance of the extended rhizomorph networks that arise from spread (Fox, 2000). Two maps of rhizomorph networks of *Armillaria lutea*, growing in soil over an area of 25 m² of a tree plantation, are presented and analysed from an ecological perspective in Chapter 6. Both networks had numerous branches and anastomoses resulting in cyclic paths, i.e. regions of the system that start and end at the same point. Network characteristics like total rhizomorph length, number of cyclic paths, fractal dimension, etc. are determined, and in Chapter 7 other possible applications of graph-theoretic concepts (Wilson, 1979) are explored. In particular both exploitative and explorative foraging strategies (Ritz & Crawford, 1990) of *Armillaria* are apparent, and we speculate about the underlying reasons and interpretations for these. The introduction of graph-theoretic properties to fungal growth may lead to an improved ecological understanding of fungal networks in general, when relevant biological interpretations can be drawn. Finally, the main conclusions are given in Chapter 8.

Section I

Chapter 2

Modelling the growth of soil-borne fungi in response to carbon and nitrogen

LAMOUR, A., VAN DEN BOSCH, F., TERMORSHUIZEN, A.J. & JEGER, M.J. 2001
IMA J. Math. Appl. Med. Biol. 17, 329-346

Abstract

Growth of soil-borne fungi is poorly described and understood, largely because non-destructive observations on hyphae in soil are difficult to make. Mathematical modelling can help in the understanding of fungal growth. Except for a model by Paustian & Schnürer (1987a), fungal growth models do not consider carbon and nitrogen contents of the supplied substrate, although these nutrients have considerable effects on hyphal extension in soil. We introduce a fungal growth model in relation to soil organic matter decomposition dealing with the detailed dynamics of carbon and nitrogen. Substrate with a certain carbon:nitrogen ratio is supplied at a constant rate, broken down and then taken up by fungal mycelium. The nutrients are first stored internally in metabolic pools and then incorporated into structural fungal biomass. Standard mathematical procedures were used to obtain overall-steady states of the variables (implicitly from a cubic equation) and the conditions for existence. Numerical computations for a wide range of parameter combinations show that at most one solution for the steady state is biologically meaningful, specified by the conditions for existence. These conditions specify a constraint, namely that the 'energy' (in terms of carbon) invested in breakdown of substrate should be less than the 'energy' resulting from breakdown of substrate, leading to a positive carbon balance. The biological interpretation of the conditions for existence is that for growth the 'energy' necessary for production of structural fungal biomass and for maintenance should be less than the mentioned positive carbon balance in the situation where all substrate is colonised. In summary, the analysis of this complicated fungal growth model gave results with a clear biological interpretation.

1. Introduction

An important mechanism for active dispersal of soil-borne fungi is the formation of hyphae. A prerequisite for growth is the availability of substrate. In nature, dead plant parts are returned to the soil and can serve as a substrate for microorganisms. The activities of soil fauna, bacteria, and fungi degrade the complex organic components, using carbon for energy and mineral elements for biomass production. Colonisation of substrate by a given fungal species is dictated by the ability to utilise the resource (often referred to as the substrate quality), the time of arrival at the resource, and the ability to compete against other fungal species with similar physiological competence. Decomposition arises from enzyme activity. The types of enzymes required depend on the chemical constituents of the substrate. Fungal species differ in the range of enzymes they are capable of producing, resulting in a change in species composition as different plant substrates undergo a cascade of decomposition processes. Following decomposition, nutrients are taken up and incorporated into fungal biomass (Dighton, 1997).

Carbohydrates are among the most readily available sources of carbon for fungi. Monosaccharides are widely utilised, but polyhydric alcohols are also good carbon sources. As a source for nitrogen, ammonium (NH_4^+) is preferred, but also nitrate (NO_3^-) can be utilised by many fungi. Organic nitrogen compounds are decomposed by some fungi to produce ammonia (Cooke & Whipps, 1993). Phosphorus is usually taken up in inorganic form. Most of this phosphate is of mineral origin but some may be derived from enzymatic breakdown of soil organic matter. Sulphur is provided by mineralization of soil organic matter, producing sulphate (SO_4^{2-}). Microbes require other mineral elements only in very low concentrations, mainly as activators of various enzymes (Richards, 1987).

Growth of soil-borne fungi is poorly understood, largely because non-destructive observations on hyphae in soil are difficult to make. However, in laboratory culture outgrowth patterns have been observed, e.g. on mycelial cord systems of *Phanerochaete velutina* and *Hypholoma fasciculare* extending into soil from woody resource bases (Bolton & Boddy, 1993), on *Armillaria* mycelia and rhizomorphs (Mihail et al., 1995), or on *Rhizoctonia solani* (Gilligan & Bailey, 1997). The soil microbial ecosystem is very complex in terms of the number and diversity of organisms and their interactions. Mathematical modelling is a useful complement to experimental research, since it helps to focus attention on the fundamental properties of the system and enables predictions to be made under a wide range of conditions. Mathematical modelling has already become a recognised tool in mycology,

aiding to some extent in the understanding of fungal growth in culture (for reviews see Bull & Trinci, 1977; Prosser, 1979; Righelato, 1979).

Growth models should be based on biological assumptions regarding growth mechanisms and generate predictions, which can be tested experimentally. For example, Prosser & Trinci (1979) developed a mechanistic model for hyphal growth and branching and compared the predictions from the model with experimentally observed growth kinetics of mycelia of *Geotrichum candidum* and *Aspergillus nidulans*. Other fungal growth models include also the dynamics of a substrate source (e.g. Edelstein & Segel, 1983; Molin et al., 1993; Regalado et al., 1996; Davidson et al., 1997). Paustian & Schnürer (1987a&b) model fungal growth in response to the carbon:nitrogen ratio of the supplied substrate, in the context of decomposition processes in soil. Carbon and nitrogen sources have considerable effects on hyphal extension in soil (e.g. Stack et al., 1987). We introduce a fungal growth model dealing with the detailed dynamics of carbon and nitrogen for fungi with different growth potentials. The model describes a system of organic matter decomposition in soil by saprophytic fungi or those with a saprophytic phase. In this paper we do not direct the model to a particular biological system, but point to its general form. We examine the qualitative behaviour of the model, e.g. criteria determining growth potential, persistence and steady state values for the variables, in relation to substrate supply. We make a simple assumption that there is a continuous and constant supply of substrate and obtain qualitative and numerical results that we interpret biologically. Another option would be to examine the impact of a sinusoidal substrate input, e.g. representing fluctuations in leaf litter. In subsequent papers we examine how fungal growth may track substrate supply (either as a single or periodic supply) and, by making simplifying assumptions on the relative time-scales of carbon and nitrogen compared with growth dynamics, show how the model can be linked to experimental observations.

Fungal growth involves a spatial process, namely the extension of fungal hyphae. Edelstein (1982) described growth and branching in mycelial fungi and derived a spatial mathematical model (Edelstein & Segel, 1983). Spatial heterogeneity is important in terms of the persistence or maintenance of a biological system. However, the model as presented does not focus on the spatial nature of fungal growth but on detailed substrate dynamics and resulting changes in fungal biomass as a mean field approximation.

2. Model description

The fungal growth model describes the colonisation and decomposition of substrate, subsequent uptake of nutrients, and incorporation into fungal biomass. The symbol S (Table 1) indicates the substrate source that is encountered by the fungus by outgrowth of mycelium (Fig. 1). Besides supply (e.g. dead organic matter) and removal (e.g. by other decomposers, leaching, or harvesting), fungal colonisation determines the dynamics of substrate S . Colonised substrate (I) is decomposed by exoenzymes to carbon and nitrogen in readily available form, involving an energetic cost. Many fungal species secrete exoenzymes to support decomposition, for example manganese-dependent peroxidase, lignin peroxidase or glyoxal oxidase (Archer & Wood, 1995; Datta et al., 1991). Fungi need mostly carbon and nitrogen to grow, therefore we concentrate on the dynamics of these nutrients only. Thus, as a result of substrate decomposition, carbon and nitrogen are formed externally (and therefore indicated by an asterisk: C^* , N^*). Subsequently, carbon and nitrogen are taken up by the fungus and stored internally in metabolic pools. Uptake is by means of osmosis, therefore without an energetic cost. The nutrients in the metabolic pools can be used for growth of structural fungal biomass (B). Fungal biomass can be considered as two components, cytoplasm and cell walls, differing in their nutrient demands. Cytoplasm contains high amounts of carbon and nitrogen, but the cell wall is composed primarily of polysaccharides (Peberdy, 1990), where the nitrogen concentration is only 1-2% (Paustian & Schnürer, 1987a). A constant carbon:nitrogen ratio is assumed for cell walls (Burnett, 1979) by considering storage products as a separate component; the same is true for the cytoplasm. Therefore, we consider biomass as one variable. Experimentally, it is difficult to distinguish between the cytoplasmic and cell wall components.

The carbon and nitrogen that are present externally (C^* and N^*) can also be partially assimilated by competing bacteria and other fungi. Therefore at the C^* and N^* level an outflow termed *loss* is indicated. For nitrogen an inflow also exists due to mineralization. As a result of the rapid turnover of soil organic matter by microorganisms, nutrient elements are released into soil solution as simple inorganic compounds, a process termed mineralization (Dighton, 1997). The energetic cost involved in maintenance is modelled as carbon costs out of the metabolic carbon pool. The same holds for the energetic cost involved in substrate decomposition. The carbon and nitrogen metabolic pools both have an outflow due to leakage out of the mycelium. The balance between uptake and leakage depends on the degree of insulation, i.e. the resistance to deformation and penetration, of the hyphal boundaries which must always be partly deformable or penetrable if the system is not to

stagnate (Rayner et al., 1994). The system is described by seven state variables (Table 1). The dimensions are expressed in arbitrary carbon or nitrogen units per unit volume of soil. These units could be moles or units of biomass (for example μg).

Table 1. Model variables with dimensions.

State		dimension [#]
S	substrate available to be colonised by the fungus	$N_{\text{C-units}}$
I	colonised substrate	$N_{\text{C-units}}$
C*	external carbon	$N_{\text{C-units}}$
N*	external nitrogen	$N_{\text{N-units}}$
C	carbon in the metabolic carbon pool	$N_{\text{C-units}}$
N	nitrogen in the metabolic nitrogen pool	$N_{\text{N-units}}$
B	structural fungal biomass	$N_{\text{C-units}}$

[#]where N = number of

Table 2. Parameters, dimensions, default values, and ranges for numerical computations.

Parameter		dimension [#]	value (range)
σ	substrate supply per time unit	$N_{\text{C-units}} \text{T}^{-1}$	10^6 ($1-10^8$)
ρ	substrate removal rate	T^{-1}	0.05 ($10^{-2}-10^5$)
α	substrate colonisation probability per carbon unit biomass	$(N_{\text{C-units(B)}})^{-1}$	0.1 ($10^{-6}-10^2$)
τ	fungal growth rate per C/B per N/B	see @	10^{-6}
β	substrate decomposition rate	T^{-1}	0.15
v_{C^*}	C* loss rate	T^{-1}	0.1 ($0-1$)
v_{N^*}	N* loss rate	T^{-1}	0.1
k_1	C* uptake rate	T^{-1}	0.1 ($10^{-3}-10^8$)
k_2	C leakage rate	T^{-1}	0.1
k_3	N* uptake rate	T^{-1}	0.1
k_4	N leakage rate	T^{-1}	0.1
ψ	carbon:nitrogen ratio of supplied substrate	$N_{\text{C-units}}(N_{\text{N-units}})^{-1}$	9
ξ	extra mineralization per time unit	$N_{\text{N-units}} \text{T}^{-1}$	10^3
ω	maintenance rate of structural fungal biomass	T^{-1}	0.02 ($10^{-2}-10^4$)
Δ	carbon units invested in decomposition per carbon unit substrate	$N_{\text{C-units(C-pool)}}(N_{\text{C-units(I)}})^{-1}$	0.1 ($0-1$)
ϕ	carbon:nitrogen ratio of structural fungal biomass	$N_{\text{C-units}}(N_{\text{N-units}})^{-1}$	10
μ	mortality rate of structural fungal biomass	T^{-1}	0.01 ($10^{-8}-10^2$)

[#]where N = number of; T = time unit (day)

@ where the dimension of τ is $\text{T}^{-1} \frac{N_{\text{C-units(B)}}}{N_{\text{C-units(C-pool)}}} \frac{N_{\text{C-units(B)}}}{N_{\text{N-units(N-pool)}}$

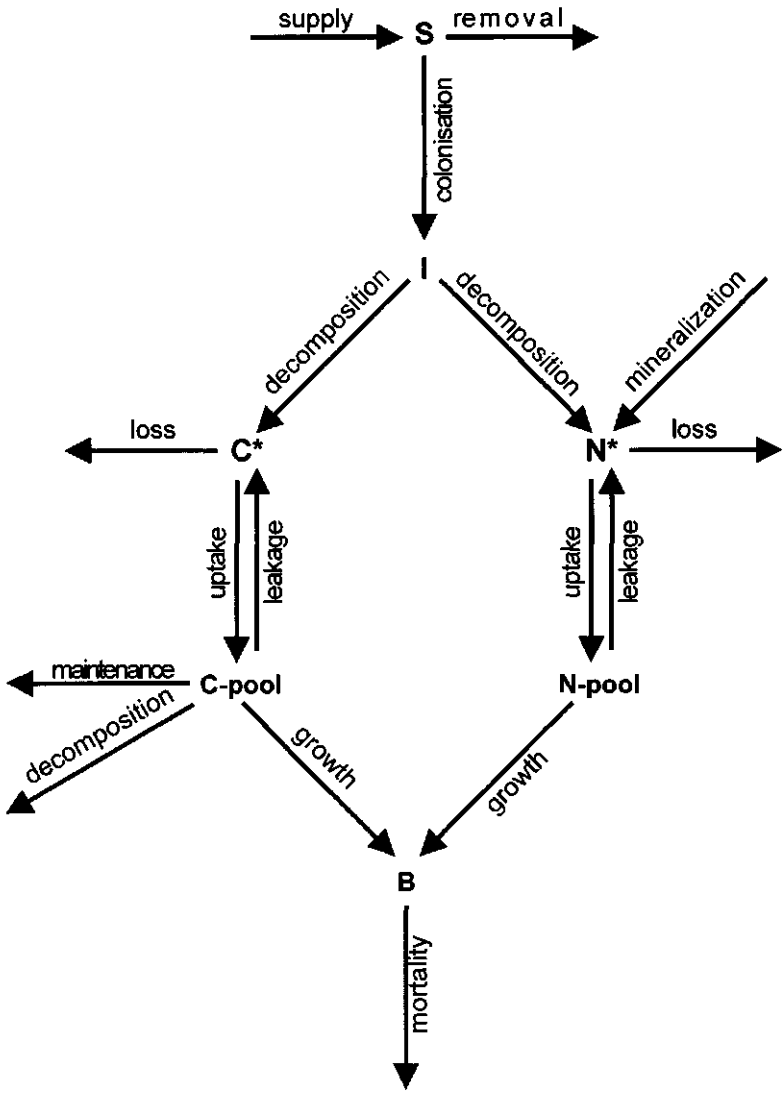


Figure 1. In the fungal growth model substrate (S) is colonised, colonised substrate (I) is externally decomposed to carbon (C*) and nitrogen (N*), subsequently taken up into a metabolic carbon (C) and nitrogen (N) pool, and incorporated into structural fungal biomass (B).

The model structure then takes the form:

$$\frac{dS}{dt} = \text{supply} - \text{removal} - \text{colonisation} \quad [\text{substrate}]$$

$$\frac{dI}{dt} = \text{colonisation} - \text{decomposition} \quad [\text{colonised substrate}]$$

$$\frac{dC^*}{dt} = \text{decomposition} - \text{loss} - \text{uptake} + \text{leakage} \quad [\text{external carbon}]$$

$$\frac{dN^*}{dt} = \text{decomposition} - \text{loss} - \text{uptake} + \text{leakage} + \text{mineralization} \quad [\text{external nitrogen}]$$

$$\frac{dC}{dt} = \text{uptake} - \text{leakage} - \text{growth} - \text{maintenance} - \text{decomposition} \quad [\text{metabolic carbon pool}]$$

$$\frac{dN}{dt} = \text{uptake} - \text{leakage} - \text{growth} \quad [\text{metabolic nitrogen pool}]$$

$$\frac{dB}{dt} = \text{growth} - \text{mortality} \quad [\text{structural fungal biomass}]$$

We now derive expressions for all terms on the right-hand side of these differential equations. All model parameters have a biological or physical description (Table 2). *Supply* of substrate is assumed to be a constant amount per time unit, σ , whereas *removal* by e.g. other decomposers proceeds at a constant rate, ρ . *Colonisation* of substrate is linearly related to new growth of biomass, because substrate is encountered by the outgrowth of mycelium, where it is assumed that substrate is homogeneously distributed. There are many options to model fungal *growth*, where one of the simplest is it to be linearly proportional to $\frac{C}{B}$, i.e. carbon in the metabolic pool divided by structural fungal biomass, and also to $\frac{N}{B}$, i.e. nitrogen in the metabolic pool divided by structural fungal biomass. With τ being the proportionality constant, fungal growth is then modelled as $\tau \frac{C}{B} \frac{N}{B} B$, which simplifies to $\tau \frac{CN}{B}$. Colonisation of substrate is also linearly related to substrate with proportionality constant α , i.e. the substrate colonisation probability per carbon unit biomass, leading to a colonisation term $\alpha \tau \frac{CN}{B} S$. *Decomposition* is assumed to proceed at a constant rate, β , because it is assumed that there always is a sufficient amount of fungal biomass (and a sufficient amount of exoenzymes) available for decomposition. Colonised substrate is expressed in carbon units. Therefore, carbon derived from decomposition is βI , and nitrogen derived from decomposition is $\frac{1}{\psi} \beta I$, where ψ is the constant carbon:nitrogen ratio of the incoming substrate. Bacteria or other competing microorganisms cause *loss* of nutrients at rates v_c . For

carbon and v_N for nitrogen. *Uptake* and *leakage* of nutrients by the fungus are linearly related to the amount of nutrients in the two metabolic pools, with rates k_1 and k_2 respectively for carbon and k_3 and k_4 respectively for nitrogen. *Mineralization* is assumed to occur at a constant amount per time unit, ξ . For growth of structural fungal biomass (B), carbon is necessary at an amount $\tau \frac{CN}{B}$ per time unit. To achieve growth of biomass in terms of nitrogen, this quantity is multiplied by $\frac{1}{\phi}$, where ϕ is the carbon:nitrogen ratio of the structural fungal biomass. Because ϕ refers only to structural biomass and not to storage products, this ratio is assumed to be constant. For each unit of fungal biomass a fixed amount of energy, in terms of carbon, is necessary per time unit for *maintenance*, ω . *Decomposition* of colonised substrate demands carbon units out of the metabolic carbon pool at an amount Δ per carbon unit colonised substrate, leading to a carbon loss term $\Delta\beta I$ per time unit. This carbon loss term involves energy for production of enzymes. Because enzymes contain only little nitrogen, a nitrogen loss term is neglected. A constant *mortality* rate μ of biomass is assumed, where dead biomass is not a qualitatively good substrate source. In case substrate supply is large, dead biomass as a substrate source can be neglected anyway. The fungal growth model (2.1) can then be written as:

$$2.1 \text{ (a). } \quad \frac{dS}{dt} = \sigma - \rho S - \alpha \tau \frac{CN}{B} S \quad \text{[substrate]}$$

$$2.1 \text{ (b). } \quad \frac{dI}{dt} = \alpha \tau \frac{CN}{B} S - \beta I \quad \text{[colonised substrate]}$$

$$2.1 \text{ (c). } \quad \frac{dC^*}{dt} = \beta I - v_C C^* - k_1 C^* + k_2 C \quad \text{[external carbon]}$$

$$2.1 \text{ (d). } \quad \frac{dN^*}{dt} = \frac{1}{\psi} \beta I - v_N N^* - k_3 N^* + k_4 N + \xi \quad \text{[external nitrogen]}$$

$$2.1 \text{ (e). } \quad \frac{dC}{dt} = k_1 C^* - k_2 C - \tau \frac{CN}{B} - \omega B - \Delta \beta I \quad \text{[metabolic carbon pool]}$$

$$2.1 \text{ (f). } \quad \frac{dN}{dt} = k_3 N^* - k_4 N - \frac{1}{\phi} \tau \frac{CN}{B} \quad \text{[metabolic nitrogen pool]}$$

$$2.1 \text{ (g). } \quad \frac{dB}{dt} = \tau \frac{CN}{B} - \mu B \quad \text{[structural fungal biomass]}$$

$$\text{where the maintenance rate} = \begin{cases} \omega & \text{if } C > 0 \\ 0 & \text{if } C = 0 \end{cases}$$

$$\text{and the decomposition rate} = \begin{cases} \Delta & \text{if } C > 0 \\ 0 & \text{if } C = 0 \end{cases}$$

These restrictions avoid that the maintenance or decomposition term in equation 2.1 (e) drive variable C negative when C is small relative to B or I.

3. Qualitative analysis and results

The model (2.1) was analysed to establish whether steady state values for all variables existed. Rates of change of all variables are then zero. The steady state value for substrate, \hat{S} , follows implicitly from the cubic equation $a_1\hat{S}^3 + a_2\hat{S}^2 + a_3\hat{S} + a_4 = 0$, where a_1 , a_2 , a_3 , and a_4 are composites of the original parameters (Appendix 1). The three roots of this cubic equation are not biologically meaningful if they give negative or complex values. If \hat{S} is biologically meaningful, then the remaining steady state variables are directly related to \hat{S} :

$$3.1 (a). \quad \hat{I} = \frac{\sigma - \rho\hat{S}}{\beta}$$

$$3.1 (b). \quad \hat{C} = \frac{(\alpha\mu[\Delta - 1]\hat{S} + \mu + \omega)(\rho\hat{S} - \sigma)}{\alpha\mu\nu_C\hat{S}}$$

$$3.1 (c). \quad \hat{N} = \frac{\alpha\phi\psi\xi\hat{S} + (\sigma - \rho\hat{S})(\alpha\phi\hat{S} - \psi)}{\alpha\nu_{N^*}\phi\psi\hat{S}}$$

$$3.1 (d). \quad \hat{C} = \frac{(\alpha\mu[\Delta(k_1 + \nu_C) - k_1]\hat{S} + (k_1 + \nu_C)(\mu + \omega)(\rho\hat{S} - \sigma))}{\alpha k_2 \mu \nu_C \hat{S}}$$

$$3.1 (e). \quad \hat{N} = \frac{\alpha\phi\psi k_3 \xi \hat{S} + (\sigma - \rho\hat{S})(\alpha\phi k_3 \hat{S} - \psi[\nu_{N^*} + k_3])}{\alpha \nu_{N^*} \phi \psi k_4 \hat{S}}$$

$$3.1 (f). \quad \hat{B} = \frac{(\sigma - \rho\hat{S})}{\alpha\mu\hat{S}}$$

To have a biological interpretation, all steady state expressions derived from \hat{S} (3.1) should also be larger than zero resulting in a cascade of conditions for existence:

$$3.2 (a). \quad \hat{S} > 0$$

$$3.2 (b). \quad \hat{S} < \frac{\sigma}{\rho}, \text{ necessary for } \hat{I} > 0 \text{ and } \hat{B} > 0$$

$$3.2 (c). \quad \hat{S} > \frac{1 + \frac{\omega}{\mu}}{\alpha(1 - \Delta)} \text{ with } \Delta < 1, \text{ necessary for } \hat{C}^* > 0$$

$$3.2 (d). \quad \alpha\phi\psi\xi\hat{S} + (\sigma - \rho\hat{S})(\alpha\phi\hat{S} - \psi) > 0, \text{ necessary for } \hat{N}^* > 0$$

$$3.2 (e). \quad \hat{S} > \frac{1 + \frac{\omega}{\mu}}{\alpha \left(\frac{k_1}{k_1 + v_{C^*}} - \Delta \right)} \text{ with } \Delta < \frac{k_1}{k_1 + v_{C^*}}, \text{ necessary for } \hat{C} > 0$$

$$3.2 (f). \quad \alpha \phi \psi k_3 \xi \hat{S} + (\sigma - \rho \hat{S}) (\alpha \phi k_3 \hat{S} - \psi [v_{N^*} + k_3]) > 0, \text{ necessary for } \hat{N} > 0$$

Conditions 3.2 (d) and 3.2 (f) can be written as complicated intervals with \hat{S} written explicitly as a root of the cubic equation (Appendix 1), but are difficult to interpret biologically. Condition 3.2 (b) can be combined with condition 3.2 (e), which is a sufficient condition for 3.2 (a) and 3.2 (c), to give:

$$3.3. \quad \frac{1 + \frac{\omega}{\mu}}{\alpha \left(\frac{k_1}{k_1 + v_{C^*}} - \Delta \right)} < \hat{S} < \frac{\sigma}{\rho} \text{ with } \Delta < \frac{k_1}{k_1 + v_{C^*}}$$

Clearly, for equation 3.3 to hold requires $\frac{1 + \frac{\omega}{\mu}}{\alpha \left(\frac{k_1}{k_1 + v_{C^*}} - \Delta \right)} < \frac{\sigma}{\rho}$, which can be rewritten as:

$$3.4. \quad \alpha \left(\frac{k_1}{k_1 + v_{C^*}} - \Delta \right) \frac{\sigma}{\rho} > 1 + \frac{\omega}{\mu} \text{ implying } \Delta < \frac{k_1}{k_1 + v_{C^*}} \text{ (since } 1 + \frac{\omega}{\mu} > 0 \text{)}.$$

We start with the biological interpretation of the constraint $\Delta < \frac{k_1}{k_1 + v_{C^*}}$ (3.4). The carbon

formed as a result of decomposition is either taken up by the fungus (k_1) or lost due to assimilation by other microorganisms (v_{C^*}) (Fig. 1). Therefore $\frac{k_1}{k_1 + v_{C^*}}$ is the carbon fraction

that is taken up by the fungus or, in other words, the number of carbon units resulting from decomposition per carbon unit substrate. It is biologically relevant that the number of carbon units invested in decomposition per carbon unit substrate (Δ) should be less than the number of carbon units resulting from decomposition per carbon unit substrate ($\frac{k_1}{k_1 + v_{C^*}}$).

The left-hand side of condition 3.4 can be explained as follows. In absence of the fungus the steady state value for substrate depends only on substrate supply per time unit (σ) and substrate removal rate (ρ), so $\frac{dS}{dt} = \sigma - \rho S$, leading to $\hat{S} = \frac{\sigma}{\rho}$, which gives an upper limit to

\hat{S} . The left-hand side (3.4) has a biological interpretation, indicating a positive carbon balance, $\frac{k_1}{k_1 + v_{C^*}} - \Delta$, in the case where substrate is at $\frac{\sigma}{\rho}$ with colonisation probability α (per carbon unit biomass). It is evident that the amount of substrate in absence of the fungus, $\frac{\sigma}{\rho}$, will never be reached in the presence of the fungus. The first part of the right-hand side (3.4), the quantity 1, represents the fact that the number of carbon units extracted from the metabolic carbon pool, $\tau \frac{CN}{B}$, is equal to the number of carbon units incorporated into structural fungal biomass, $\tau \frac{CN}{B}$ (model 2.2). The second part of the right-hand side is $\frac{\omega}{\mu}$, where ω is the number of carbon units necessary out of the metabolic carbon pool for maintenance of structural fungal biomass per unit time (per carbon unit biomass). With μ being the biomass mortality rate, $\frac{\omega}{\mu}$ is the number of carbon units necessary for maintenance during the whole life time of a carbon unit biomass (per carbon unit biomass). The right-hand side thus represents the number of carbon units necessary for production of structural biomass and for maintenance (per carbon unit biomass). From a biological viewpoint it is clear that for growth this quantity should be less than the left-hand side, being the positive carbon balance in the situation where all substrate is colonised.

4. Numerical analysis and results

The fungus can colonise an environment when the parameter values satisfy the existence criteria discussed in the previous section. After fungal invasion the system can either stabilise at the internal steady state, or periodic fluctuations might arise. An example of the first possibility is shown in Fig. 2. To determine whether the internal steady state might lose stability, giving rise to a periodic solution, can be calculated using linearised stability analysis. These calculations, combined with implicitly defined steady state values (Appendix 1), result however in a characteristic equation too unwieldy to be of any practical value. Our numerical simulations for wide ranges of all parameter values, however, indicate that the system always converges to the internal steady state, meaning that no periodic solutions are observed. We simulated the system for such a wide variety of parameter values that we feel safe to conclude that at least for biological reasonable values the internal steady state is always stable.

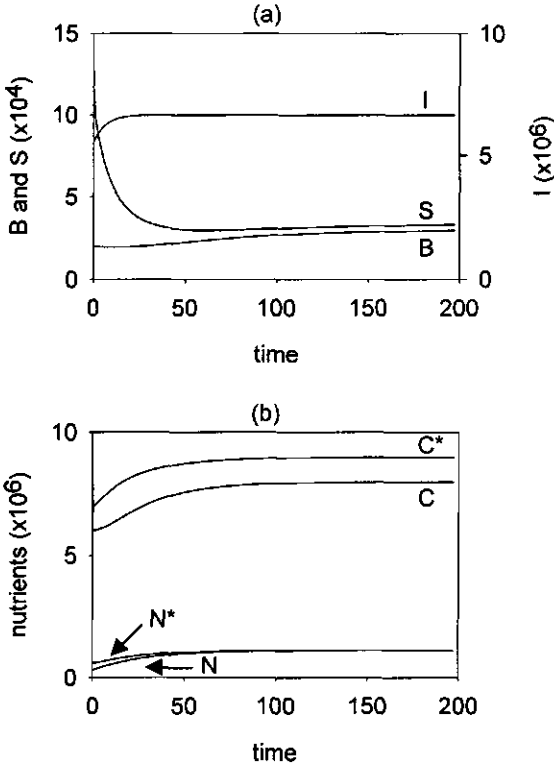


Figure 2. Time plots of structural fungal biomass (B), substrate (S), and colonised substrate (I) in (a), and of the nutrients in (b).

Time plots for default parameter values (Table 2), where appropriate taken from Paustian & Schnürer (1987b), show stabilisation of all variables at single point steady states (Fig. 2). Substrate is colonised by the fungus, resulting in an increase in fungal biomass (Fig. 2(a)). Carbon (both C and C*) stabilises at higher levels than nitrogen (Fig. 2(b)). A time plot of the carbon:nitrogen ratio in the metabolic pools ($\frac{C}{N}$) shows stabilisation at a level below the constant carbon:nitrogen ratio of the structural biomass ϕ (Fig. 3). Experimentally nutrients in the metabolic pools (C, N) cannot be measured separately from nutrients in the structural biomass, but the overall carbon:nitrogen ratio of the mycelium can be measured. Carbon present in the structural biomass (C_B) is calculated from $\frac{\phi}{\phi + 1}B$, and nitrogen present in the

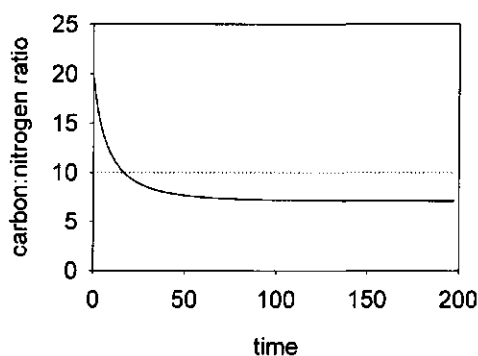


Figure 3. Time plot of the carbon:nitrogen ratio in the metabolic pools ($\frac{C}{N}$, solid line). The constant carbon:nitrogen ratio of the structural fungal biomass (ϕ) has default value 10 (dotted line).

structural biomass (N_B) is calculated from $\frac{1}{\phi+1}B$, where $\frac{C_B}{N_B}$ equals ϕ . The curve of the overall carbon:nitrogen ratio of the mycelium ($\frac{C+C_B}{N+N_B}$) is almost similar to the $\frac{C}{N}$ curve (not shown). Numerical output shows that $\frac{C}{N}$ is slightly higher than $\frac{C+C_B}{N+N_B}$ until both curves cross, and slightly lower afterwards. The curves cross where $\frac{C}{N} = \frac{C+C_B}{N+N_B}$, thus where $\frac{C}{N} = \frac{C_B}{N_B} = \phi$. The expression for the steady state carbon:nitrogen ratio $\frac{\hat{C}+\hat{C}_B}{\hat{N}+\hat{N}_B}$ is given in

Appendix 2.

The steady state value for structural fungal biomass (3.1 (f)) shows an inverse relationship with \hat{S} , indicating a high sensitivity to the efficiency of substrate utilisation (Fig. 4(a)). At high \hat{B} there is little *non-colonised* substrate remaining and vice versa. Curves are also shown for biomass mortality rates 10 times higher or lower than the default value 0.01, indicating higher \hat{B} at lower mortality rates. The higher the steady state fraction of colonised substrate, $\hat{I}/(\hat{I}+\hat{S})$, the higher the steady state value for fungal biomass (Fig. 4(b)).

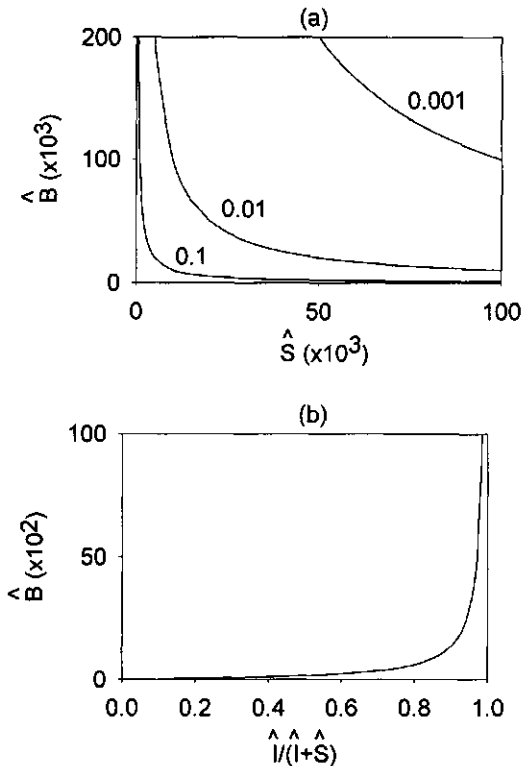


Figure 4. Steady state of structural fungal biomass (\hat{B}) versus steady state of substrate (\hat{S}) for biomass mortality rates of 0.1, 0.01 and 0.001 d^{-1} in (a), and versus steady state fraction of colonised substrate ($\hat{I}/(\hat{I} + \hat{S})$) in (b).

The three steady state solutions for substrate, resulting from the cubic equation (Appendix 1) were calculated for the default parameter values (used in Fig. 2) and with varying values of those parameters that appear in 3.3 (see range in Table 2). It was then checked whether each of these solutions is biologically meaningful with respect to the conditions for existence of the steady state variables (3.2). For all cases investigated (see Table 2 and Figs. 5&6) the result of this analysis was that of the three solutions for \hat{S} at most one solution had biological interpretation. The biologically meaningful solution for \hat{S} is plotted versus various parameters to study the sensitivity of \hat{S} to parameter values. Plots involving the parameters of the constraint of condition 3.3 (Δ , k_1 , v_c) show a lower, asymptotic boundary and an upper, strict boundary for \hat{S} (Fig. 5).

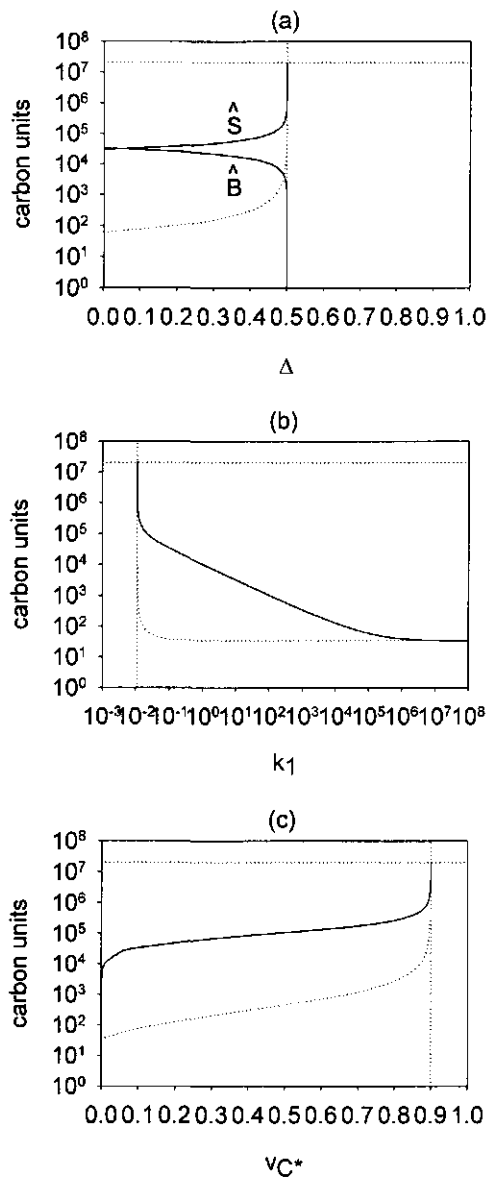


Figure 5. Biologically meaningful solution for the steady state of substrate (\hat{S} , solid line) versus carbon units invested in decomposition per carbon unit substrate (Δ) in (a), versus carbon uptake rate (k_1) in (b), and versus carbon loss rate (v_{C^*}) in (c). Fig. 5(a) shows also the corresponding steady state of structural fungal biomass (\hat{B}). The boundaries (dotted lines) are formed by conditions for existence of the steady state variables (3.2 (b) and (e)).

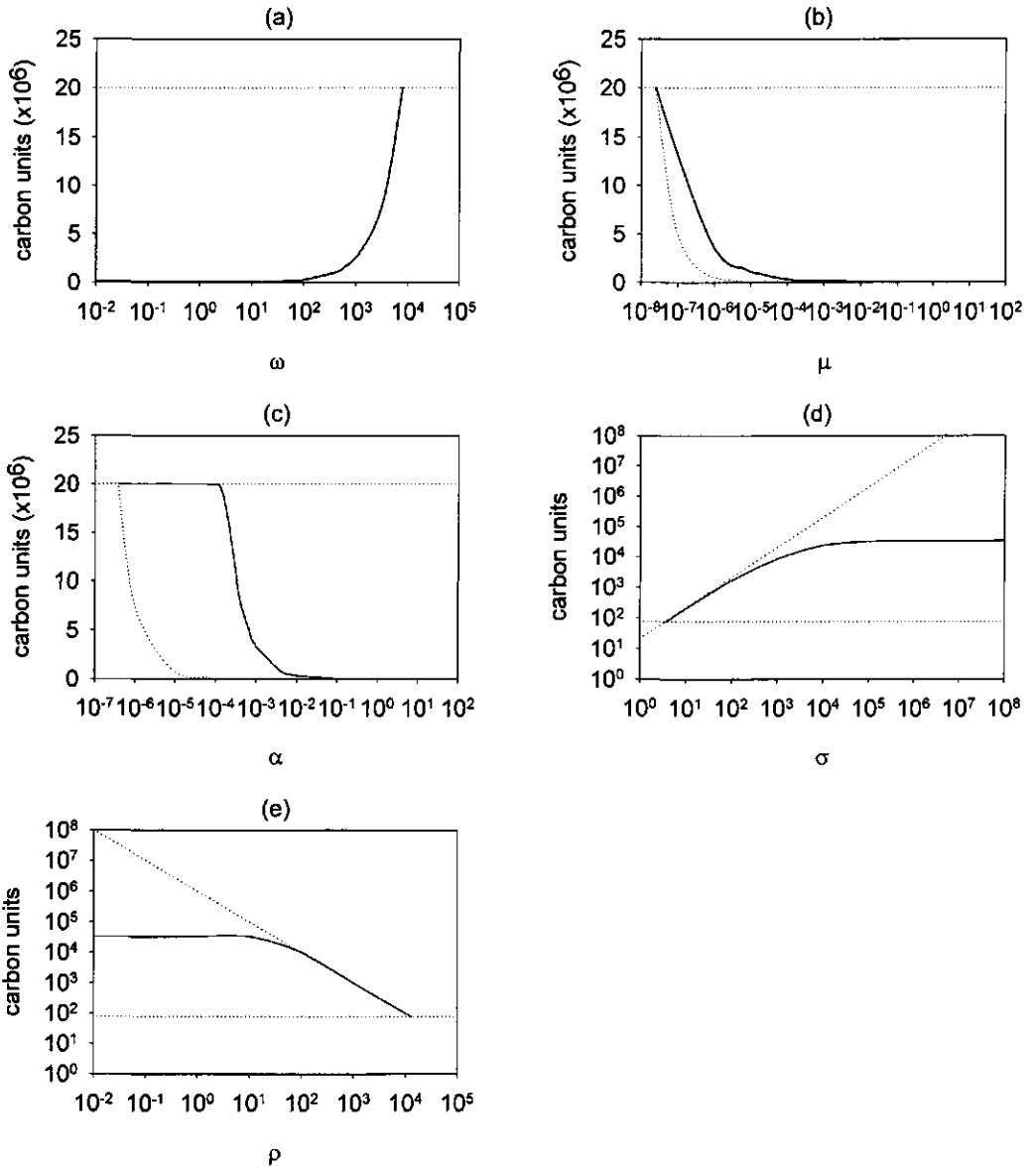


Figure 6. Biologically meaningful solution for the steady state of substrate (\hat{S} , solid line) versus ω , μ , α , σ , and ρ in Fig. 6 (a) to (e) respectively. For parameter descriptions see Table 2. The boundaries (dotted lines) are formed by conditions for existence of the steady state variables (3.2 (b) and (e)).

These two boundaries are set by the left-hand side and right-hand side of condition 3.3. The lower boundaries of the intervals specified by condition 3.2 (d) and 3.2 (f) are ensured by condition 3.2 (e) while the upper boundaries are ensured by condition 3.2 (b). A boundary for

Δ is given by the constraint of condition 3.3, $\Delta < \frac{k_1}{k_1 + v_c}$ (Fig. 5(a)). The parameters

involved in this constraint do not appear in condition 3.2 (d) or 3.2 (f). Rewriting the

constraint as $k_1 > \frac{\Delta v_c}{(1-\Delta)}$ or $v_c < \frac{k_1(1-\Delta)}{\Delta}$ gives the boundaries for k_1 (Fig. 5(b)) and v_c .

(Fig. 5(c)). Plotting the biologically meaningful solution for \hat{S} versus the remaining parameters of condition 3.3 (ω , μ , α , σ , and ρ) shows also a lower and upper boundary

for \hat{S} (Fig. 6), again set by the left-hand side and right-hand side of condition 3.3. All curves do not cross the boundaries indicated, however, some are very close to them. The curves indicate the cases where one biologically meaningful solution for the steady state was found. Beyond the boundaries no biologically meaningful solution exists (that is for $\omega \geq 8000$, $\mu \leq 2.5 \cdot 10^{-8}$, $\alpha \leq 3.75 \cdot 10^{-7}$, $\sigma \leq 3.75$, and $\rho \geq 13333$).

5. Discussion and conclusions

In this paper we studied fungal growth as a result of substrate decomposition. The model includes detailed dynamics of carbon and nitrogen, whereas other models proposed thus far do not. Steady states of the model were analysed qualitatively and by numerical simulations. In the case where a continuous substrate input is changed into a batch input, the amount of substrate approaches zero and the fungus does not persist. Then, the system does not stabilise at an internal steady state, as explained by Garrett (1946). Insofar as the final product of organic matter decomposition in soil, namely humus, is a more or less permanent constituent of the soil ecosystem, the theoretical zero end-point will never be reached.

The model presented assumes a constant carbon:nitrogen ratio for structural fungal biomass, because the metabolic pools are considered as separate components. Paustian & Schnürer (1987a) also assumed constant carbon:nitrogen ratios for cytoplasm and cell walls. The overall carbon:nitrogen ratio for the mycelium may vary greatly depending on the degree of metabolic nutrient accumulation (Fig. 3, where $\frac{C + C_B}{N + N_B}$ is almost similar to $\frac{C}{N}$). Nicolardot

et al. (1989) found that the carbon:nitrogen ratio for one species (*Aspergillus flavus*) could vary from 5.8 to 11.9. A constant carbon:nitrogen ratio is also assumed for substrate (S),

implying that the substrate is of a constant quality. This is a limitation of the model, since the carbon:nitrogen ratio of substrate should decrease due to continuous loss of carbon and conservation of the limiting nitrogen in an immobilised form (Swift et al., 1979). Fungal colonisation of dead fern litter resulted in a decrease in carbon:nitrogen ratio from some 200:1 to 30:1, as a result of the rate of loss of cellulose and lignin (Frankland, 1994). Changes in available resources are related to succession of fungal species. Sugar is first consumed by, for example, mucoraceous fungi and bacteria, followed by cellulose by many ascomycetes and basidiomycetes, and lignin by predominantly basidiomycetes. In the model presented here we do not see this phenomenon, since we have a constant carbon:nitrogen ratio, which is, as already mentioned, a limitation of the model. Use of substrate by other microorganisms is included implicitly by using a substrate removal term, and loss terms of external carbon and nitrogen (Fig. 1).

Where the carbon:nutrient ratio is very high, as in wood, the model of Swift et al. (1979) suggests that during initial stages of decomposition the carbohydrate component is used as an energy source until the fungal resource carbon:nutrient ratio approaches that of the fungus. Wood-decay fungi are able not only to extract nitrogen from wood but also to concentrate it, by which is meant that the overall carbon:nitrogen ratio in mycelium is much lower than in wood. Considerable immobilisation of nutrients is suggested by Stark (1972), who showed that hyphae had 193 to 272% greater nitrogen content and 104 to 223% greater phosphorus content than the pine needle litter on which they were found. In the default parameter set used to analyse the model presented, the fungus is assumed to colonise substrate having approximately the same carbon:nitrogen ratio as the structural fungal biomass ($\psi=9$, $\phi=10$). Simulations showed that a larger difference ($\psi=90$, $\phi=10$) also resulted in a steady state (lower value for structural fungal biomass, higher value for substrate and almost the same value for colonised substrate).

Qualitative analysis of the model shows three solutions for the steady state. However, numerical computations for a wide range of parameter combinations (Table 2) show that either one or no solution for the steady state is biologically meaningful, specified by conditions for existence with biological interpretation (section 3). We have been unable to show that two or three biologically meaningful solutions exist or to prove that this is impossible. The biologically meaningful solution for the steady state of substrate (\hat{S}) was plotted versus various parameters (Figs. 5&6). If many carbon units are invested in decomposition per carbon unit substrate (Δ), much carbon is extracted from the C-pool and

therefore not available for incorporation into structural fungal biomass, where less biomass results in more *non*-colonised substrate \hat{S} (Fig. 5(a)). At low carbon uptake rates (Fig. 5(b)) or high carbon loss rates (Fig. 5(c)), less carbon enters the C-pool, again resulting in a high value for \hat{S} . As Δ approximates the boundary specified by the constraint in equation 3.3, the steady state of structural fungal biomass (\hat{B}) becomes so small that substrate can not be colonised. The same holds for the carbon uptake and loss rate. A high maintenance rate of structural fungal biomass implies that much carbon is extracted from the C-pool and therefore not available for incorporation into structural fungal biomass, where less biomass results in more *non*-colonised substrate \hat{S} (Fig. 6(a)). In case this maintenance rate is too high, the fungus cannot persist. A high mortality rate of structural fungal biomass gives a low value for \hat{S} (Fig. 6(b)). This is also shown in Fig. 4(a) where for a given value for \hat{B} , increasing the mortality rate reduces the steady state value for substrate. On the other hand, for a given value for \hat{S} , increasing the mortality rate reduces the steady state value for structural fungal biomass, because the mortality rate appears in the steady state expression for B (3.1.(f)). A high substrate colonisation probability α gives more colonised substrate, and therefore less *non*-colonised substrate \hat{S} (Fig. 6(c)). If \hat{S} is too small, the fungus cannot colonise enough substrate to persist. A higher substrate supply per time unit (Fig. 6(d)) or a lower substrate removal rate (Fig. 6(e)) leads to more substrate in the steady state. If you supply too little or remove too much, the fungus can no longer persist.

Paustian and Schnürer (1987a) included translocation of cytoplasm in their model. Translocation is the movement of cytoplasm from existing hyphae into the zone of new growth, creating evacuated hyphal lengths. Hyphal outgrowth is then possible without a net increase in cytoplasm, where limiting growth resources are preferentially allocated to cell wall synthesis. Jennings (1975) reported that in most fungi hyphal extension is associated with the translocation of cytoplasmic constituents to apical regions. Furthermore, fungi may be highly differentiated with regions of actively-growing hyphae and degenerate or autolyzing hyphae existing within the same mycelium (Ricciardi et al., 1974). Although the phenomenon of translocation can be included in the model presented, we chose to keep the model simple to enable a detailed study of the dynamics of carbon and nitrogen.

One option to validate the model presented is to supply substrate with a known carbon:nitrogen ratio to a fungus with well-described growth characteristics such as

maintenance rate and mortality rate. Several parameters can effectively be set to zero, for example substrate removal rate, loss rates of carbon and nitrogen, by excluding competition and extra mineralization per time unit. The nutrients in the structural fungal biomass (C_B , N_B) and the pools (C, B) can in principle be measured. For a known carbon:nitrogen ratio of structural fungal biomass, time plots for C and N can be produced and compared with numerical simulations. The unknown parameters remaining can then be optimised by appropriate procedures to produce the best fit. In conclusion we can say that this complicated fungal growth model gave qualitative results with a clear biological interpretation, and which in simplified form can be evaluated with experimental data.

Appendix 1. The coefficients of the cubic equation in which the steady state variable substrate (\hat{S}) is expressed implicitly.

$$a_1 = \alpha^2 \mu k_3 \rho \tau [\Delta(k_1 + v_{C^*}) - k_1] / [\psi k_2 k_4 v_{C^*} v_{N^*}]$$

$$a_2 =$$

$$- \alpha \tau \left\{ \alpha \phi \psi \mu k_3 \xi [\Delta(k_1 + v_{C^*}) - k_1] + \alpha \phi \mu k_3 \sigma [\Delta(k_1 + v_{C^*}) - k_1] + \right. \\ \left. \rho [\Delta \psi \mu (k_3 + v_{N^*}) (k_1 + v_{C^*}) - v_{N^*} \psi k_1 \mu - k_3 \{ \phi (k_1 + v_{C^*}) (\mu + \omega) + \psi k_1 \mu \}] \right\} / [\psi \phi k_2 k_4 v_{C^*} v_{N^*}]$$

$$a_3 =$$

$$- \left\{ \alpha \phi \psi k_3 \tau \xi (k_1 + v_{C^*}) (\mu + \omega) - \right. \\ \left. \alpha \tau \sigma [\Delta \psi \mu (v_{N^*} + k_3) (k_1 + v_{C^*}) - v_{N^*} \psi k_1 \mu - k_3 \{ \phi (k_1 + v_{C^*}) (\mu + \omega) + \psi k_1 \mu \}] - \right\} / [\psi \phi k_2 k_4 v_{C^*} v_{N^*}] \\ \left\{ \psi \rho [v_{N^*} \{ \phi k_2 k_4 v_{C^*} - \tau (k_1 + v_{C^*}) (\mu + \omega) \}] - k_3 \tau (k_1 + v_{C^*}) (\mu + \omega) \right\}$$

$$a_4 = \sigma \{ k_3 \tau (k_1 + v_{C^*}) (\mu + \omega) - v_{N^*} [\phi k_2 k_4 v_{C^*} - \tau (k_1 + v_{C^*}) (\mu + \omega)] \} / [\phi k_2 k_4 v_{C^*} v_{N^*}]$$

Appendix 2. The expression for the steady state carbon:nitrogen ratio $\frac{\hat{C} + \hat{C}_B}{\hat{N} + \hat{N}_B}$, where C

and N refer to carbon and nitrogen in the metabolic pools, and C_B and N_B refer to carbon and nitrogen in the structural fungal biomass.

$$\frac{v_{N^*} \phi \psi k_4 \{ \alpha \mu \hat{S} (\phi + 1) [\Delta(k_1 + v_{C^*}) - k_1] + \phi [(k_1 + v_{C^*}) (\mu + \omega) - k_2 v_{C^*}] + (k_1 + v_{C^*}) (\mu + \omega) \} (\rho \hat{S} - \sigma)}{k_2 v_{C^*} \{ \alpha \psi \phi \mu k_3 \xi \hat{S} (\phi + 1) + (\sigma - \rho \hat{S}) [\alpha \phi \mu k_3 \hat{S} (\phi + 1) + \psi (v_{N^*} [\phi (k_4 - \mu) - \mu] - \mu k_3 (\phi + 1))] \}}$$

Chapter 3

Quasi-steady state approximation to a fungal growth model

LAMOUR, A., VAN DEN BOSCH, F., TERMORSHUIZEN, A.J. & JEGER, M.J.

Submitted to *IMA J. Math. Appl. Med. Biol.*

Abstract

In Chapter 2, we proposed a fungal growth model (Lamour *et al.*, 2001), describing the colonization and decomposition of substrate, subsequent uptake of nutrients, and incorporation into fungal biomass, and performed an overall-steady state analysis. In this paper we assume that where nutrient dynamics are much faster than the dynamics of fungal biomass and substrate, the system will reach a quasi-steady state relatively quickly. We show how the quasi-steady state approximation is a simplification of the full fungal growth model. We then derive an explicit fungal invasion criterion, which was not possible for the full model, and characterise parameter domains for invasion and extinction. Importantly, the fungal invasion criterion takes two forms: one for systems where carbon is limiting, another for systems where nitrogen is limiting. We focus attention on what happens in the short term immediately following the introduction of a fungus to a fungal-free system by analysing the stability of the trivial steady state, and then check numerically whether the fungus is able to persist. The derived invasion criterion was found to be valid also for the full model. Knowledge of the factors that determine invasion is essential to an understanding of fungal dynamics. The simplified model allows the invasion criterion to be tested with experimental data.

1. Introduction

In Chapter 2 of this thesis, we proposed a fungal growth model with detailed consideration of carbon and nitrogen dynamics arising from colonization of a substrate source (Lamour *et al.*, 2001). The model describes the colonization and decomposition of substrate, subsequent uptake of carbon and nitrogen into internal metabolic pools, and incorporation into fungal biomass. An overall-steady state analysis was performed for the model with the conditions for existence of the steady state having a clear biological interpretation. However, it was not possible to derive an explicit invasion criterion for the fungus to establish in the described system.

In the overall-steady state analysis no *a priori* assumptions were made with respect to possibly differing rates for the various processes involved. Indeed for the default parameter set used in analysing the overall-steady state, these were of the same order of magnitude. However, the process of uptake of nutrients through the fungal membrane may proceed much faster than the process of growth of fungal biomass. Thus, in this paper we consider the possible outcomes if we assume that processes proceed at strongly differing rates. In particular the relatively fast nutrient dynamics will reach equilibrium, referred to as quasi-steady state (QSS), in a relatively short period of time as compared to the relatively slow dynamics of fungal biomass and substrate.

In plant growth models the assumption of fast nutrient dynamics compared to crop growth is common, and this approach has been applied successfully (Thornley & Johnson, 1990). In fungal growth, we are not aware of reports in the literature of direct measurements of rates related with substrate decomposition, acquisition (the crossing of extracellularly decomposed substrates through the cell wall and the plasmalemma), and usage for growth (notably the production of new cell walls). However, from the high energy required for decomposition of some substrates such as cellulose and lignin, and the high complexity of chemical reaction cascades involved in both substrate decomposition and structural growth, we deduce that these processes occur more slowly, per unit of carbon or nitrogen, than the relatively simple processes of low molecular weight compounds entering the fungal cell (Cooke & Whipps, 1993). Therefore, the assumption of fast nutrient dynamics compared to fungal growth makes a reasonable working hypothesis.

The QSS approximation is probably the most frequently used method of model simplification in mathematical models of complex biological phenomena across a wide range of time

scales. For chemical reaction networks, where reaction steps can be grouped as 'fast' and 'slow', the QSS approximation is seen to apply, for example to the communication system of slime moulds (Stiefenhofer, 1998). Also in predator-prey models (Borghans *et al.*, 1996; Huisman & De Boer, 1997) and models of HIV infection (Lenbury *et al.*, 2000) the QSS approximation can be applied. A QSS approximation often yields revealing analytical formulae and frequently circumvents problems of stiffness in the numerical integration of systems of differential equations.

We show how a QSS approximation simplifies the full fungal growth model (Lamour *et al.*, 2001). We investigate the conditions under which a fungus is able to invade a fungal-free habitat containing substrate for fungal growth, and alternatively when the fungus goes extinct. From an ecological and experimental point of view, it is relevant to derive a quantitative criterion that determines whether fungal invasion or extinction will take place. In this context an analogy can be made with the basic reproductive number of a pathogen, R_0 , defined as the average number of new infections produced following the introduction of a single infective individual to an infection-free system (e.g. Diekmann *et al.*, 1990). Clearly, for an individual to invade requires $R_0 > 1$. If $R_0 \leq 1$, then the epidemic dies out. In the fungal growth model, knowledge of factors that determine fungal invasion and extinction is essential to an understanding of the fungal dynamics.

In this paper we derive an explicit fungal invasion criterion for the simplified model, which was not possible for the full model. Lack of a priori knowledge of the behaviour of the limit of the fungal growth term ($\tau \frac{CN}{B}$ in equation 2.1 (g) below) as B approaches zero, made it impossible to carry out a direct linear stability analysis of the full problem. We circumvent this problem by simplifying the model by a quasi-steady state approximation. We use the fungal invasion criterion to characterise parameter domains for invasion and extinction. We then apply this invasion criterion to the dynamics of the full model. In a subsequent paper, we relate the invasion criterion to experimental data and estimate model parameters based on quantitative data on growth of fungal hyphae in response to a substrate source.

2. Model description

The fungal growth model is described in detail in Lamour *et al.* (2001), i.e. Chapter 2. Briefly (Tables 1 & 2), the model describes the colonization of substrate (S), decomposition of colonized substrate (I), subsequent uptake of carbon (C*) and nitrogen (N*) into an internal carbon (C) and nitrogen (N) pool, and incorporation into fungal biomass (B).

Table 1. Model variables with dimensions.

State		dimension [#]
S	substrate available to be colonised by the fungus	$N_{C\text{-units}}$
I	colonised substrate	$N_{C\text{-units}}$
C*	external carbon	$N_{C\text{-units}}$
N*	external nitrogen	$N_{N\text{-units}}$
C	carbon in the metabolic carbon pool	$N_{C\text{-units}}$
N	nitrogen in the metabolic nitrogen pool	$N_{N\text{-units}}$
B	structural fungal biomass	$N_{C\text{-units}}$

[#]where N = number of

Table 2. Parameters with dimensions and default values for numerical computations.

Parameter		dimension [#]	value
σ	substrate supply per time unit	$N_{C\text{-units}} T^{-1}$	10^6
ρ	substrate removal rate	T^{-1}	0.05
α	substrate colonisation probability per carbon unit biomass	$(N_{C\text{-units}(B)})^{-1}$	0.1
τ	fungal growth rate per C/B per N/B	see @	10^{-6}
β	substrate decomposition rate	T^{-1}	0.15
v_{C^*}	C* loss rate	T^{-1}	0.1
v_{N^*}	N* loss rate	T^{-1}	0.1
k_1	C* uptake rate	T^{-1}	0.1
k_2	C leakage rate	T^{-1}	0.1
k_3	N* uptake rate	T^{-1}	0.1
k_4	N leakage rate	T^{-1}	0.1
ψ	carbon:nitrogen ratio of supplied substrate	$N_{C\text{-units}}(N_{N\text{-units}})^{-1}$	9
ξ	extra mineralization per time unit	$N_{N\text{-units}} T^{-1}$	10^3
ω	maintenance rate of structural fungal biomass	T^{-1}	0.02
Δ	carbon units invested in decomposition per carbon unit substrate	$N_{C\text{-units}(C\text{-pool})}(N_{C\text{-units}(I)})^{-1}$	0.1
ϕ	carbon:nitrogen ratio of structural fungal biomass	$N_{C\text{-units}}(N_{N\text{-units}})^{-1}$	10
μ	mortality rate of structural fungal biomass	T^{-1}	0.01

[#]where N = number of; T = time unit (day)

@ where the dimension of τ is $T^{-1} \frac{N_{C\text{-units}(B)}}{N_{C\text{-units}(C\text{-pool})} \frac{N_{C\text{-units}(B)}}{N_{N\text{-units}(N\text{-pool})}}$

Supply of substrate is a constant amount per time unit, σ , whereas *removal* proceeds at a constant rate, ρ . *Colonization* of substrate is linearly related to new growth of biomass. Fungal *growth* is linearly proportional to $\frac{C}{B}$, i.e. a measure of the carbon concentration, and also to $\frac{N}{B}$. With τ being the proportionality constant, fungal growth is then modelled as $\tau \frac{C}{B} B$, which simplifies to $\tau \frac{CN}{B}$. Colonization of substrate is also linearly related to substrate with a proportionality constant α , leading to the colonization term $\alpha \tau \frac{CN}{B} S$. *Decomposition* is assumed to proceed at a constant rate, β . Carbon derived from decomposition (expressed in carbon units) equals βI , therefore nitrogen derived from decomposition is $\frac{1}{\psi} \beta I$, where ψ is the constant carbon:nitrogen ratio of the incoming substrate. *Loss* of nutrients is at rates v_C for carbon and v_N for nitrogen. *Uptake* and *leakage* of nutrients by the fungus are at rates k_1 and k_2 respectively for carbon, and k_3 and k_4 respectively for nitrogen. *Mineralization* is assumed to occur at a constant amount per time unit, ξ . For growth of structural fungal biomass (B), carbon is utilized at an amount $\tau \frac{CN}{B}$ per time unit. To achieve growth of biomass in terms of nitrogen, this quantity is multiplied by $\frac{1}{\phi}$, where ϕ is the constant carbon:nitrogen ratio of structural fungal biomass. *Maintenance* of fungal biomass is a constant rate, ω . *Decomposition* of colonized substrate demands carbon units out of the metabolic carbon pool at an amount Δ per unit of colonized substrate, leading to a carbon loss term $\Delta \beta I$ per time unit. A constant *mortality* rate μ of biomass is assumed. The fungal growth model reads

$$2.1 \text{ (a). } \frac{dS}{dt} = \sigma - \rho S - \alpha \tau \frac{CN}{B} S \quad \text{[substrate]}$$

$$2.1 \text{ (b). } \frac{dI}{dt} = \alpha \tau \frac{CN}{B} S - \beta I \quad \text{[colonized substrate]}$$

$$2.1 \text{ (c). } \frac{dC^*}{dt} = \beta I - v_C C^* - k_1 C^* + k_2 C \quad \text{[external carbon]}$$

$$2.1 \text{ (d). } \frac{dN^*}{dt} = \frac{1}{\psi} \beta I - v_N N^* - k_3 N^* + k_4 N + \xi \quad \text{[external nitrogen]}$$

$$2.1 \text{ (e). } \frac{dC}{dt} = k_1 C^* - k_2 C - \tau \frac{CN}{B} - \omega B - \Delta \beta I \quad \text{[metabolic carbon pool]}$$

$$2.1 \text{ (f). } \frac{dN}{dt} = k_3 N^* - k_4 N - \frac{1}{\phi} \tau \frac{CN}{B} \quad \text{[metabolic nitrogen pool]}$$

$$2.1 \text{ (g). } \frac{dB}{dt} = \tau \frac{CN}{B} - \mu B \quad \text{[structural fungal biomass]}$$

$$\text{where the maintenance rate} = \begin{cases} \omega & \text{if } C > 0 \\ 0 & \text{if } C = 0 \end{cases}$$

$$\text{and the decomposition rate} = \begin{cases} \Delta & \text{if } C > 0 \\ 0 & \text{if } C = 0 \end{cases}$$

To avoid C going negative in equation 2.1 (e), we set the maintenance and decomposition rates to zero for $C=0$. Another option would be to use a Michaelis-Menten term in which these rates gradually decline to zero as C tends to zero. However, the situation where C is small relative to B and I is arguably not interesting in terms of fungal growth, therefore the simple linear term is preferred in the model.

3. Quasi-steady state approximation

If the nutrient dynamics of model (2.1) are very fast compared to the dynamics of fungal biomass, substrate and colonized substrate, then after a fast transient the nutrients can be regarded as in equilibrium. The quasi-steady states for the nutrients are dependent on the sizes of other variables. Under this assumption the rates of change in the nutrients are set to zero, resulting in the simplified model

$$3.1 \text{ (a). } \frac{dS}{dt} = \sigma - \rho S - \alpha\tau \frac{CN}{B} S \quad \text{[substrate]}$$

$$3.1 \text{ (b). } \frac{dI}{dt} = \alpha\tau \frac{CN}{B} S - \beta I \quad \text{[colonized substrate]}$$

$$3.1 \text{ (c). } \frac{dC^*}{dt} = 0 \quad \text{[external carbon]}$$

$$3.1 \text{ (d). } \frac{dN^*}{dt} = 0 \quad \text{[external nitrogen]}$$

$$3.1 \text{ (e). } \frac{dC}{dt} = 0 \quad \text{[metabolic carbon pool]}$$

$$3.1 \text{ (f). } \frac{dN}{dt} = 0 \quad \text{[metabolic nitrogen pool]}$$

$$3.1 \text{ (g). } \frac{dB}{dt} = \tau \frac{CN}{B} - \mu B \quad \text{[structural fungal biomass]}$$

Solving equations 3.1 (c) to 3.1 (f) as a subset of the model, gives large, non-intuitive QSS expressions for the nutrients as functions of variables I and B (and of various parameters). The variable S does not appear in the rate of change in the nutrients. It is assumed that the levels of substrate, colonized substrate, and biomass change negligibly during the fast

transient. Differential equations for S, I, and B (equations 3.1 (a), (b), and (g) respectively), which are valid after the fast transient, are derived by substituting the QSS expressions for \hat{C} and \hat{N} in the fungal growth term $\tau_{\frac{CN}{B}}$. The fungal growth term is then also a function of variables I and B (Appendix 1).

The QSS assumption should provide a good approximation for calculating the post-transient development of the system under consideration. The time that characterises the duration of the fast transient should be much smaller than the magnitude of time required for a significant change in S, I, or B during the post-transient period. Also, the change in I and B should be small in the fast transient, since the QSS expressions for the nutrients are functions of I and B. The QSS approximation thus reduces model (2.1) to three differential equations, i.e. for substrate, colonized substrate, and fungal biomass.

4. Fungal invasion criterion

Introducing a small amount of fungal biomass to a fungal-free system may lead to fungal invasion of the system or to extinction. Invasion implies that the trivial steady state is unstable and the introduced fungus will start growing. In cases where the trivial steady state is stable, the system will return to this trivial steady state after introduction of the fungus, i.e. it fails to invade. Before we calculate the invasion criterion, we simplify the fungal growth term $\tau_{\frac{CN}{B}}$ (Appendix 1), since this is a large non-intuitive function of variables I and B. We show that $\tau_{\frac{CN}{B}}$ is linear in I for small values of B.

The QSS expressions for C and N were obtained from 3.1 (c) to 3.1 (f). These functions of variables I and B were substituted in the fungal growth term $\tau_{\frac{CN}{B}}$ (Appendix 1), and calculated using the default parameter set (Table 2). On logarithmic scales, $\tau_{\frac{CN}{B}}$ is linearly related to colonized substrate I for various values of B (Fig. 1 (a)). For small values of B this is a perfect linear relationship (for $B=10^{-4}$, $R^2=1$), and for large values of B the relationship is reasonably linear (for $B=10^8$, $R^2=0.963$). The slope and intercept of the curves in Fig. 1 (a) are plotted against $\ln(B)$ in Fig. 1 (b) & (c) respectively. For decreasing values of B the slope approaches 1, indicating that $\tau_{\frac{CN}{B}}$ is linear in I. Since B is assumed to be small at the time of invasion, we consider the limit of $\tau_{\frac{CN}{B}}$ as B approaches zero. This can be analytically computed, or derived by hand (Appendix 1). For simplicity, we take mineralization (appearing in 2.1 (d)) zero, although the analysis can also be done for non-zero values, giving

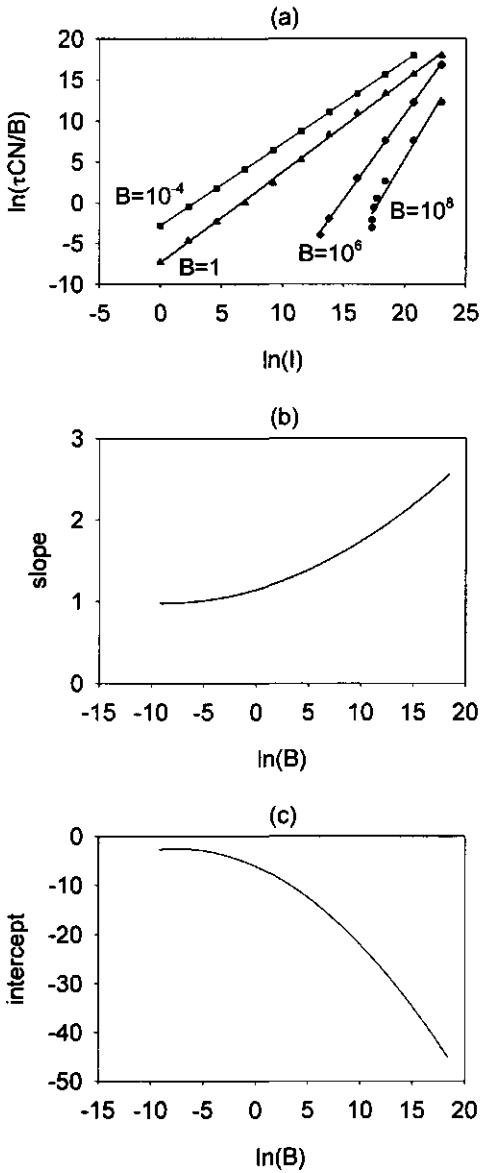


Figure 1. The fungal growth term (τ_{CN}/B in Appendix 1) versus colonized substrate (I) for various amounts of fungal biomass (B) in (a); The slope of these relationships in (b), and the intercept in (c) (default parameter values in Table 2).

$$4.1 \quad \lim_{B \rightarrow 0} \tau \frac{CN}{B} = \begin{cases} \left(\frac{k_1}{k_1 + v_{C^*}} - \Delta \right) \beta I & \text{if } \phi \frac{k_3}{k_3 + v_{N^*}} \frac{\beta}{\psi} I > \left(\frac{k_1}{k_1 + v_{C^*}} - \Delta \right) \beta I \\ \phi \frac{k_3}{k_3 + v_{N^*}} \frac{\beta}{\psi} I & \text{if } \phi \frac{k_3}{k_3 + v_{N^*}} \frac{\beta}{\psi} I < \left(\frac{k_1}{k_1 + v_{C^*}} - \Delta \right) \beta I \end{cases}$$

$$\text{implying } \Delta < \frac{k_1}{k_1 + v_{C^*}}$$

The inequality determining the form of $\lim_{B \rightarrow 0} \tau \frac{CN}{B}$ that is valid has a biological interpretation.

Starting on the right-hand side of the inequality, carbon formed as a result of decomposition is either taken up by the fungus (k_1) or lost due to assimilation by other microorganisms (v_{C^*}).

Therefore, $\frac{k_1}{k_1 + v_{C^*}}$ is the carbon fraction that is taken up by the fungus per unit carbon

substrate. Since Δ is the number of carbon units invested in decomposition per unit carbon

substrate, $\frac{k_1}{k_1 + v_{C^*}} - \Delta$ indicates the positive carbon balance, which is gained for each

substrate amount βI colonized per time unit, where βI is in terms of carbon units (Tables 1 &

2). Thus, the right-hand side of the condition indicates the carbon inflow per time unit.

Similarly, for the left-hand side $\frac{k_3}{k_3 + v_{N^*}}$ is the nitrogen fraction that is taken up by the

fungus, and $\frac{k_3}{k_3 + v_{N^*}} \frac{\beta}{\psi} I$ indicates the nitrogen inflow per time unit (βI is in terms of carbon

units, thus $\frac{\beta I}{\psi}$ is in terms of nitrogen units). The left-hand side is multiplied by ϕ , to compare

both sides of the inequality in the same carbon units. If the nitrogen inflow (in terms of carbon

units) exceeds the carbon inflow, then fungal growth is set by the limiting carbon inflow (at

the time of invasion). However, if the nitrogen inflow is limiting, then fungal growth is set by

the nitrogen inflow. The default parameter set (Table 2) represents a system of limiting

carbon inflow.

If $\lim_{B \rightarrow 0} \tau \frac{CN}{B}$ is indicated by GI, where G equals $\left(\frac{k_1}{k_1 + v_{C^*}} - \Delta \right) \beta$ in cases where carbon is

limiting, and $\phi \frac{k_3}{k_3 + v_{N^*}} \frac{\beta}{\psi}$ in cases where nitrogen is limiting, then the model reads

$$4.2 (a). \quad \frac{dS}{dt} = \sigma - \rho S - \alpha GIS$$

$$4.2 (b). \quad \frac{dI}{dt} = \alpha GIS - \beta I$$

$$4.2 (c). \quad \frac{dB}{dt} = GI - \mu B$$

The trivial steady state for model (4.2) is

$$4.3 \quad (\hat{S}, \hat{I}, \hat{B}) = \left(\frac{\sigma}{\rho}, 0, 0 \right)$$

Substituting the trivial steady state (4.3) in the Jacobian matrix for model (4.2) gives the characteristic equation

$$4.4 \quad \det \begin{pmatrix} -\rho - \lambda & -\alpha G \frac{\sigma}{\rho} & 0 \\ 0 & \alpha G \frac{\sigma}{\rho} - \beta - \lambda & 0 \\ 0 & G & -\mu - \lambda \end{pmatrix} = 0$$

from which we find the real eigenvalues

$$4.5 (a). \quad \lambda_1 = -\rho$$

$$4.5 (b). \quad \lambda_2 = \alpha G \frac{\sigma}{\rho} - \beta$$

$$4.5 (c). \quad \lambda_3 = -\mu$$

Only for (one or more) positive eigenvalues does the solution of the system grow with time.

The fungal invasion criterion is then

$$4.6 \quad \alpha G \frac{\sigma}{\rho} - \beta > 0 \quad \text{which can be rewritten as}$$

$$4.7 \quad \alpha \left(\frac{k_1}{k_1 + v_{C^*}} - \Delta \right) \frac{\sigma}{\rho} > 1 \quad \text{implying } \Delta < \frac{k_1}{k_1 + v_{C^*}} \quad \text{for limiting carbon, and}$$

$$4.8 \quad \alpha \phi \frac{k_3}{k_3 + v_{N^*}} \frac{1}{\psi} \frac{\sigma}{\rho} > 1 \quad \text{for limiting nitrogen}$$

5. Biological interpretation of the invasion criterion

In the previous paper (Lamour *et al.*, 2001) the overall-steady state of the full model required a cascade of conditions for existence. The conditions providing the steady state expressions

\hat{S} , \hat{I} , \hat{B} , \hat{C}^* , and \hat{C} to be positive, could be combined to give

$$5.1 \quad \alpha \left(\frac{k_1}{k_1 + v_C} - \Delta \right) \frac{\sigma}{\rho} > 1 + \frac{\omega}{\mu} \quad \text{implying } \Delta < \frac{k_1}{k_1 + v_C}$$

This equation (5.1) is almost similar to the fungal invasion criterion for a limiting carbon inflow (4.7). The left-hand side of (4.7) and (5.1) have the same biological interpretation, indicating a positive carbon balance, $\frac{k_1}{k_1 + v_C} - \Delta$, in the situation where all substrate ($\frac{\sigma}{\rho}$) is colonized with probability α (per carbon unit biomass). On the right-hand side of (4.7) and (5.1), quantity 1 represents the number of carbon units necessary for production of structural fungal biomass, and $\frac{\omega}{\mu}$ (5.1 only) represents the number of carbon units necessary for maintenance (per carbon unit biomass). It is a clear biological interpretation that for growth the left-hand side should be larger than the right-hand side. Clearly, (5.1) is a stronger criterion than (4.7).

Similarly, the conditions providing the steady state expressions \hat{N}^* and \hat{N} to be positive (Lamour *et al.*, 2001) can be combined (assuming mineralization to be zero) to give

$$5.2 \quad \alpha \phi \frac{k_3}{k_3 + v_{N^*}} \frac{1}{\psi} \frac{\sigma}{\rho} > 1$$

Expression (5.2) is identical to the fungal invasion criterion in the case of a limiting nitrogen inflow (4.8). The left-hand side indicates the positive nitrogen balance, $\frac{k_3}{k_3 + v_{N^*}}$, in the situation where all substrate ($\frac{\sigma}{\rho}$ in terms of carbon units, thus $\frac{1}{\psi} \frac{\sigma}{\rho}$ in terms of nitrogen units) is colonized. It is then converted to carbon units by ϕ , where the colonization probability is α (per carbon unit biomass).

6. Parameter domains for invasion and extinction

The values of the parameters determine whether carbon or nitrogen is limiting and, therefore, which form of the invasion criterion is valid. For both forms (4.7 & 4.8), parameters involved in the invasion criterion are varied over a wide range, and parameter domains for fungal invasion and extinction are shown (Fig. 2 & 3). For the default parameter set (Table 2), carbon is limiting and fungal invasion takes place. If substrate supply is low per time unit, the fungus can only invade the system if the substrate removal rate is small, whereas at higher supply rates, the removal rate may increase and still allow invasion (Fig. 2 (a) & Fig. 3 (a)).

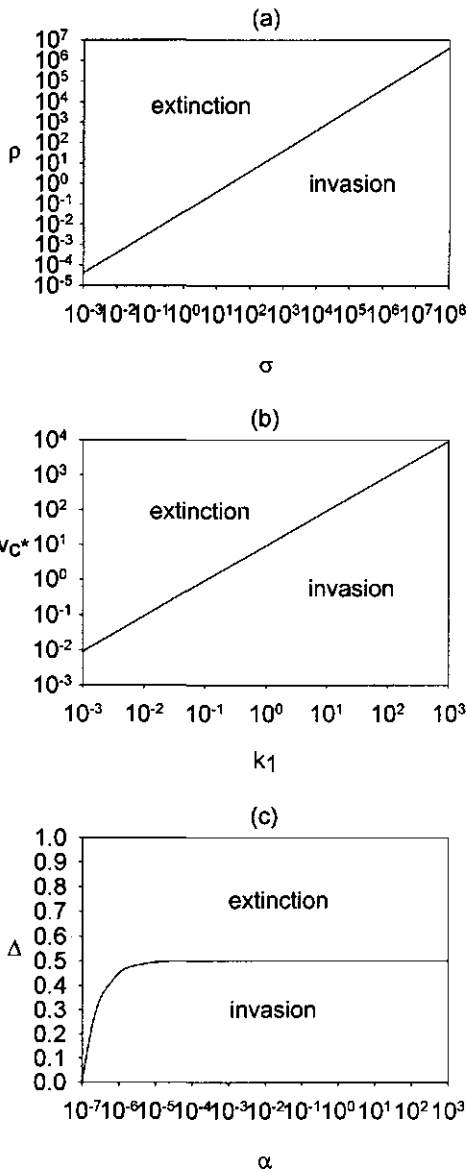


Figure 2. Parameter domains for fungal invasion and extinction in cases where carbon is limiting (default parameter values in Table 2). All parameters of the invasion criterion (4.7) are varied. Substrate removal rate (ρ) versus substrate supply per time unit (σ) in (a); Carbon loss rate (v_c) versus carbon uptake rate (k_1) in (b); Carbon units invested in decomposition per carbon unit substrate (Δ) versus substrate colonization probability per carbon unit biomass (α) in (c).

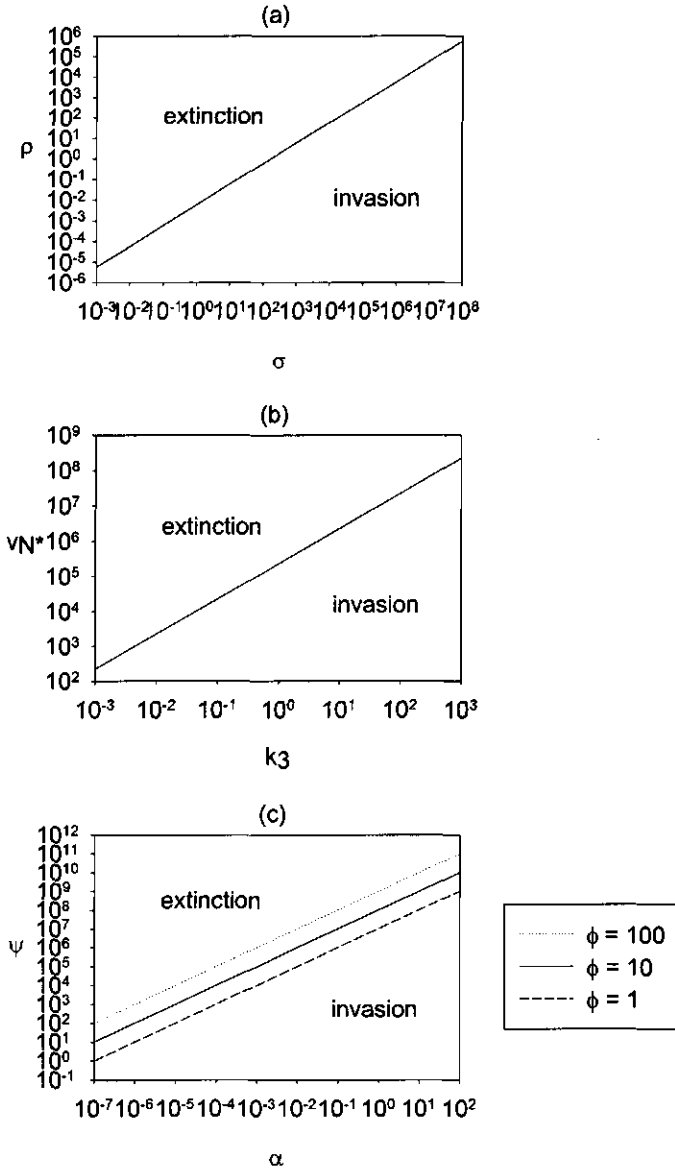


Figure 3. Parameter domains for fungal invasion and extinction in cases where nitrogen is limiting (default parameter values in Table 2, except for $\psi=90$). All parameters of the invasion criterion (4.8) are varied. Substrate removal rate (ρ) versus substrate supply per time unit (σ) in (a); Nitrogen loss rate (v_N) versus nitrogen uptake rate (k_3) in (b); Carbon:nitrogen ratio of supplied substrate (ψ) versus substrate colonization probability per carbon unit biomass (α) for various values of the carbon:nitrogen ratio of structural fungal biomass (ϕ) in (c).

At high nutrient uptake rates, the nutrient loss rate may be higher than at low uptake rates for invasion to be possible (Fig. 2 (b) & Fig. 3 (b)). In cases where carbon is limiting it is shown that at high values of the colonization probability α , Δ should be lower than the asymptote of 0.5, where Δ is the number of carbon units invested in decomposition per carbon unit substrate (Fig. 2 (c)). Smaller values of α require a decreasing value of Δ . In cases where nitrogen is limiting, small values of α require low values of ψ , i.e. the carbon:nitrogen ratio of the supplied substrate, where at higher α this ratio may increase (Fig. 3 (c)). For a higher carbon:nitrogen ratio of structural fungal biomass, ϕ , the parameter domain for invasion is larger.

7. Validity of the invasion criterion

The validity of the invasion criterion was numerically checked for model (4.2). This was done for systems of limiting carbon (default parameter set, Table 2), and also for systems of limiting nitrogen (default parameter set, except for $\psi=90$), determined by the inequality in (4.1). The system returned to the trivial steady state, i.e. the fungal-free habitat, if the invasion criterion was not fulfilled. In case the invasion criterion was fulfilled, the system persisted in the long run. The validity of the invasion criterion was also tested for the QSS model (3.1). This is graphically demonstrated for a system of limiting carbon for values of Δ approaching the border (4.7) between invasion and extinction (Fig. 4). When the invasion criterion was tested for the overall-steady state model (2.1), it was found to predict accurately the qualitative outcome in terms of invasion or extinction (Fig. 5). Here, extinction could be shown for $\Delta \geq 0.51$, which is very close to the predicted border of $\Delta=0.5$ (equation 4.7). Quantitatively, the time plots in Figures 4 and 5 show a close relationship.

8. Discussion

We reduced a system of 7 differential equations to 3 by assuming 'slow' and 'fast' subsystems. In the slow system the fast variables (nutrients) are assumed to converge to their equilibrium values instantaneously, where the slow variables are subject to slow dynamics. In the fast system the slow variables (biomass, substrate, and colonized substrate) are assumed to be constant and act as parameters, where the fast variables are subject to fast dynamics.

This QSS approximation reduced the full model to three differential equations, representing substrate, colonized substrate, and fungal biomass. For small values of B , the fungal growth term simplified to a linear term in I . The resulting system of equations bears similarity with the

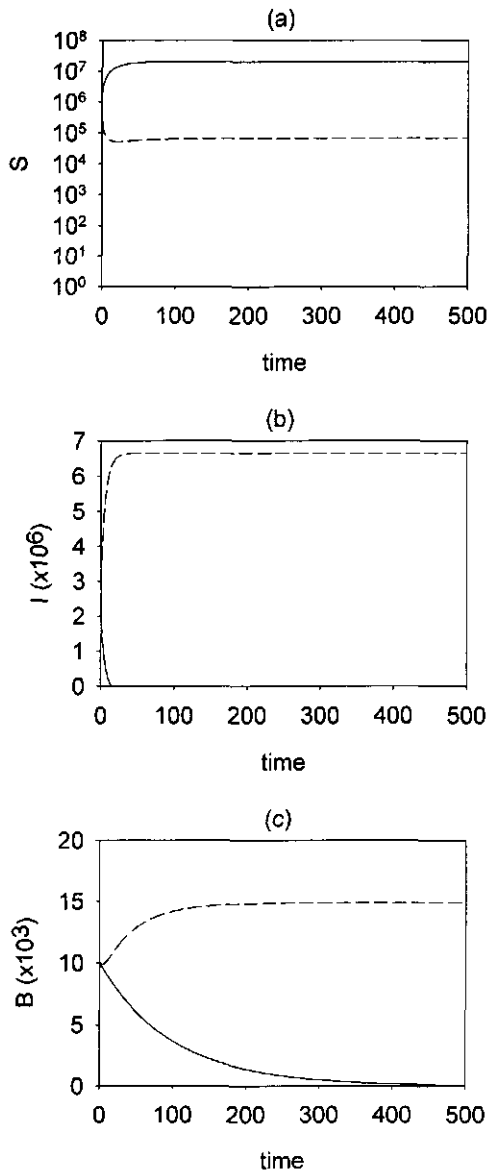


Figure 4. Invasion (dashed line) and extinction (solid line) in a system of limiting carbon of substrate (S) in (a), colonized substrate (I) in (b), and structural fungal biomass (B) in (c). The quasi-steady state model (3.1) and the default parameter set (Table 2) are used except for $\Delta=0.4$ (invasion), or $\Delta=0.5$ (extinction). Equation (4.7) predicts invasion for $\Delta < 0.5$, and extinction for $\Delta \geq 0.5$.

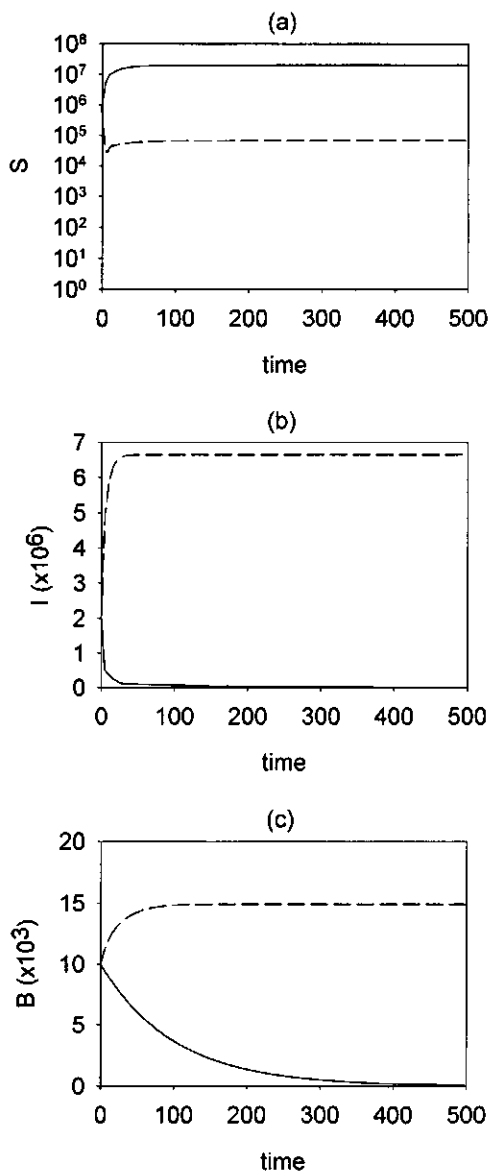


Figure 5. Invasion (dashed line) and extinction (solid line) in a system of limiting carbon of substrate (S) in (a), colonized substrate (I) in (b), and structural fungal biomass (B) in (c). The overall-steady state model (2.1) and the default parameter set (Table 2) are used except for $\Delta=0.4$ (invasion), or $\Delta=0.51$ (extinction). Equation (4.7) predicts invasion for $\Delta < 0.5$, and extinction for $\Delta \geq 0.5$.

well-known dynamics of *SIR* epidemic models, since substrate passes from a *susceptible* state (i.e. uncolonized substrate, *S*) to an *infected* state (i.e. colonized substrate, *I*). Although the system studied was developed to describe saprotrophic fungal growth, the model is sufficiently general to be applicable to a broad range of host-parasite associations, involving biological control. Other models of host-parasite associations include the model of Gubbins and Gilligan (1996), describing a parasite-hyperparasite system from which the parasite's host is excluded, using Lotka-Volterra equations modified to incorporate infected and uninfected parasites. Although the mathematical expressions used to model the various processes involved are different, the parasites (infected and uninfected) are related to substrate (colonized and uncolonized), and the hyperparasite to the fungus. Stolk *et al.* (1998) developed a model for mycoparasitism, which was based on the energy contents of the host fungus and the mycoparasite, and which is comparable with the *SIR* model. The central question in these papers is whether or not the biological control agent (hyperparasite or mycoparasite) can invade the host population (parasite or host fungus) and persist sufficiently to maintain control during the period of susceptibility of the crop.

By reducing the full model to three differential equations only, the qualitative behaviour is more readily investigated. For the reduced model we were able to derive an explicit fungal invasion criterion, which was not possible for the full model. In the derivation of the invasion criterion, we have focussed attention on what happens in the short term immediately following the introduction of a fungus to a fungal-free system by analysing the stability of the trivial steady state. We have then checked numerically whether the fungus was able to maintain itself in the long term. If the system returned to the trivial steady state, this was termed *extinction*. In cases where the system remained bounded away from zero, this was termed *invasion*. In fact, this is also persistence, because, if substrate supply is non-zero, invasion will always result in persistence since the system will approach a steady state.

The fungal invasion criterion takes two forms: one for systems where carbon is limiting, another for systems where nitrogen is limiting. Both forms were compared with results from the overall-steady state analysis of the full model. The full model had a cascade of conditions for existence of the overall-steady state, where one composite condition (5.1) varied slightly from the invasion criterion for limiting carbon (4.7) derived from the reduced model. The QSS assumption results in a model that is an approximation of the full model, and therefore (5.1) varies slightly from (4.7). The remaining conditions for existence of the overall-steady state could be combined to an expression (5.2) identical to the fungal invasion criterion in the case

of limiting nitrogen (4.8). Although the composite conditions for existence of the steady state were similar to the invasion criterion, this was not clear from the overall-steady state analysis. In addition, the overall-steady state analysis could not indicate which nutrient was limiting, as did the QSS analysis (inequality in 4.1), so the QSS approach was essential and has yielded valuable new insights.

The fungal invasion criterion derived for the reduced model was found to be also valid for the full model, even though a QSS assumption for the nutrients was not explicitly involved. It is important to discuss the applicability of a QSS assumption, since a QSS approximation of a high dimensional biological model may result in a low dimensional, less realistic, mathematical model, not making reliable predictions (e.g. Hunding & Kærn, 1998). However, the usually cited requirements for a QSS assumption to be valid can also be wrong (Palsson, 1987; Segel, 1988; Segel & Slemrod, 1989). Borghans *et al.* (1996) extended the QSS approximation by introducing a new variable, as a result of the addition of two model variables. In their approach the parameter domain for which the QSS assumption was valid was considerably extended, as shown for a variety of biologically significant examples taken from enzyme kinetics, immunology and ecology.

Bailey *et al.* (2000) distinguished between invasive and non-invasive fungal spread occurring amongst discrete sites of nutrient resources in a Petri dish. The fungus continued to spread provided it made contact with these nutrient sites, creating an expanding patch, the size of which was limited only by the size of the system in which the fungus was growing. This invasive spread is not comparable to the invasion phenomenon in our model, since it does not show whether the fungus is able to maintain itself in the long term. The fungus stopped spreading if it failed to make contact with uncolonized resources, resulting in a patch of finite size. This non-invasive spread is not comparable to extinction, because the experimental data do not clarify whether the fungal population goes extinct and the system returns to the fungal-free equilibrium. Clearly, the aim of the experiments was to visualise initial fungal spread, since, if nutrient sources are too far apart, local invasion ceases as the fungus exhausts its nutrient supply before colonizing a new resource. In this situation stochastic variation and spatial aspects are likely to be important.

Our model is a mean-field deterministic model leading, in the QSS approximation, to clear thresholds for invasion under the contrasting nutrient limiting conditions of decomposition processes in soil. We assume, for example, that a constant proportion of substrate is

colonized per unit of time, irrespective of spatial heterogeneity in substrate or fungal presence. The limitations of this approach were recognized in the previous paper (Lamour et al., 2001). Spatially explicit percolation models applied to the experimental system described by Bailey et al. (2000) again lead to the derivation of critical thresholds for invasion. In stochastic analogues of these types of models, thresholds deal only with the probability of invasion, and are consistently higher than in the deterministic models (Nåsell, 1995). Stochastic variation is increasingly important at low population densities and invasion probabilities, or where a population is spatially stratified as in a metapopulation. However, as previously described (Lamour et al., 2001), our primary concern is to focus on substrate dynamics and the resulting changes in fungal biomass.

In this paper, parameter domains for fungal invasion and extinction were derived, with parameters varying over a wide range (Fig. 2 & 3). Criteria for invasion are of considerable practical importance for the implementation of biological control by introduced hyperparasitic microorganisms, for example the mycoparasite *Sporidesmium sclerotivorum* which utilizes sclerotia of the plant pathogen *Sclerotinia minor* (Adams, 1990; Adams & Ayers, 1982; Fravel, 1997).

Carbon and nitrogen limitation arises in the inflow of nutrients from external and metabolic pools to structural fungal biomass, and therefore the lowest nutrient inflow limits fungal growth. Both nutrients are incorporated in biomass according to the carbon:nitrogen ratio of the structural fungal biomass (ϕ). Experimental data on fungal growth in response to the C:N ratio of substrate are scarce. Jackson *et al.* (1991) found growth of four soil-borne fungi (*Gliocladium virens*, *Trichoderma pseudokoningii*, and two strains of *T. viride*) in pure liquid culture to occur at C:N ratios varying between 5:1 and 155:1. Fungal dry weight increased with C:N ratio when the same amount of N was provided. However, dry weight production per gram C provided in the medium was optimal at a C:N ratio of 15:1 for all fungi tested, slightly more than the C:N ratio of 8-12:1 of most micro-organisms (Deacon, 1980). However, Park *et al.* (1991) found that mycelial growth of *G. virens in vitro* was not affected by a C:N ratio of the medium varying between 18:1 and 80:1. Growth of two isolates of *Fusarium oxysporum* f.sp. *elaeidis* increased as the concentration of carbon in the medium increased, but not with increase in the nitrogen concentration (Oritsejafor, 1986), indicating that the important factor influencing fungal growth is the concentration of carbon in the medium, rather than the C:N ratio *per se*.

The experimental data cited above relate to liquid cultures or agar plates where nutrients diffuse throughout the medium. Nutrients are therefore in contact with the total amount of fungal biomass. In reality, however, fungal hyphae grow towards substrate patches, whereby the newly produced hyphae are involved in substrate colonization. To our knowledge experimental data obtained for these situations barely exist, probably because the experimental difficulties involved. In future studies we will generate appropriate experimental data to link with qualitative results of both the overall-steady state (Lamour *et al.*, 2001) and quasi-steady state (this paper) analysis. In particular we will test the invasion criterion by monitoring fungal growth at varying amounts of substrate supply, and at varying C:N ratios of the supplied substrate (ψ).

9. Acknowledgements

The authors are grateful to Mark Huiskes (Agricultural University, Wageningen, The Netherlands) for his help and advice on the numerical simulations. IACR-Rothamsted receives grant aided support of BBSRC.

Appendix 1

Derivation of the two forms of the invasion criterion (4.1): Firstly, the quasi-steady state expressions for C and N, derived by solving equations 3.1 (c) to 3.1 (f) as a subset of the model, are substituted in the fungal growth term $\tau \frac{CN}{B}$; Secondly, the limit situation as B approaches zero is described, leading to (4.1).

$$\text{Define: } P_1 = \left(\frac{k_1}{k_1 + v_{C^*}} - \Delta \right) \beta I \quad P_2 = \left(\frac{k_1}{k_1 + v_{C^*}} - 1 \right) k_2$$

$$P_3 = \frac{k_3}{k_3 + v_{N^*}} \frac{\beta}{\psi} I \quad P_4 = \left(\frac{k_3}{k_3 + v_{N^*}} - 1 \right) k_4$$

$$\text{Then: } \tau \frac{CN}{B} = \frac{\tau(P_1 - \omega B)N}{-BP_2 + \tau N} \quad \text{where}$$

$$N = \left[-\left(P_3 \tau - BP_2 P_4 - \frac{\tau}{\phi} (P_1 - \omega B) \right) \pm \sqrt{\left(P_3 \tau - BP_2 P_4 - \frac{\tau}{\phi} (P_1 - \omega B) \right)^2 + 4P_4 \tau BP_2 P_3} \right] / [2P_4 \tau]$$

Now $\lim_{B \rightarrow 0} \tau \frac{CN}{B}$ depends on the behaviour of N as B approaches zero, therefore we study:

$$\lim_{B \rightarrow 0} N = \left[-P_3 \tau + \frac{\tau}{\phi} P_1 \pm \sqrt{\left(P_3 \tau - \frac{\tau}{\phi} P_1 \right)^2} \right] / [2P_4 \tau] \quad \text{giving}$$

$$\left\{ \begin{array}{ll} [-P_3\tau + \frac{\tau}{\phi}P_1 + (P_3\tau - \frac{\tau}{\phi}P_1)] / [2P_4\tau] = 0 & \text{if } P_3\tau - \frac{\tau}{\phi}P_1 > 0 \quad (\text{A.1}) \\ [-P_3\tau + \frac{\tau}{\phi}P_1 + (-P_3\tau + \frac{\tau}{\phi}P_1)] / [2P_4\tau] = \frac{-(P_3\tau - \frac{\tau}{\phi}P_1)}{P_4\tau} & \text{if } P_3\tau - \frac{\tau}{\phi}P_1 < 0 \quad (\text{A.2}) \\ [-P_3\tau + \frac{\tau}{\phi}P_1 - (P_3\tau - \frac{\tau}{\phi}P_1)] / [2P_4\tau] = \frac{-(P_3\tau - \frac{\tau}{\phi}P_1)}{P_4\tau} & \text{if } P_3\tau - \frac{\tau}{\phi}P_1 > 0 \quad (\text{A.3}) \\ [-P_3\tau + \frac{\tau}{\phi}P_1 - (-P_3\tau + \frac{\tau}{\phi}P_1)] / [2P_4\tau] = 0 & \text{if } P_3\tau - \frac{\tau}{\phi}P_1 < 0 \quad (\text{A.4}) \\ [-P_3\tau + \frac{\tau}{\phi}P_1 \pm 0] / [2P_4\tau] = 0 & \text{if } P_3\tau - \frac{\tau}{\phi}P_1 = 0 \quad (\text{A.5}) \end{array} \right.$$

There are 2 cases:

(i) $\lim_{B \rightarrow 0} N = \frac{-(P_3\tau - \frac{\tau}{\phi}P_1)}{P_4\tau}$ which is non-zero and biologically relevant if $P_3\tau - \frac{\tau}{\phi}P_1 > 0$

(since $P_4 < 0$), and $\lim_{B \rightarrow 0} \tau \frac{CN}{B} = \lim_{B \rightarrow 0} \frac{\tau(P_1 - \omega B)N}{-BP_2 + \tau N} = \frac{\tau P_1 N}{\tau N} = P_1$ (implying $\Delta < \frac{k_1}{k_1 + v_C}$). This is

the first form of the invasion criterion (4.1).

(ii) $\lim_{B \rightarrow 0} N = 0$ where we approximate N by a first order Taylor expansion around $B=0$,

giving $N = \left(\frac{\partial N}{\partial B} \right)_{B=0} \bullet B$ where $\left(\frac{\partial N}{\partial B} \right)_{B=0}$ should be positive, and find

$$\frac{\partial N}{\partial B} = \frac{1}{2P_4\tau} \left[P_2P_4 - \frac{\tau\omega}{\phi} \pm \frac{2\{P_3\tau - BP_2P_4 - \frac{\tau}{\phi}(P_1 - \omega B)\}(-P_2P_4 + \frac{\tau\omega}{\phi}) + 4P_2P_3P_4\tau}{2\sqrt{\{P_3\tau - BP_2P_4 - \frac{\tau}{\phi}(P_1 - \omega B)\}^2 + 4P_4\tau BP_2P_3}} \right] \text{ and}$$

$$\left(\frac{\partial N}{\partial B} \right)_{B=0} = \frac{1}{2P_4\tau} \left[P_2P_4 - \frac{\tau\omega}{\phi} \pm \frac{2\{P_3\tau - \frac{\tau}{\phi}P_1\}(-P_2P_4 + \frac{\tau\omega}{\phi}) + 4P_2P_3P_4\tau}{2\sqrt{\{P_3\tau - \frac{\tau}{\phi}P_1\}^2}} \right] \text{ where } P_3\tau - \frac{\tau}{\phi}P_1 \neq 0$$

In (A.1) the plus is used in \pm and $P_3\tau - \frac{\tau}{\phi}P_1 > 0$, where in (A.4) the minus is used in \pm and

$P_3\tau - \frac{\tau}{\phi}P_1 < 0$, both leading to

$$\left(\frac{\partial N}{\partial B}\right)_{B=0} = \frac{1}{2P_4\tau} \left[P_2P_4 - \frac{\tau\omega}{\phi} + \frac{2\{P_3\tau - \frac{\tau}{\phi}P_1\}(-P_2P_4 + \frac{\tau\omega}{\phi}) + 4P_2P_3P_4\tau}{2(P_3\tau - \frac{\tau}{\phi}P_1)} \right] = \frac{P_2P_3}{P_3\tau - \frac{\tau}{\phi}P_1}$$

Since $P_2 < 0$, $P_3 > 0$, and therefore $P_2P_3 < 0$, the value of $\left(\frac{\partial N}{\partial B}\right)_{B=0}$ is positive if $P_3\tau - \frac{\tau}{\phi}P_1 < 0$

(implying that $P_1 > 0$, thus $\Delta < \frac{k_1}{k_1 + v_C}$) giving

$$N = \frac{P_2P_3}{P_3\tau - \frac{\tau}{\phi}P_1} \bullet B \text{ which is substituted in}$$

$$\lim_{B \rightarrow 0} \tau \frac{CN}{B} = \lim_{B \rightarrow 0} \frac{\tau(P_1 - \omega B)N}{-BP_2 + \tau N} = \lim_{B \rightarrow 0} \frac{\tau(P_1 - \omega B) \frac{P_2P_3}{P_3\tau - \frac{\tau}{\phi}P_1} B}{-BP_2 + \tau \frac{P_2P_3}{P_3\tau - \frac{\tau}{\phi}P_1} B} = \lim_{B \rightarrow 0} \frac{\tau P_1 P_2 P_3 B}{-BP_2(P_3\tau - \frac{\tau}{\phi}P_1) + \tau P_2 P_3 B} = \phi P_3$$

This is the second form of the invasion criterion (4.1).

Chapter 4

A fungal growth model fitted to carbon limited dynamics of *Rhizoctonia solani*

Abstract

A simplified mean-field model of fungal growth (Lamour et al., 2001) was fitted to growth data of the soil-borne plant pathogen *Rhizoctonia solani*. Fungal growth and colonisation of discrete nutrient sites (1.5 mg agar droplets) in Petri plates was assessed under a dissecting microscope. Colonisation was faster for a high (0.016 mg) compared with low (0.0074 mg) carbon concentration of the substrate. The model predicts a lower asymptote for non-colonised substrate and this was estimated from the data by non-linear regression. A key composite parameter, the positive carbon balance per carbon unit of colonised substrate, was derived. The estimated value was lower at the high carbon concentration of the substrate. The carbon decomposition rate was estimated by least squares minimisation, after correction for a lag phase expected after robust handling of the inoculated fungus. The delay in subsequent fungal growth after inoculation was extended when there was less carbon available for physical recovery and physiological adaptation to the new environment. The simplified mean-field model with parameters estimated as described above produced a good fit to the data.

1. Introduction

In Chapter 2, we proposed a model of fungal growth arising from colonisation of a substrate source (Lamour et al., 2001). Carbon and nitrogen derived as a result of decomposition, are taken up into internal metabolic pools, and incorporated into fungal biomass. The model is based on a detailed specification of carbon and nitrogen dynamics, and leads to analysis of steady state values, and criteria for the fungus to invade and persist in a given environment. It is, however, difficult to relate the model to experimental data without further simplification. In this paper, we assume that only carbon is limiting fungal growth, and exclude nitrogen dynamics from the model. We follow a quasi-steady state approach in simplifying the model, as was done for the original fungal growth model (Chapter 3, Lamour et al., submitted). The resulting model is simple, and can be fitted to experimental data to obtain estimates of the biologically relevant parameters.

Growth of fungal hyphae is intrinsically a spatial process, whereby newly produced hyphae grow towards substrate patches to establish colonisation. Spatially explicit models can be developed to model this situation, but these require more advanced analytical and numerical techniques than the usual mean-field or mass-action approaches. The *mean-field* approach is the simplest and most widely used approximation in spatial problems in which it is assumed that the states of any two individual sites on a spatial frame are independent. In this paper we examine whether our simplified mean-field model can be fitted to spatial experimental data, as was done by others (e.g. Kleczkowski et al., 1996).

As a model system (Bailey et al., 2000) we observed fungal growth in Petri plates containing discrete substrate sites in the form of nutritionally defined agar droplets, and measured colonisation of these sites in time as a result of saprophytic growth of *Rhizoctonia solani* Kühn. This fungus is a ubiquitous facultative soil-borne plant pathogen, causing damping-off and root and stem diseases in a wide range of wild and cultivated plants (Sneh et al. 1996). As a hyphal tip of *R. solani* was robustly cut from the growing edge of a fresh colony before inoculation of one of the droplets, we anticipated delays in the subsequent growth from this tip to allow for physical recovery and physiological adaptation to the new environment. Specifically, we address the following questions: (1) Does the mean-field model provide a good fit to the spatial data? (2) How does colonisation of substrate proceed in relation to carbon concentration of the substrate? (3) Is any delay in subsequent growth from the hyphal tip related to carbon concentration of the substrate?

2. The Model

2.1 Model description

If it is assumed that nitrogen does not limit fungal growth, then nitrogen dynamics can be excluded from the original fungal growth model. The resulting model then describes the flow of carbon arising from colonisation of substrate (S), decomposition of colonised substrate (I), subsequent uptake of carbon (C*) into an internal carbon (C) pool, and incorporation into fungal biomass (B). Briefly (Tables 1 & 2), *supply* of substrate is a constant amount per time unit, σ , whereas *removal* proceeds at a constant rate, ρ . *Colonisation* of substrate is linearly related to new growth of biomass. Fungal *growth* is linearly proportional to $\frac{C}{B}$, i.e. a measure of the carbon concentration. With τ being the proportionality constant, fungal growth is then modelled as $\tau \frac{C}{B} B$, which simplifies to τC . Colonisation of substrate is also linearly related to substrate with a proportionality constant α , leading to the colonisation term $\alpha \tau CS$. *Decomposition* is assumed to proceed at a constant rate, β . *Loss* of carbon is at a rate v_c , and *uptake* and *leakage* of carbon by the fungus are at rates k_1 and k_2 , respectively. For growth of structural fungal biomass (B), carbon is utilised at an amount τC per time unit. *Maintenance* of fungal biomass is at a constant rate, ω . *Decomposition* of colonised substrate demands carbon from the metabolic carbon pool at an amount Δ per unit of colonised substrate, leading to a carbon loss term $\Delta \beta I$ per time unit. A constant *mortality* rate μ of biomass is assumed, giving

$$1 \text{ (a). } \frac{dS}{dt} = \sigma - \rho S - \alpha \tau CS \quad \text{[substrate]}$$

$$1 \text{ (b). } \frac{dI}{dt} = \alpha \tau CS - \beta I \quad \text{[colonised substrate]}$$

$$1 \text{ (c). } \frac{dC^*}{dt} = \beta I - v_c C^* - k_1 C^* + k_2 C \quad \text{[external carbon]}$$

$$1 \text{ (d). } \frac{dC}{dt} = k_1 C^* - k_2 C - \tau C - \omega B - \Delta \beta I \quad \text{[metabolic carbon pool]}$$

$$1 \text{ (e). } \frac{dB}{dt} = \tau C - \mu B \quad \text{[structural fungal biomass]}$$

$$\text{where the maintenance rate} = \begin{cases} \omega & \text{if } C > 0 \\ 0 & \text{if } C = 0 \end{cases}$$

$$\text{and the decomposition rate} = \begin{cases} \Delta & \text{if } C > 0 \\ 0 & \text{if } C = 0 \end{cases}$$

The maintenance and decomposition rate are set to zero for $C=0$ to avoid C going negative in equation 1 (d).

Table 1. Model variables with dimensions.

State		dimension [#]
S	substrate available to be colonised by the fungus	$N_{C\text{-units}}$
I	colonised substrate	$N_{C\text{-units}}$
C*	external carbon	$N_{C\text{-units}}$
C	carbon in the metabolic carbon pool	$N_{C\text{-units}}$
B	structural fungal biomass	$N_{C\text{-units}}$

[#]where N = number of

Table 2. Parameters with dimensions.

Parameter		dimension [#]
σ	substrate supply per time unit	$N_{C\text{-units}} T^{-1}$
ρ	substrate removal rate	T^{-1}
α	substrate colonisation probability per carbon unit biomass	$(N_{C\text{-units}(B)})^{-1}$
τ	fungal growth rate per C/B	see @
β	substrate decomposition rate	T^{-1}
v_{C^*}	C* loss rate	T^{-1}
k_1	C* uptake rate	T^{-1}
k_2	C leakage rate	T^{-1}
ω	maintenance rate of structural fungal biomass	T^{-1}
Δ	carbon units invested in decomposition per carbon unit substrate	$N_{C\text{-units}(C\text{-pool})}(N_{C\text{-units}(I)})^{-1}$
μ	mortality rate of structural fungal biomass	T^{-1}

[#]where N = number of; T = time unit (day)

@ where the dimension of τ is $T^{-1} \frac{N_{C\text{-units}(B)}}{N_{C\text{-units}(C\text{-pool})}}$

2.2 Quasi-steady state approximation

If the carbon dynamics of the model (i.e. equations 1c and 1d) are very fast compared to the dynamics of fungal biomass, substrate and colonised substrate, then after a fast transient carbon can be regarded as in equilibrium. Under this assumption the rates of change in C^* and C are approximately zero, resulting in quasi-steady state expressions for \hat{C}^* and \hat{C} .

$$2 \text{ (a). } \hat{C}^* = \frac{\beta I (k_2 + \tau - k_2 \Delta) - \omega B k_2}{v_{C^*} (k_2 + \tau) + \tau k_1}$$

$$2 \text{ (b). } \hat{C} = \frac{\beta I (k_1 - v_{C^*} \Delta - k_1 \Delta) - \omega B (k_1 + v_{C^*})}{v_{C^*} (k_2 + \tau) + \tau k_1}$$

In this paper we describe experiments in which substrate supply (σ) and removal (ρ) are zero, substrate supply is given by the initial condition S_0 , and $v_{C^*}=0$ as the experimental system is sterile. Incorporating these conditions produces a simpler quasi-steady state expression for \hat{C} , which can then be substituted in equations 1a, 1b, and 1e. This gives a simplified model where the parameters τ , k_1 , and k_2 cancel out.

$$3 \text{ (a). } \frac{dS}{dt} = -\alpha(1-\Delta)\beta I S + \alpha\omega B S$$

$$3 \text{ (b). } \frac{dI}{dt} = \alpha(1-\Delta)\beta I S - \alpha\omega B S - \beta I$$

$$3 \text{ (c). } \frac{dB}{dt} = (1-\Delta)\beta I - (\omega + \mu)B$$

2.3 Fungal invasion

In a system where the fungus is absent, introducing a small amount of fungal biomass may lead to fungal invasion, or to extinction. Since B is assumed to be small at the time of invasion, we consider the limit situation in which B is close to zero, as was done in the quasi-steady state approximation to the original growth model (Lamour et al., submitted). Experimentally it is very difficult to measure fungal biomass (B), and therefore we focus only on the equations for non-colonised substrate (S) and colonised substrate (I), giving

$$4 \text{ (a). } \frac{dS}{dt} = -\alpha(1-\Delta)\beta I S$$

$$4 \text{ (b). } \frac{dI}{dt} = \alpha(1-\Delta)\beta I S - \beta I$$

Consequently, the two parameters to consider are the composite parameter $\alpha(1-\Delta)$ and the decomposition rate β . Colonised substrate droplets decrease in carbon content as a result of decomposition, which makes I , in term of carbon units, very difficult to measure. Therefore, the two differential equations (4a and 4b) were fitted to the data for non-colonised substrate only.

2.4 Asymptotic behaviour of non-colonised substrate

Dividing equation (4b) by (4a) gives

$$5. \quad \frac{dl}{dS} = \frac{1}{\alpha(1-\Delta)S} - 1$$

and by integrating l with respect to S gives

$$6. \quad l = \frac{1}{\alpha(1-\Delta)} \ln S - S + A \text{ where } A \text{ is the constant of integration}$$

Suppose $S=S_0$ when $l=l_0$, then substituting in equation 6 gives

$$7. \quad l = S_0 + l_0 - S + \frac{1}{\alpha(1-\Delta)} \ln \frac{S}{S_0}$$

As time goes to infinity, S approaches a final value $S^* < S_0$ and l approaches zero due to decomposition. Substituting the final value S^* and the final zero value for l in equation (7) gives, after re-arranging

$$8. \quad S^* = S_0 + l_0 + \frac{1}{\alpha(1-\Delta)} \ln \frac{S^*}{S_0}$$

3. The Experiment

3.1 Materials and Methods

3.1.1 Pilot experiments

Agar droplets were positioned at pre-set distances on an empty Petri plate. In pilot experiments fungal growth from one agar droplet, inoculated with a single hyphal tip, was observed for three candidate fungal species (*R. solani*, *Trichoderma viride*, *Talaromyces flavus*). A second agar droplet was positioned at a given distance (e.g. 6 mm), and colonisation of this droplet from the first was observed. The experiment was repeated for a wide range of carbon concentrations of the agar medium (Table 3), and for many replicates. The hypothesis was that the second agar droplet would be colonised in a high proportion of replicates for a high carbon concentration of the first droplet, but less so for a low concentration, given that the pre-set distance was within an appropriate range. *T. viride* showed colonisation in about half of the replicates only, irrespective of the carbon concentration, and was not considered a suitable experimental system. *T. flavus* showed an inconsistent relationship between growth distance and carbon concentration. *R. solani* colonised the second agar droplet in all cases at a 6 mm distance, and this experiment was repeated at a distance of 10 mm. At this distance, however, hardly any colonisation was observed. Since *R. solani* successfully colonised the second agar droplet in all cases for a distance of 6 mm, this suggested expansive growth of the fungus in a population of agar

droplets for a wide range of carbon concentrations. Therefore, *R. solani* was used in the main experiment at a distance between droplets of 6 mm. This effectively ensured experiments in which colonised substrate increases, and carbon flows from non-colonised to colonised substrate to fungal biomass, i.e. invasion.

Table 3. Agar components (in g), where the sucrose concentration is indicated as high or low

component	high	low
NaNO ₃	2.0	2.0
KH ₂ PO ₄	1.0	1.0
MgSO ₄ .7H ₂ O	0.5	0.5
KCl	0.5	0.5
FeSO ₄ .7H ₂ O	0.01	0.01
Sucrose (C ₁₂ H ₂₂ O ₁₁)	27.0	12.0
Technical agar (Oxoid)	12.0	12.0
Reverse osmosis water	1000	1000

3.1.2 Main experiment

Small agar droplets measuring 3 mm in diameter and 1.5 mg in weight of a defined agar medium were distributed in a Petri plate (diameter 9 cm). The agar was derived from the defined medium Czapek Dox, having two different carbon contents (Table 3). A metal rod was dipped in liquid agar from a beaker on a hot plate (70 °C), and a droplet was allowed to roll off the rod into a Petri plate. The agar droplets, which were consistent in size, were positioned on a two-dimensional triangular lattice (Figure 1), where the distance between the droplets (from centre to centre) was 6 mm, leading to 127 droplets per Petri plate.

The central agar droplet of each plate was inoculated with a single hyphal tip, about 1 mm in length, removed from the growing edge of a 3-day old colony of *R. solani* (IMI 385768; AG 4) grown on water agar. Moist filter paper was placed into the lid of each Petri plate to avoid desiccation of the agar, and the plates were sealed and incubated in the dark at 23°C. There were 10 replicates, and two carbon concentrations containing 27.0 and 12.0 g sucrose per litre (Table 3) in a fully randomised design. Every 12 hours plates were assessed under a dissecting microscope, and agar droplets were scored as colonised or non-colonised. Scoring stopped when the fungal colony reached one edge of the Petri Plate, which was after 9.5 days at latest.

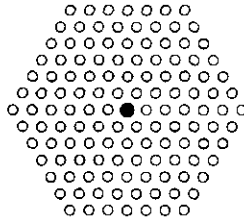


Figure 1. Positioning of the agar droplets on a two-dimensional triangular lattice. The central droplet was inoculated with a hyphal tip of *Rhizoctonia solani*.

3.1.3 Calculations

Non-colonised substrate was expressed in carbon units (Table 1 & 2) according to the formula: carbon content per droplet (g) = relative concentration of sucrose in agar medium x carbon fraction of sucrose x weight of one droplet. One litre of agar contained 27.0 g sucrose per 1043.01 g agar medium for the high concentration, and 12.0 g sucrose per 1028.01 g agar medium for the low concentration (Table 3). The carbon fraction of sucrose ($C_{12}H_{22}O_{11}$) equals 144/342. Since the weight of a non-colonised agar droplet is 1.5 mg, the carbon content per droplet equals 0.016 mg for the high agar concentration, and 0.0074 mg for the low agar concentration.

3.2 Results

3.2.1 Time plots

Time plots of the mean values of non-colonised substrate (S), expressed in carbon units, for the two sucrose concentrations (Figure 2) show a smooth decrease. At the low sucrose concentration (Figure 2b) there is clear evidence of levelling off. The standard errors were very low, although they increased towards the end of the experiment, as the number of replicates declines due to growth reaching one side of the Petri plate. Until day 7 the high sucrose concentration has 9 or 10 replicates, and a coefficient of variation ranging from close to zero to 0.03. Thereafter, the number of replicates declines to 6, 4, and 2 until there is only one at day 9 (Figure 2a). The low sucrose concentration has 10 replicates until day 8, giving a coefficient of variation ranging from close to zero to 0.05. After day 8, the number of replicates declines to 8, 6, and finally 3 (Figure 2b).

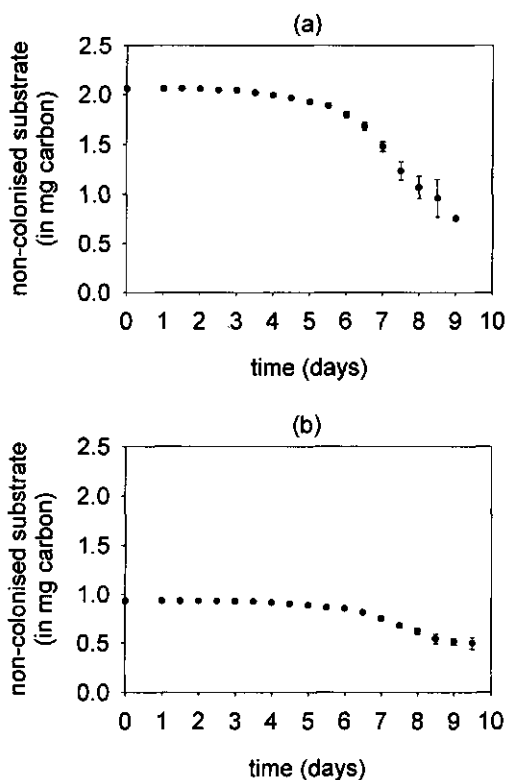


Figure 2. Time plots of the mean values of non-colonised substrate (S) for the high (2a) and the low (2b) sucrose concentration (Table 3) after inoculation with a hyphal tip of *Rhizoctonia solani* at $t=0$. Error bars represent standard errors.

3.2.2 Lower asymptotes

The data for the low sucrose concentration show a clear levelling off to a lower asymptote (Figure 2b). Also at the high sucrose concentration a lower asymptote would be expected if growth is adequately described by the model, although this is not readily apparent from the data. The lower asymptote (carbon units per Petri plate) was estimated by the following formula for a decreasing sigmoid curve.

$$9. \quad S = S_0 - \frac{a}{1 + e^{-\left(\frac{t-t_0}{b}\right)}} \quad \text{where } (S_0 - a) \text{ is the lower asymptote}$$

Non-linear regression gave an estimate for the lower asymptote of $0.48 (\pm 0.074)$ mg for the high sucrose concentration, and of $0.43 (\pm 0.016)$ mg for the low sucrose concentration (Figure 3). These asymptotic values were substituted in equation 8 together with the known values for S_0 and I_0 calculated from the carbon units for 126 and 1 droplets respectively (Figure 1). Equation 8 then gives an estimated value for $\alpha (1 - \Delta)$ of 0.91 for the high sucrose concentration, and 1.5 for the low sucrose concentration (see dimensions, Table 2). As discussed later, the composite parameter $\alpha (1 - \Delta)$ gives the positive carbon balance per carbon unit of colonised substrate.

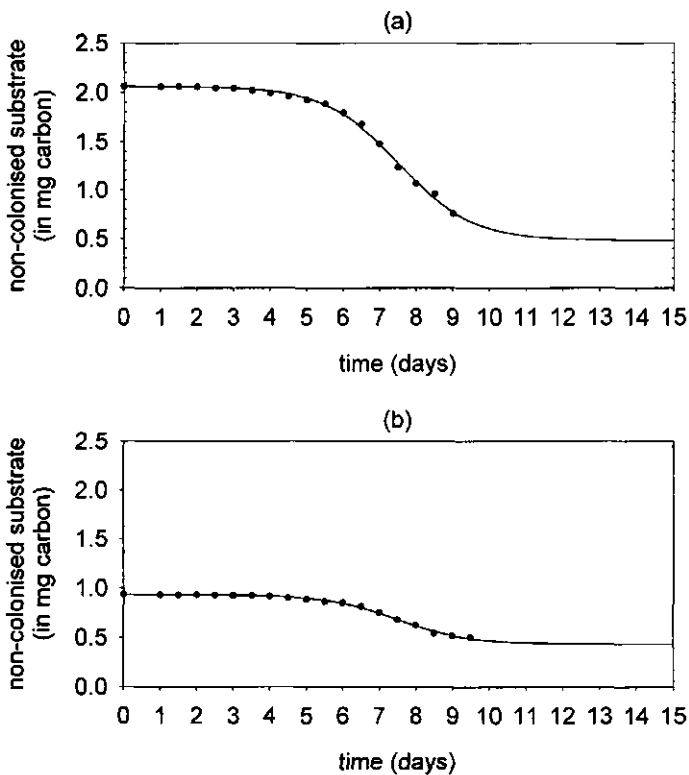


Figure 3. A sigmoid curve (equation 9) fitted to the mean of non-colonised substrate (S), showing the lower asymptote for the high (3a) and the low (3b) sucrose concentration (Table 3).

3.2.3 Fitting the model

Model (4) was fitted to the mean of the data for non-colonised substrate (S) by least squares minimisation using a Statistical Analysis System (SAS 6.12; SAS Institute Inc., Cary, USA). This was valid since the shape of the curve fitted to the mean data was not different from those fitted to each replicate separately (Kleczkowski, 1998). Since the value for the composite parameter $\alpha(1-\Delta)$ was derived from the estimated lower asymptote, only parameter β was estimated by directly fitting the model, both for the high and the low carbon concentration. The model produced a reasonable fit in both cases, which improved when corrected for a lag phase. A delay in growth would be expected due to effects caused by the experimental procedures as discussed earlier. The correction for the lag phase was done by excluding the first one or more data points. The best estimate for parameter β was then the one corresponding to the lag giving the lowest Residual Sum of Squares in the fitted model. This was 1.12 (± 0.015) per unit time for the high sucrose concentration, and 2.46 (± 0.051) per unit time for the low sucrose concentration (Table 4), where the time between assessments was 12 hours. Using this value for β in combination with the estimated value for $\alpha(1-\Delta)$ derived from the lower asymptote, model (4) produced a good fit to the data for both carbon concentrations (Figure 4).

Table 4. Estimated β and Residual Sum of Squares (RSS) for the complete data set of mean values for non-colonised substrate, and for data sets where the first one or more data points are excluded. The total number of data points is 18 for the high, and 19 for the low sucrose concentration. The lowest RSS is presented in bold.

high sucrose concentration			low sucrose concentration		
# data points excluded	estimated β	RSS	# data points excluded	estimated β	RSS
0	0.5715	0.3899	0	0.9495	0.0755
1	0.6693	0.2471	1	1.1141	0.0527
2	0.7301	0.1823	2	1.2161	0.0418
3	0.8015	0.1245	3	1.3356	0.0316
4	0.8864	0.0761	4	1.4775	0.0223
5	0.9890	0.0399	5	1.6482	0.0143
6	1.1152	0.0203	6	1.8572	0.0082
7	1.2738	0.0210	7	2.1189	0.0043
8	1.4791	0.0480	8	2.4556	0.0033
9	1.7542	0.1097	9	2.9049	0.0058
10	2.1417	0.2152	10	3.5345	0.0125

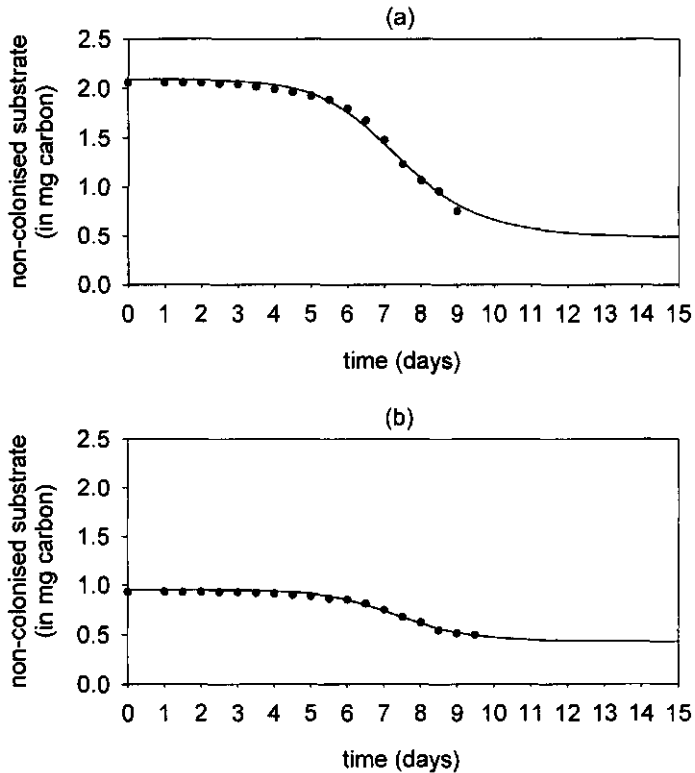


Figure 4. Model (4) fitted to the mean of non-colonised substrate (S) for the high (4a) and the low (4b) sucrose concentration (Table 3). In (4a) parameter $\alpha(1-\Delta)=0.91$ and $\beta=1.1152$, where in (4b) parameter $\alpha(1-\Delta)=1.5$ and $\beta=2.4556$ (Table 4).

4. Discussion

In *mean-field* models sites are assumed to be perfectly mixed and independent. This is different from a spatially explicit model where sites are correlated, for example between nearest-neighbours. A spatial aspect, either confined to a plane or extended into three dimensions, is implicitly included in model (4), since newly produced hyphae grow towards substrate patches to establish colonisation, which is intrinsically a spatial process. Although complicated spatial patterns in biochemical and biological processes may affect the time evolution, mean-field models have been widely used and successfully applied. For example in modelling biological control of fungal plant pathogens, in both deterministic (e.g.

Kleczkowski et al., 1996; Kleczkowski & Grenfell, 1999) and stochastic (e.g. Gibson et al., 1999) formulations.

Excluding the nitrogen dynamics from the original fungal growth model resulted in a simplified model that could be fitted to experimental data. A similar approach can be taken by excluding the carbon dynamics. In both approaches it is assumed that one of the nutrients is non-limiting, thereby focusing on the nutrient that is to some extent limiting.

The original fungal growth term $\tau \frac{CN}{B}$ then simplifies to τN , leading to equations for substrate, colonised substrate, fungal biomass, external nitrogen and a nitrogen pool. However, the equivalents to equations (4a) and (4b) describing nitrogen dynamics then include a composite parameter formed from three parameters of a complex form, which would make it more difficult to interpret any particular estimated value, compared to the simpler $\alpha (1 - \Delta)$.

Since all variables in the model are expressed in carbon units (Table 1), we focused on the data for the non-colonised droplets, for which the carbon content is known, and not on colonised droplets that gradually decrease in carbon content due to decomposition. The data for the low carbon concentration clearly levelled off to a lower asymptote (Figure 2b), which was also expected for the high concentration in the long term. The estimated value for the high carbon concentration was higher than for the low concentration, 0.48 and 0.43 mg respectively. These values correspond with 29 and 58 non-colonised droplets respectively.

The value for the lower asymptote could be used (equation 8) to derive the composite parameter $\alpha (1 - \Delta)$, giving for the high and the low sucrose concentration values of 0.91 and 1.5 respectively. As explained in detail in Lamour et al. (2001), it is biologically relevant that the number of carbon units *invested in* decomposition per carbon unit of substrate (Δ) should be less than the number of carbon units *resulting from* decomposition per carbon unit of substrate, which is 1 for a zero loss term v_C . Therefore, $(1 - \Delta)$ is the positive carbon balance per carbon unit of substrate. Multiplied by the colonisation probability per carbon unit of substrate, $\alpha (1 - \Delta)$ represents the positive carbon balance per carbon unit of colonised substrate. In the case of the higher sucrose concentration, the fungus can colonise more substrate and therefore $\alpha (1 - \Delta)$ is lower since it is expressed per carbon unit of colonised substrate.

Parameter β was then estimated by least squares minimisation, after correction for the lag phase (Table 4). The best estimates for β were 1.12 and 2.46 per unit time (i.e. 12 hours) for the high and the low sucrose concentration respectively, which is about a two-fold difference. The difference between I_0 at the high and low concentration is also about a two-fold difference. The net effect is that at $t=0$ absolute decomposition βI_0 is the same for both carbon concentrations. The relationship between decomposition rate and carbon availability is clearly an area for further study.

Correction for a lag phase involved exclusion of 6 and 8 data points for the high and the low carbon concentration respectively. Apparently, the hyphal tip needs more time when there is less carbon available for physical recovery and physiological adaptation to the new environment, after being cut from the growing edge of a fresh colony. For both carbon concentrations model (4) produced a good fit to the data when the estimates for $\alpha(1-\Delta)$ and β were used (Figure 4).

For each replicate, the fungus was able to reach the border of the Petri plate, although the rate of spread was higher for the high than for the low carbon concentration (Figure 2). A higher rate of spread results in less substrate that is not colonised. Clearly, carbon limitation is shown in Figure 2b. An increase in hyphal extension rate with increasing sugar concentration was also reported for *Botrytis cinerea* (Vercesi et al., 1997), and for the soil-borne fungal antagonists *Gliocladium roseum* and *Thielavia terricola* (Stack et al., 1987). As well as the nutrient content of the agar, the distance to grow to a new substrate source, before the fungus exhausts its endogenous nutrient supply, may also limit fungal growth. In this study, the given combinations of carbon concentration and distance between agar sites showed expansive growth initially, however, the first signs of a lower asymptote were soon apparent for the low carbon concentration (Figure 2b). Therefore, patches of finite size would be expected in the long term if the experimental system was larger, as was shown by Bailey et al. (2000).

The invasion criterion derived in a previous paper (Lamour et al., submitted) for a mean-field model predicts that there is a nutritional threshold below which the fungus will be unable to invade the system. In our experiments the procedures adopted were designed to ensure that fungal growth to non-colonised substrate would occur. This nutritional threshold differs from the percolation threshold of Bailey et al. (2000) which gives a critical threshold distance

between nutrient sites in a spatial model. Below the percolation threshold, growth leads to patches of finite size, whereas above this threshold, growth may result in a single patch of potentially infinite size. Further research will be needed to distinguish between a nutritional threshold in a mean-field model and a percolation threshold. It may then be possible to test the invasion criterion defined in Lamour et al. (submitted) which focuses on what happens in the short time immediately following the introduction of a fungus to a fungal-free system: fungal invasion or extinction?

5. Acknowledgements

We thank Prof. Dr. C.A. Gilligan for his hospitality and collaboration, and are grateful to Dr. D.J. Bailey and Dr. W. Otten for helpful advice (Cambridge University: Epidemiology and Modelling).

Section II

Chapter 5

Quantitative aspects of the epidemiology of *Armillaria* in the field

LAMOUR, A. & JEGER, M.J. 2000

In: *Armillaria* root rot: biology and control of honey fungus (R.T.V. Fox, ed.).

Andover, Hants: Intercept Ltd.

Abstract

Armillaria root rot is a serious disease in many forests and horticultural tree crops worldwide. Consequently, there is much interest in determining how different silvicultural practices influence disease incidence and options for avoiding or restricting the spread of disease. However, published information on the biology and ecology of *Armillaria* frequently is not available in a form that can directly assist decision-making. A model to forecast disease development and severity would be invaluable in forest management to facilitate choices between different silvicultural practices. It would also serve as a quantitative statement of hypotheses about root disease dynamics, behaviour, and impact. Serious data gaps can be identified and thus research needs can be defined and prioritised. Studies are reviewed in which the number and dry weight of *Armillaria* rhizomorphs are determined and the distributions of rhizomorphs, both vertically and horizontally, are quantified. Studies on disease progress, both temporal and spatial, in permanent plots are also reviewed and models developed to simulate disease progress are described, notably the Western Root Disease Model.

1. Introduction

Armillaria root rot is a cause of continuing concern in forest management. Even-aged plantations and silvicultural measures such as soil cultivation favour infection and spread of the disease. Consequently, there is considerable interest in knowing how silvicultural practices influence quantitatively disease incidence and how to avoid or restrict spread of the disease. The wealth of information available on the biology and ecology of *Armillaria* and on root rot disease is frequently not in a form that can directly assist decision making by forest managers. Besides, a cost-benefit analysis of control options is often lacking (Pawsey and Rahman, 1976). *Armillaria* species can be both plant pathogenic and saprotrophic and have a wide host range (Termorshuizen, 2000). Colonisation of substrate provides the energy for production of rhizomorphs to explore the soil for new substrates, often giving rise to an extensive network by means of branching and anastomosis. Various studies have focussed on *Armillaria* rhizomorphs, which are the major means of spread in the temperate regions. Infection spreads from plant to plant when roots encounter rhizomorphs growing from stump roots or when crop roots directly contact infected roots.

Quantification of disease processes can be made with respect to the pathogen and the disease, or ideally both. Quantitative data should then be placed in an appropriate framework so that the consequences for management can be determined. We summarise here what biological data have been quantified, what techniques have been used, and how they have been integrated in predictive models of disease progress. Data on weight and distribution of rhizomorphs in soil are presented (Table 1). Concepts of fractal geometry (Mandelbrot, 1982) have been used to describe branching patterns and have been applied to a variety of organisms ranging from microorganisms to plant roots (for example Eghball et al., 1993; Mihail et al., 1994). For quantification of *Armillaria* the fractal dimension is a measure of branching density (Mihail et al., 1995). Studies on disease incidence, both temporal and spatial, in permanent long-term forest plots are presented (Table 2). A predictive model to forecast disease incidence may prove invaluable in forest management planning to facilitate choices between different silvicultural practices. Such a model can also serve as a quantitative statement of hypotheses about root disease dynamics, behaviour, and impact and can aid scientists in identifying serious data gaps and thus help to define and prioritise research needs. A specific example concerns the Western Root Disease Model (Stage et al., 1990).

Table 1. Summary of literature references on the rhizomorph distribution of various *Armillaria* species. Data are from the field, unless indicated.

reference	species
Ono 1965	<i>Armillaria</i> sp..
Redfern 1973	<i>A. mellea</i> (lab experiment in soil)
Morrison 1976	<i>A. mellea</i>
Singh 1981	<i>A. mellea</i>
Stanosz & Patton 1991	<i>Armillaria</i> sp.
Rishbeth 1972	<i>A. mellea</i>
Twery et al. 1990	<i>Armillaria</i> spp.
Mihail et al. 1995	<i>A. gallica</i> , <i>A. ostoyae</i> (lab experiment on agar)
Mihail & Bruhn 1995	<i>A. gallica</i> , <i>A. mellea</i> (lab experiment on agar)
Termorshuizen et al. 1998	<i>A. ostoyae</i>

Table 2. Summary of literature references on fungal species causing root and butt rot disease in the field.

reference	species
Marsh 1951	<i>A. mellea</i>
Vollbrecht & Agestam 1995	<i>Armillaria</i> spp., <i>Heterobasidion annosum</i>
Vollbrecht & Jørgensen 1995	<i>Armillaria</i> spp., <i>Heterobasidion annosum</i>
Williams & Leaphart 1978	<i>A. mellea</i> , <i>Phellinus weirii</i>
Williams & Marsden 1982	<i>A. mellea</i> , <i>Phellinus weirii</i>
Lundquist 1993	<i>Armillaria</i> sp.
van der Kamp 1995	<i>A. ostoyae</i>
Klein-Gebbinck et al. 1990	<i>A. ostoyae</i>
Bruhn et al. 1996	<i>A. ostoyae</i>
Hughes & Madden 1998	<i>A. ostoyae</i>
Chadoeuf et al. 1993	<i>Rigidoporus lignosus</i> , <i>Phellinus noxius</i>
Wiensczyk et al. 1997	<i>A. ostoyae</i>
Stage et al. 1990	<i>Armillaria</i> spp., <i>Phellinus weirii</i>

2. Distribution of *Armillaria* rhizomorphs

In temperate forests rhizomorphs provide a major means of spread and subsequent infection of many tree species by most *Armillaria* species (Morrison, 1976). In general, rhizomorphs are produced most abundantly from wood that was colonised years previously. Studies indicate that the vertical distribution of *Armillaria* rhizomorphs is restricted to a particular part of the soil layer. The pattern of spread from a food base is usually radial (Ono, 1970) and, as a result of branching and anastomosis of individual rhizomorphs, a network is formed (Redfern, 1973). Clearly, on an infested site the chances of contact between rhizomorph growing tips and a root are related to the number of tips present in a unit volume of soil at any given time.

2.1 Vertical distribution

In Japan, Ono (1965) found more rhizomorphs in the upper 0-10 cm of soil than at 10-20 cm soil depth. Redfern (1973) reported that at four sites in East Anglia the distribution of rhizomorphs in soil varied with depth, but the highest densities occurred at 2.5-20 cm soil depth, and they were only rarely found below 30 cm. Morrison (1976) found that the distribution patterns of mature (black) rhizomorphs of *A. mellea* varied from site to site. On moist sites rhizomorphs were concentrated in the upper 10 cm of soil, whereas on dry sites they were found deeper in the soil profile. In contrast, distribution patterns of immature (red) rhizomorphs were independent of soil moisture conditions. It was suggested that a minimum soil moisture content determines the upper limit of rhizomorph growth. On the other hand, the lower limit of rhizomorph growth, 30-35 cm, seems to be controlled by oxygen or carbon dioxide concentrations. Rhizomorphs initiated on inoculum segments buried at 30 or 60 cm depth frequently grew toward the soil surface. Laboratory experiments showed that the direction of rhizomorph growth was along gradients of increasing oxygen and decreasing carbon dioxide concentrations (Morrison, 1976). Singh (1981) showed that the vertical distribution of rhizomorphs in Newfoundland forests depended not only on soil moisture conditions but also on the type of site (cutover or burned-cutover from a mixed softwood stand, and pastureland), and host species.

2.2 Horizontal distribution

Stanosz and Patton (1991) studied the capacity of aspen stumps following clear-cutting to support the production and growth of rhizomorphs over time by sampling rhizomorphs using ring-trench and core soil sampling methods. Weights of rhizomorphs of undetermined *Armillaria* sp. obtained using the two sampling methods around aspen stumps at different

intervals after harvest were highly correlated. The mean quantities obtained generally increased as a function of the interval after harvest. In laboratory experiments (Redfern, 1973) the number and dry weight of rhizomorphs produced from woody inocula containing *A. mellea* and buried in soil varied with soil type and incubation temperature. In the same soil fewer rhizomorphs were initiated at 15°C than at 25°C, but the total dry weight of rhizomorphs was approximately the same. The ability of *A. mellea* to produce rhizomorphs from stump samples was tested by a standard laboratory method by Rishbeth (1972). The amount produced from stumps of broad-leaved trees at first increased with the length of period after felling. Later the yield decreased, although some rhizomorphs were still produced after 40 years. The rate of decay varies between tree species and between individuals within a species, so that in a given area food bases are available for *A. mellea* over a long period. Wood from stems or roots of broad-leaved trees generally provides a better substrate for rhizomorph production than similar material from pines. Rishbeth (1972) suggests that other fungi compete more effectively with *A. mellea* in pine stumps than in stumps of broad-leaved trees, although clear proof of this does not exist in the literature. Twery et al. (1990) quantified the abundance and distribution of rhizomorphs of *Armillaria* spp. in the soil in undisturbed stands and in stands defoliated 1 and 5 years previously by insects. Trees weakened by biotic stress are often colonised and killed by *Armillaria* and other secondary pathogens. Rhizomorph distribution within the 0.04 ha study plots was uniform in the undisturbed stands, but was significantly greater near dead trees in the defoliated stands. Total rhizomorph abundance was greater on plots defoliated 5 years before sampling than on more recently defoliated plots, and it was least on undefoliated plots. Rhizomorph density near dead trees was highly correlated with overall rhizomorph density.

2.3 Quantification of horizontal distribution

Historically, fungal branching patterns have been described graphically or in qualitative terms. With the development of fractal geometry (Mandelbrot, 1982), a quantitative tool is available for the investigation of branching phenomena in a systematic fashion. For any object showing self-similarity at different scales (Pfeifer and Obert, 1989), the fractal dimension can be calculated. Most applications have been made to fungal branching patterns in vitro, not in the field. However, fractal geometry has been applied to *Armillaria* rhizomorphs in growth cultures (Mihail et al., 1995) and in the field (Termorshuizen et al., 1998). A model that can be adapted to quantify rhizomorph growth (Brown et al., 1997) has been described.

2.3.1 Description of fractal dimension

To conceptualise the applications of fractal geometry to fungal branching (Mihail et al., 1994), first consider a germinating propagule from which a single, unbranched hyphen extends across the surface of an agar medium. Geometrically, this system is represented as a line, which is a one-dimensional object (dimension=1) measured in units of length, e.g. mm. Next consider the case of a fungal thallus growing on a nutrient-rich agar medium such that the *entire* surface of the medium is completely covered. Geometrically, this system can be represented as a two-dimensional object (dimension=2), measured in units of area, e.g. mm². For both of these systems the dimension of the object is an integer. Finally, consider the more typical (and more interesting) case of a less densely branched fungal thallus growing on an agar surface. Geometrically, the branched thallus should have a dimension greater than 1.0 (that of a line), but smaller than 2.0 (that of a plane), for example 1.6. Mandelbrot (1982) proposed the term "fractal" to describe objects with "fractional" dimensions. The fractal dimension (D) describes the space-filling characteristics of an object. Thus, D would be close to 1.0 for a sparsely branched thallus, and close to 2.0 for a highly branched thallus.

2.3.2 Description of self-similarity

Fractal objects are by definition self-similar (Pfeifer and Obert, 1989). This means that if a small portion of a fractal object is expanded to the same size as the entire object, the expanded part is indistinguishable from the total object. An idealised fractal object is identically self-similar over an infinite range of scales. However, real-world fractal objects are self-similar only over a finite range of scales. For fungal thalli, the lower scaling limit is set by the hyphal diameter, and the upper scaling limit may be no greater than the largest diameter of the thallus, which increases as the thallus grows (Obert et al., 1990). Also, real-world fractal objects are self-similar only in the statistical sense that the objects have the same branching density within a defined range of scales.

2.3.3 Calculation of fractal dimension

Evaluation of the fractal dimension using a box-counting method can be carried out as follows. The mycelium is covered with a grid of cells (boxes) of side length ϵ and the number of boxes, $N_{\text{box}}(\epsilon)$ intersected by the mycelium is counted. $N_{\text{box}}(\epsilon)$ is then calculated over a range of different side lengths ϵ . The mycelium has a well-defined fractal dimension if $\log\{N_{\text{box}}(\epsilon)\} = |D| \log\{\epsilon\} + C$, where C is a proportionality constant. In the case where N_{box} is plotted versus ϵ on logarithmic scales and a linear relationship is apparent, then the

absolute value of the slope of the regression line represents the fractal dimension D . There are many examples of successful applications of this procedure (for example Mihail et al., 1994). Rather than counting how many boxes are intersected by the mycelium, the mycelial mass contained within a given radius r (originating from the centre of the colony), $M(r)$, can be calculated over a range of different radii (Ritz and Crawford, 1990). The mathematical representation is then $\log\{M(r)\} = D \log\{r\} + C$. Instead of mass, area of mycelium can also be used (Bolton and Boddy, 1993), where for example the mycelial area is calculated from photographs using image analysis (Bolton et al., 1991).

2.3.4 Application of fractal geometry to *Armillaria*

Fractal dimension (D) is a useful descriptor of foraging pattern, described as a balance between exploratory and exploitative growth strategies (Rayner, 1991), as it provides a quantitative summary of two-dimensional space utilisation. Although rhizomorph systems occur in a three-dimensional soil matrix, the depth dimension is small in comparison with the two-dimensional area (Morrison, 1976; Rishbeth, 1978). Thus, the reduction of rhizomorph branching from three to two dimensions is quite appropriate. Within a specified environment, D is highly consistent for multiple thalli representing a genet, which implies a strong degree of genetic control over rhizomorph branching pattern (Mihail et al., 1995). In these studies, D for rhizomorph systems ranged from 1.4 to 1.9, depending on the genet and species examined (Mihail et al., 1995; Mihail and Bruhn, 1995). Indeed, it was possible to distinguish rhizomorph branching patterns of *A. gallica* and *A. mellea* based solely on the magnitude of D (*A. gallica*, $D=1.57$; *A. mellea*, $D=1.68$; $P<0.05$) (Mihail and Bruhn, 1995). Further, D was temporally constant for rhizomorph systems, which is consistent with their foraging function. Although consistent in a specified environment, D is, however, sensitive to varying environmental conditions.

In tree plantations heavily affected by *Armillaria* root rot, dense rhizomorph networks of *A. lutea* were mapped over an area of 25 m² and described quantitatively (Chapter 6; Termorshuizen et al., 1998). Basic characteristics of the networks were: rhizomorph length, number of branches, number of cases in which rhizomorphs crossed each other both with and without forming connections, and number of rhizomorph cycles. The cycles varied in size from very small (lengths 1-5 cm) to fairly large (lengths up to 800 cm). The fractal dimensions of the networks (D) were 1.30 and 1.38. Quantitative description of branching density using the fractal dimension might become a novel supplement to the morphological criteria traditionally used in fungal taxonomy.

2.3.5 Rhizomorph growth model

There are no examples of mathematical models specifically designed to describe rhizomorph growth, although Brown et al. (1997) presented a step towards a generic framework for modelling root-architecture and the spatial structure of associated microbial ecosystems. This framework can be adapted for other root system features, such as rhizomorph interactions with root systems. A simulation programme produces and manipulates computer representations of a plant root-microbial ecosystem. The root system is described by a set of nodes. A node records a position in three-dimensional space and may represent the origin of another root, a bend, or some change in the root's microbial status. Disease lesions, closely associated microbial populations such as mycorrhizal fungi, and free soil microbial populations may also be represented. A multi-dimensional matrix structure provides a useful conceptual framework for the numerous stochastic functions required by the model. Procedures for composing the node-based root map, and for simulating root growth and microbial interaction, are presented in terms of the matrix structure, which in conjunction with the necessary manipulations of the node lists represents the root system.

3. *Armillaria* disease distribution

To study *Armillaria* root rot, dead and decaying tree species have been mapped in various regions over long periods of time using ground surveys (Vollbrecht and Agestam, 1995; Vollbrecht and Jørgensen, 1995) and aerial photography (Williams and Leaphart, 1978; Lundquist, 1993). Studies in which the rate of temporal disease mortality increase was determined or the spatial distribution was evaluated are given below and models developed to simulate disease progress are described.

3.1 Distribution in time

Records of *A. mellea* infections were made in a blackcurrant plantation from 1932-1941 (Marsh, 1951). The progress of infection could reasonably be explained by assuming that the major factor influencing fungal spread from bush to bush was root contact, and that it could invade the root system of a blackcurrant sufficiently quickly to bring about death of the entire bush in the season of initial infection. Vollbrecht and Agestam (1995) presented an empirical model to forecast the incidence of butt rot caused by *Heterobasidion annosum* and *Armillaria* spp. at the stand level. The model is based on data from 152 permanent plots of pure Norway spruce plantations in southern Sweden, where the incidence of butt rot at stump height in thinned trees had been recorded after each thinning. According to simulations with the model, areas previously used as fields or for grazing were particularly susceptible to butt

rot, while old hardwood sites were less susceptible. Furthermore, the model predicted that the earlier, the harder or more often a stand was thinned, the faster will be development of the disease. Development of butt rot in permanent plots of pure Norway spruce had also been recorded in Denmark (Vollbrecht and Jørgensen, 1995). Regression analysis was carried out to predict incidence of butt rot using variables describing site, stand, and silvicultural treatments. The model predicted the fastest disease development in stands that had been planted on previous hardwood sites and in thinned stands. This result does not corroborate the data from the study in Sweden (Vollbrecht and Agestam, 1995), where Norway spruce on old hardwood sites exhibited the slowest disease development. As the epidemiology of the disease is complex, the many simplifications introduced in empirical models makes application to different geographical areas or soils dangerous.

It is useful to identify sites with a high probability of developing root disease centres, making it possible to allocate land usage or manage appropriately on a short-term basis. Perhaps more importantly, the development of a model will help determine factors that contribute to damage and provide specific long-range direction for alleviating or managing these factors. Williams and Leaphart (1978) reported a survey system employing aerial photography with follow-up ground evaluations of root disease centres, indicated by openings in the forest canopy. The most frequently identified root pathogens in the disease centres were *Phellinus weirii* and *A. mellea*. Williams and Marsden (1982) evaluated their data and correlated forest stand and site characteristics with occurrence of root disease centres, among which stand age, average stand diameter, timber type, soil type, aspect, habitat type, and elevation showed significant associations. A logistic regression model was used for predicting the probability of root disease centre occurrence as a function of stand conditions. For wet aspects, the highest probability was found on soils with lowest year-round moisture availability. The reverse was true for dry aspects. Increased slope was associated with increased probability of the development of a root disease centre. Root disease centre frequency was inversely related to elevation and positively related to occurrence of *Pseudotsuga menziesii* and *Abies grandis*. Maximum probability of root disease centre occurrence was at 60-100 years of stand age across all habitat types (Williams and Marsden, 1982). Lundquist (1993) also used aerial photo surveys together with roadside reconnaissance to characterise the frequency and size of canopy gaps caused by *Armillaria* root disease in stands of *Pinus spp.* in the eastern Transvaal, South Africa. Disease severity (proportion of stand area with gaps) increased rapidly to age 3, remained nearly constant between ages 6-17, increased rapidly again between 17-28, and then decreased abruptly

between ages 28-40. Gap incidence (proportion of all stands with gaps) rapidly increased to age 10, after which it remained nearly constant. Host species present in previous stands influenced whether disease developed in current stands. Lundquist (1993) also presented empirical models describing the various phases of the disease progress curves.

3.2 Spatial distribution

The following three questions can be posed: (1) Does *Armillaria* infection occur in clusters, and if so, how large are these clusters? (2) Is *Armillaria* infection associated with old stumps? (3) Is the spatial distribution such that removal of all trees within a set distance of *Armillaria* killed or dying trees has a reasonable chance of preventing further spread? To answer these questions, van der Kamp (1995) developed an analytical procedure to distinguish between spatial clustering of *Armillaria* infection attributable to clustering of the host, and clustering caused by the spatial distribution of *Armillaria* inoculum. The location, species, and infection status of all trees and stumps in nine 40 by 40 m plots located in a single large area infested by *A. ostoyae* in British Columbia were recorded. The area was logged to a diameter limit and then left undisturbed. Spatial analysis using variance-to-mean ratios of number of trees per grid square for a series of grid sizes showed that stumps were randomly distributed, trees were strongly clustered, and infected trees occurred in small clusters (1-29 trees) that were themselves randomly distributed. Van der Kamp (1995) concluded that 30 years after the last major spatial disturbance by cutting, *Armillaria* occurs largely on the root systems of trees regenerated since logging. Removing all trees in close vicinity of an infected tree may isolate most of the viable *Armillaria* inoculum from the remainder of the stand.

To determine the inoculum sources, and methods and pattern of spread by *A. ostoyae* in lodgepole pine stands in West Central Alberta, juvenile lodgepole pine was excavated at three sites (Klein-Gebbinck et al., 1991). In all cases in which *A. ostoyae* had become established in the root collar or taproot, it was also able to colonise lateral roots. In cases in which only lateral roots were infected, subsequent colonisation was primarily distal to the point of infection. Rhizomorphs were associated with 89% of 121 infected roots, whereas only 19% of 70 roots with no associated rhizomorphs were infected. Stumps, roots, and debris from the previous stand were the major source of inoculum. There was no spatial relationship between stumps and symptomatic trees. Nearest neighbour analysis (Pielou, 1961) was used to determine whether there was a spatial association between stumps and symptomatic trees and to determine if pines near symptomatic trees were at a greater risk of developing symptoms than pines near asymptomatic trees. Nearest neighbour analysis

indicated that the likelihood of an individual tree developing symptoms was dependent on whether trees within 0.15 m distance were dead or dying but independent of the apparent health of trees at greater distances. Trees within 0.15 m distance of each other often had arisen from the same cone, therefore it is likely that the same source of inoculum or secondary spread of the fungus caused infection.

In general there have been few mathematical models developed to describe the spatial dynamics of diseases caused by soil-borne pathogens (Jeger, 1990). Bruhn et al. (1996) determined the temporal progress and spatial distribution of *Armillaria* disease mortality in black spruce plantations. Between 1982 and 1989, 22 black spruce seed plantations were established on cleared jack pine forest land in north-west Ontario. These plantations were located on suboptimal sites to hasten seed production. Mortality caused by *A. ostoyae* was observed in most of these plantations within three years of establishment. In four plantations where epidemics developed, temporal disease progress was best described by a monomolecular function rather than a Gompertz or logistic function. Monomolecular rates of disease increase were 0.0062-0.0346 per year. Applying these rates, they estimated that cumulative *Armillaria* root disease mortality would be 9-41% and 25-79% at 20 and 50 years after planting, respectively. *Armillaria* root disease mortality was spatially aggregated in all four plantations. The incidence of disease mortality was significantly higher for neighbouring trees in clusters adjacent to *Armillaria*-killed trees than expected under the null hypothesis of random spatial pattern. Hughes and Madden (1998) reanalysed the data of Bruhn et al. (1996) on the basis that the use of the binomial distribution was inappropriate. They considered that the β -binomial distribution model should be used to describe aggregated patterns of binary disease incidence data, rather than the binomial distribution. Characterising heterogeneity in the patterns of diseased or dead trees, and using this information in the formulation of management recommendations relating to forest health, are important developments in forest research.

Site characteristics seem to play an important role in the incidence and spread of *Armillaria* root disease both directly, through their effects on the fungus, and indirectly, through their effects on the host. Redfern and Filip (1991) discuss several environmental factors, including soil temperature, pH, moisture, organic matter content, and nutrient status, that may directly affect the growth of *Armillaria* rhizomorphs through the soil. The ecological aspects of these interactions are described by Termorshuizen (2000). Damage by *Armillaria* root disease is known to increase in severity when trees are stressed by either abiotic and biotic factors

(Wargo and Harrington, 1991), and certain site characteristics such as soil texture and moisture regime relate well to stress susceptibility. Tree vigour and the resistance of the tree to infection may be a function of site. Wiensczyk et al. (1997) found a significant relationship between several environmental variables and *A. ostoyae* infection levels. This could predict the potential impacts of *Armillaria* root disease and therefore be helpful in forest management.

Spatial models have been developed for tree root rot diseases other than *Armillaria*. Chadoeuf et al. (1993) presented a Markov model for spread of a root rot epidemic in Côte d'Ivoire from 1977 to 1984 due to *Rigidoporus lignosus* and *Phellinus noxius*, where these root pathogens spread along planting lines without interline spread. This reduced the study of the stand to that of a single line. The health status of the trees on a planting line was considered as a Markov process. Statistical analysis showed that the two pathogens represented two independently developing processes. The pathogenicity of the fungi did not decrease with time and a healthy tree, whatever its age, always remained very susceptible to attack. Control methods aiming at reducing initial infection, secondary infection, or both could be evaluated using the model.

3.3 A specific example: the Western Root Disease Model

The Western Root Disease Model (Stage et al., 1990) was developed to simulate the spread and impact of *Armillaria spp.* and *Phellinus weirii* in western coniferous forests in the US. The simulations are sensitive to information on initial disease conditions supplied to the model, including the number, size, and location of root disease centres. The model has limited capacity to simulate the spatial pattern of root disease centres. When the disease is scattered throughout the stand, it can be simulated as a single, large centre. The model can project up to 40 growth cycles of stand development, normally of 10 years each, and operate in stands up to 100 ha. It consists of three submodels, described by Shaw et al. (1991). A root disease submodel provides the status and spread of root disease, where alternative hypotheses concerning root disease dynamics can be explored. A second submodel structures the interactions between root diseases and other mortality agents (for example wind-throw or bark beetles). Finally, the stand-interface submodel links the stand-development model, to which the Western Root Disease Model is attached, with the two above-mentioned submodels.

Forest inventory requirements and model limitations were demonstrated by Marsden (1992a). Tests of the Western Root Disease Model have identified the user-supplied parameters for which the model is most sensitive (Marsden, 1992b). Various management options for dealing with *Armillaria*, including stump removal, were also examined (Marsden et al., 1993a). A refinement in the model is documented by Marsden et al. (1993b). Modelling the initial conditions of root disease in a stand is more accurate if combined with the use of generated random proportions for the degree of root system colonised by the disease. This is necessary to reflect the variation in the proportion of root systems colonised by the disease. A truncated-binomial distribution is used to generate the sequence of proportions for each sample tree. This technique may have application in the modelling of other root rot diseases.

4. Concluding remarks

Quantification of the epidemiology of *Armillaria* is essential for the understanding of the disease in the field and for determining optimal and cost-effective control interventions. Routine management procedures carried out in forest and horticultural plantations, for example thinning, cultivation, or control of other pests and diseases, may directly influence disease development and severity, often without affecting the amount of inoculum present. In practice, such management is rarely conducted specifically for disease control because such operations are costly and because reliable information on the expected economic gain is lacking (Pawsey & Rahman, 1976). Indeed such an analysis is barely possible without appropriate quantification of the biological processes involved in disease development. The procedures used to develop the Western Root Disease Model may serve as a prototype for modelling the dynamics and behaviour of *Armillaria* root disease in other forest ecosystems or plantations. Only when existing biological data are put in a mathematical or quantitative framework can they be helpful to forest management.

Chapter 6

Networks formed by rhizomorphs of *Armillaria lutea*

Abstract

The plant pathogenic fungus *Armillaria lutea* grows through soil as specialised hyphal strands, the rhizomorphs. Maps of rhizomorphs growing in soil over areas of 25 m² at a *Pinus nigra* and a *Picea abies* tree plantation were prepared. The total rhizomorph length measured was 109 and 152 m of which 84 and 48% was interconnected in a network exhibiting many anastomoses. In separate experiments incubation of rhizomorph segments under controlled and natural environmental conditions showed that rhizomorphs were almost completely decayed within 30 weeks. Hence it is unlikely that observations were made on dead but persistent remnants of the fungus. Anastomoses of rhizomorphs resulted in 63 and 50 cyclic paths, i.e. regions of the system that start and end at the same point, respectively. The high frequency of cyclic paths may enhance redistribution of nutrients, possibly expressing a strategy of persistence. Forcing air through water-immersed rhizomorphs and cross-section X-ray microscopy showed that rhizomorph segments fused by anastomosis had a continuity of air space, indicating the potential of redistribution of nutrients in various directions. Networks of fungal hyphae growing in pure culture have been described, and photographs of mycorrhizal fungi in soil observation boxes have been published. However, this is the first report to describe quantitatively an extensive fungal network in a natural soil.

1. INTRODUCTION

The clonal dispersal of plant pathogenic *Armillaria* species occurs in temperate climatic zones by growth through soil of specialised strands, called rhizomorphs. These shoestring-like strands are 1-3 mm in diameter with a reddish brown to black outer cortex layer (Cairney et al., 1988) usually in the upper 30 cm soil layer (Redfern, 1973). *Armillaria* assembles hyphae into rhizomorphs, and clones may persist over centuries (Smith et al., 1992) if there continues to be sufficient sources of nutrition for absorption (Rizzo et al., 1992) and translocation (Granlund et al., 1985; Cairney et al., 1988; Gray et al., 1996) under turgor pressure (Eamus & Jennings, 1984). Contact with rhizomorphs can result in tree-to-tree spread of the fungus, even when direct contact between diseased and healthy roots is not made. After contact with a suitable host, a rhizomorph becomes firmly attached to roots through hardening of the mucilaginous substance covering its growing tip. Single hyphae then emerge from the rhizomorph at the points of attachment. These penetrate beneath the bark scales by mechanical force and chemical secretions (Morrison et al., 1991). The white fan-shaped mats of mycelium extend the decay up infected tree's phloem and cambium, separating the wood from the bark, killing the host, and thus encouraging wind-throw (Whitney, 1997). After a rot has been established, the mycelium may persist for many years, provided there is a sufficiently large food base. The majority of rhizomorphs is produced during the terminal stages of decay but the extent of growth is species-dependent and influenced by habitat and environmental conditions (Fox, 2000). Studies on rhizomorph abundance, disease progress, and quantitative epidemiology have been reviewed (Lamour & Jeger, 2000).

Networks of fungal hyphae growing in pure culture have been described (Bolton & Boddy, 1993; Mihail et al., 1995), and photographs have been published of the mycorrhizal fungi *Suillus bovinus* and *Thelephora terrestris* in soil observation boxes (Bending & Read, 1995). However, fungal networks in a natural soil are difficult to observe, and therefore their ecological relevance has only rarely been investigated. This is the first report to describe quantitatively extensive fungal networks in a natural soil. We analyse *Armillaria* networks using characteristics related to long-range and short-range foraging, referring to an explorative and exploitative fungal growth strategy (Ritz & Crawford, 1990) respectively, and describe the ecological significance of branching and anastomoses for rhizomorph networks. In addition, we will use graph-theoretic concepts (Wilson, 1979) for a theoretical analysis of rhizomorph networks in Chapter 7.

2. MATERIALS AND METHODS

2.1 Mapping of rhizomorph networks

In two tree plantations, we observed complex networks of rhizomorphs of *Armillaria lutea* in soil, and prepared maps of rhizomorphs over an area of 25 m². In 1997 observations were made at a 40-year-old plantation of *Pinus nigra* ssp. *maritima*, referred to as site I. In 1999 observations were made at a plantation of *Picea abies* (site II). Both sites were situated in Wageningen, The Netherlands. In addition, small shrubs of *Prunus serotina*, occurred commonly at site I. Soil and surface litter was hand-removed up to approximately 25 cm depth and rhizomorphs were located in 1 m² grids and drawn on a two-dimensional map at scale 1:10. The depth was not recorded since this was small compared to the surface dimensions. Isolates of the rhizomorphs from both sites were kindly identified by A. Pérez-Sierra (Royal Horticultural Society, Wisley, UK) as *A. lutea* Gillet (= *A. gallica* Marxm. & Romagn. = *A. bulbosa* (Barla) Kile & Watl.) with PCR-RFLP of the IGS-region of the rDNA using species-specific primers (Chillali et al., 1997; Anderson & Stasovski, 1992). At both sites, various network characteristics were determined.

2.2 Observation of internal connectedness of rhizomorph anastomoses

Anastomoses of rhizomorphs were frequently observed. To investigate whether fused rhizomorph segments were internally connected or not, air was forced through water-immersed rhizomorphs at one end and the occurrence of air bubbles was observed distally beyond the point of fusion. In addition, two rhizomorphs fused by anastomosis were shortened to approximately 2 mm each. Non-destructive information from the internal structure was obtained by transmission X-ray microscopy (Skyscan-1072 desktop X-ray microtomograph). The combination of X-ray transmission technique with tomographical reconstruction gave three-dimensional information about the internal microstructure, constructed as a set of flat cross-sections (Anonymous, 2001). Photographs were taken at 21 heights (steps of 0.091 mm), starting above the point where the rhizomorph segments were fused, and ending below this point.

2.3 Decay time of dead rhizomorphs

A key question to ask in studying a natural *Armillaria* rhizomorph network is the period of time taken for dead rhizomorphs to decay to a non-observable level. Rhizomorphs were killed by gamma radiation (25 kGray), and 10-cm pieces were incubated in pots containing forest soil of high (pF=1.6) or low (pF=2.4) water potential. Prior to incubation, soil was air dried for one week and sieved through a sieve with 1.0 mm openings. The fresh weight of the rhizomorph

pieces per pot was recorded after washing them with water and drying between filter paper. To estimate their dry weight, the water content of additional fresh rhizomorph pieces was determined. The incubation temperatures were high (20 °C) or low (10 °C), roughly corresponding to soil temperature in summer or spring/autumn respectively. A soil temperature typical of winter was not used because of low microbial activity and decay rates. At four harvest times (4, 10, 16 and 30 weeks), the soil was sieved through a 1.0 mm sieve under tap water. The dry weight of the remaining rhizomorph pieces was determined after 24 hours at 105°C, and the rhizomorph state of decay was recorded (three replicates per treatment).

Similarly, in December 1997 two dead 10-cm rhizomorph pieces were put in nets (with openings of 1.1 mm) containing sieved forest soil. The nets were buried back into the forest, thus exposed to a fluctuating soil humidity and temperature. At the same four harvest times the soil was sieved, the dry weight of the remaining rhizomorph pieces was determined, and the state of decay was recorded (6 replicates).

3. RESULTS

3.1 Mapping of rhizomorph networks

Network characteristics for each site (Figure 1) included total length of the rhizomorph system, number of short (<5 cm) and long (>5 cm) protrusions, and number of occasions that rhizomorphs crossed each other (usually at different soil depths) without anastomosis (Table 1). Also, the percentage of rhizomorphs that comprised the largest connected component was calculated. At several places (25 and 21 for site I and II respectively) interconnected rhizomorphs (black lines in Figure 1) crossed the boundary of the mapped area, indicating that the rhizomorph system was of a much larger size. Cyclic paths, i.e. regions of the system that start and end at the same point, are the result of branching and subsequent anastomoses between rhizomorph segments. In many cases, larger cycles were embracing or closely connected to one or more smaller cycles (e.g. the larger cycle A connected to the smaller cycle B in Figure 1a). Also, many small cycles were produced at this finer scale (Figure 2a), giving rise to a complex network structure.

The total rhizomorph system was reduced to the cyclic paths of the largest connected component (Figure 1, red lines). The cycles divide the soil surface into regions, termed faces,

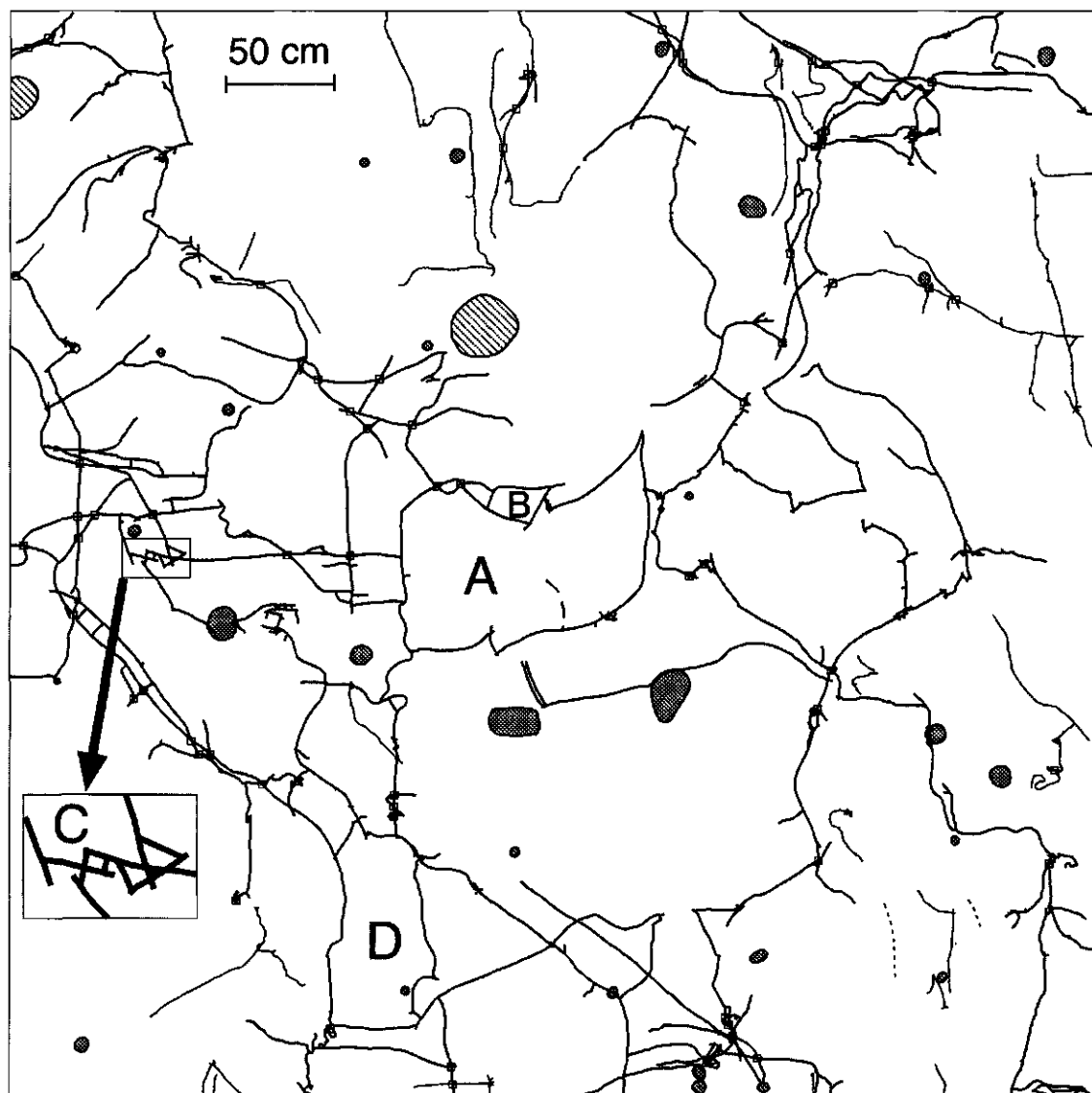


Figure 1a. Rhizomorph system at site I. Red lines: rhizomorphs contributing to the cyclic paths of the largest connected component. Black lines: rhizomorphs connected to the cyclic paths. Blue lines: other rhizomorphs. □: crossings of not-connected rhizomorphs. Green dotted circles: *Prunus serotina* shrubs. Green hatched circles: tree plantation stems. Letters refer to descriptions in the text. [For Figure 1b see page 87.]

not lying on the cycles. The number of cyclic paths is defined as the number of faces minus 1, thereby excluding the infinite (i.e. outside the cycles) face. In a number of cases several small cycles occurred closely together within the rhizomorph system (e.g. at C in Figure 1a) but in other cases cycles were larger and simpler in form (e.g. at D in Figure 1a). The systems showed self-similarity at scales from 2.5 cm up to 50 cm, and the fractal dimensions determined after Mandelbrot (1982) and Pfeifer & Obert (1989) were very similar (Table 1). At site I, the largest connected component was connected only twice to a dead stump of *P. serotina*. At site II, 73 connections to *Picea* stumps and roots were observed. Also, site II exhibited 253 rhizomorphs, not being part of the largest connected component, which were connected to tree roots and less than a few centimetres in length.

Table 1. Network characteristics of two sites (# = number of).

network characteristic	site I	site II
total rhizomorph length	109 m ($4.3 \pm 0.4 \text{ m m}^{-2}$)	152 m ($6.1 \pm 0.8 \text{ m m}^{-2}$)
# short (<5 cm) protrusions	417 ($16.7 \pm 2.2 \text{ m}^{-2}$)	491 ($19.6 \pm 4.0 \text{ m}^{-2}$)
# long (>5 cm) protrusions	127 ($5.1 \pm 0.5 \text{ m}^{-2}$)	268 ($10.7 \pm 3.5 \text{ m}^{-2}$)
# cases that rhizomorphs crossed each other without anastomosis	90 ($3.6 \pm 0.7 \text{ m}^{-2}$)	176 ($7.0 \pm 2.2 \text{ m}^{-2}$)
largest connected component	84 %	48 %
# cases that interconnected rhizomorphs left the mapped area	25	21
total length of the cyclic paths	43 m	37 m
# cyclic paths	63	50
fractal dimension	1.30	1.38
# connections of the largest connected component to stumps/roots	2	73

3.2 Observation of internal connectedness of rhizomorph anastomoses

Forcing air through one end of the rhizomorph segment showed air bubbles at the distal end beyond the point of fusion (Figure 2b), indicating a continuity of air space between the rhizomorphs. This was confirmed by X-ray cross-section analysis of two fused rhizomorph segments (Figure 2c). Of the 21 photographs taken at decreasing heights, the middle one demonstrates clearly the presence of a continuum between the two segments (Figure 2d).

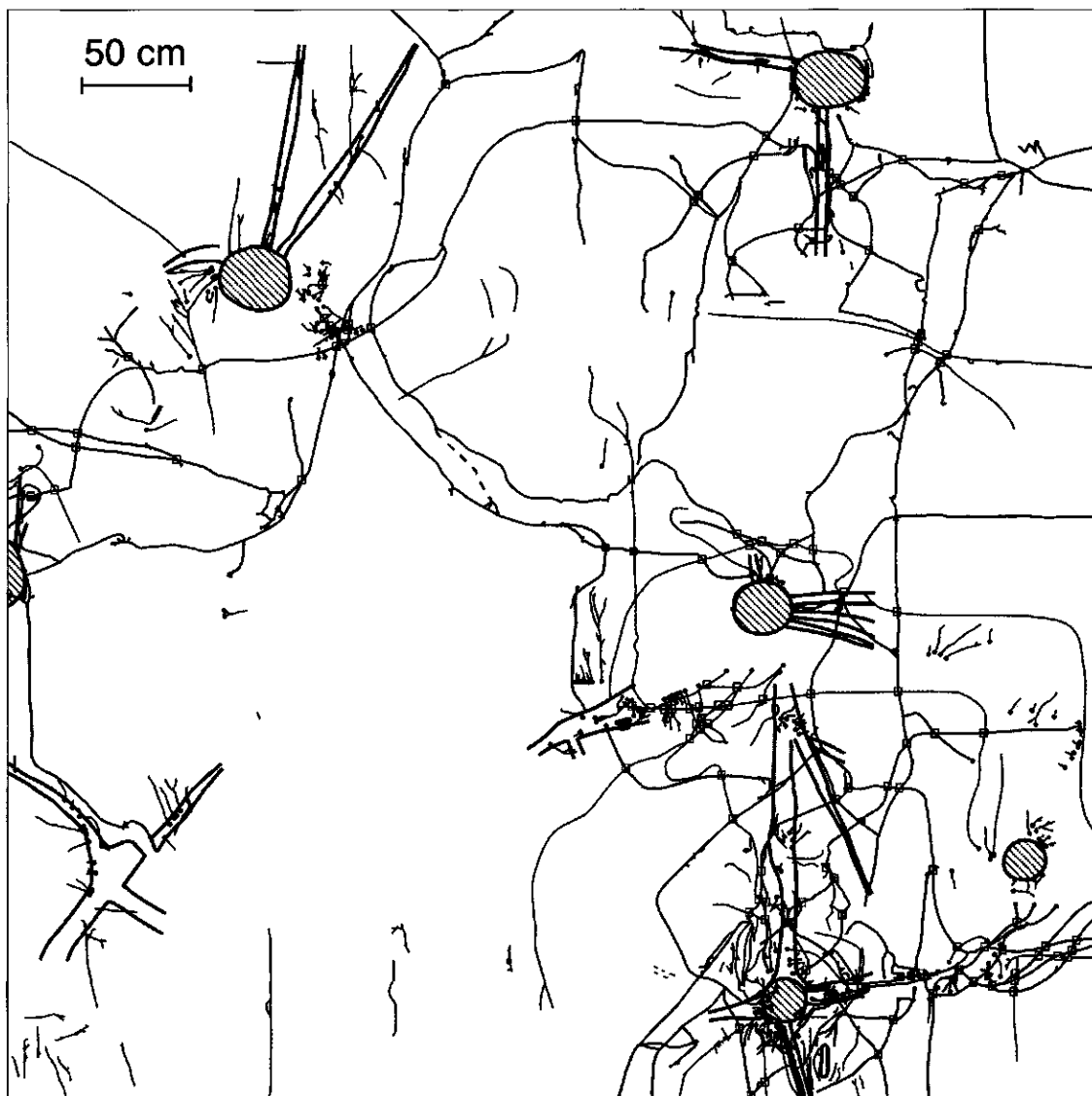
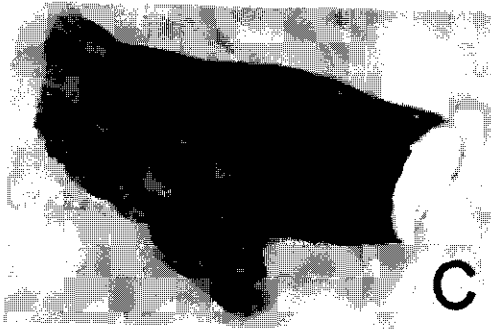
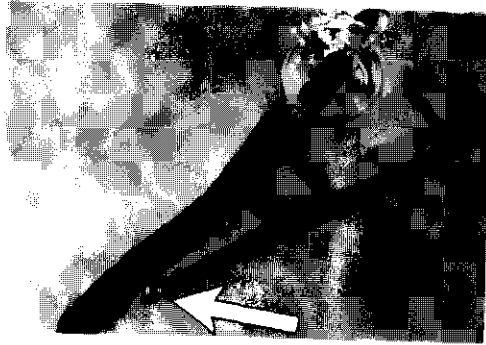
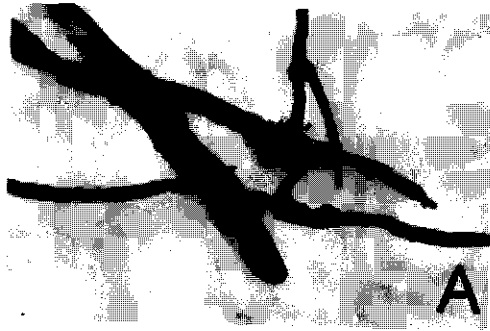


Figure 1b. Rhizomorph system at site II. Red lines: rhizomorphs contributing to the cyclic paths of the largest connected component. Black lines: rhizomorphs connected to the cyclic paths. Blue lines: other rhizomorphs. \square : crossings of not-connected rhizomorphs. Green hatched circles: tree plantation stems. Green lines: larger tree roots. Purple dots: points of attachment to trees or roots.



← **Figure 2.** Rhizomorph connections. a: Photograph of rhizomorphs of *Armillaria lutea* showing various connections. b: Demonstration of the presence of a continuum between connected rhizomorphs. Air was pressed through one end of the rhizomorph (above right) and air bubbles were observed at the low left end of the rhizomorph (arrow). c: Two fused rhizomorph segments (2 mm each). d: X-ray cross-section of the rhizomorph connection depicted in (b). The outer black line is the melanin sheath of the rhizomorphs. One rhizomorph is represented on the left side by the vertical tube, and the other perpendicularly crossing rhizomorph is represented by the right semi-circle.

3.3 Decay time of rhizomorphs

The experiments under controlled conditions and in the forest both showed that after 30 weeks many small pieces of brittle rhizomorphs could be observed, which were hollow or reduced to spiral melanin sheaths. These would not have been recorded in the network mapping. Up to 16 weeks rhizomorphs occasionally had broken down into smaller parts. However, they still maintained some physical integrity and would be recorded. High temperature and high soil water potential favoured decay of dead rhizomorphs. However, only the soil water potential effect on dry weight (Figure 3) was statistically significant ($P < 0.01$), and then only at 4 and 30 weeks.

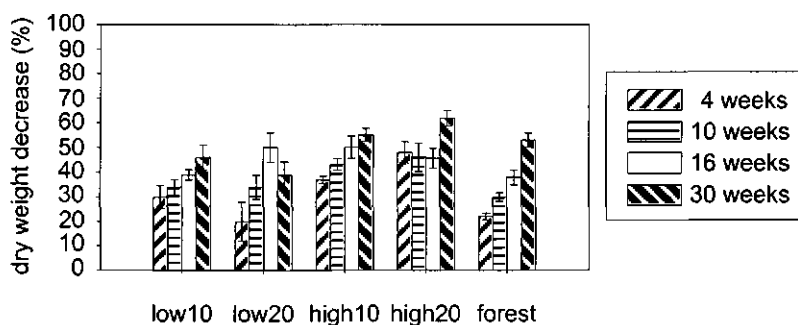


Figure 3. Dry weight decrease at four harvest times (4, 10, 16 and 30 weeks) for different treatments: Incubated under controlled conditions at a low ($pF=2.4$) and high ($pF=1.6$) soil water potential, and at 10 and 20 °C. Also incubated in forest soil.

4. DISCUSSION

We found extensive rhizomorph networks of *A. lutea* in a natural soil. Outgrowth of isolations for identification of the fungal species indicated that the majority of the rhizomorphs was viable. Experiments showed that the mapped rhizomorphs were either alive, or had died up to 30 weeks before the time of observation, indicating that we did not observe persistent dead remnants of the fungus.

Generally, two types of strategy of fungal growth are recognised: exploration and exploitation. In exploration, nutrition is limited, and the fungus reduces its investment in colonising its neighbourhood by refraining from branching, thus growing with the least energy possible to new areas where more nutrients may be available (Ritz & Crawford, 1990). This long-range foraging strategy is characterised by rapid growth, sparse branching and absence of anastomoses. In exploitative growth, or short-range foraging, nutrition is available, and the fungus quickly occupies the nutrient-rich substrate by branching structures exhibiting many anastomoses. In *Armillaria*, explorative growth is mainly accomplished through the formation of rhizomorphs, and exploitative growth through the formation of mycelial mats on substrate. Other features demonstrating the explorative character of rhizomorphs of *Armillaria* are their insulation from the environment and their relative low frequency of branching (Rayner et al., 1994). However, the ability of *Armillaria* to form networks does not fit neatly the exploration-exploitation model of fungal strategies. The frequency of branching (Figure 1), a characteristic of the networks, would point to an exploitative strategy, which is difficult to match with the clear explorative characters of rhizomorphs explained above. Therefore, we suggest that the rhizomorph network aims primarily at the strategy of persistence (Reaves et al., 1993). The high frequency of cyclic paths may limit the effects of unsuccessful exploration by enhancing the redistribution of nutrients and reducing the chance of a disconnected system when one rhizomorph breaks. Thus, the occurrence of cyclic paths may explain in part the high age of some clones of *Armillaria lutea* (Smith et al., 1992).

In intensively branched systems such as a mycelium growing in pure culture the opportunity for anastomosis is considerable due to the high probability of random encounters (Rayner et al., 1994). However, in the rhizomorph systems observed it seems unlikely that most cyclic paths have developed by random encounters. Perhaps the formation of anastomoses is the result of growth of rhizomorphs over living or dead roots, where they may have a higher chance of meeting other rhizomorphs. This would be true especially for very small cycles (e.g. at C in Figure 1) which may arise from rhizomorphic colonisation of a single piece of inoculum.

However, these roots were observed only in a few cases in our excavations. This may be due to differences in rates of decay and persistence of roots and rhizomorphs. In addition, the branching angle, being often rather perpendicular (Figure 1), will increase the probability of rhizomorph encounters. Alternatively, rhizomorphs that are not successful in attaining food substrate and that are not part of cyclic paths would be amputated relatively soon (Rayner, 1991).

The networks at site I and II showed some similarities, including the number of cyclic paths, the total length of the cyclic paths, and the fractal dimension, as well as some differences (Table 1). The total rhizomorph system at site II is 1.5 times longer compared to site I, but the largest connected component comprises at site II a two-fold lower fraction of the total rhizomorph system. We speculate that the rhizomorph system at site II is relatively young, showing many connections to stumps and tree roots. Also the largest connected component seems to be characterised by many connections to food sources. The rhizomorphs connecting the network to the sources are assumed to be amputated as the food source gets exhausted. Also, young rhizomorphs with only a few centimetres outgrowth from a nutritional source may have little chance to persist if they cannot fuse with a rhizomorph network, once the source is exhausted. Therefore, an older network, as is assumed to occur at site I, shows fewer connections to stumps, and the largest connected component is larger with more cyclic paths. Also, the number of cases that rhizomorphs cross without anastomosis is lower at site I. Thus, the rhizomorph system at site I has more characteristics related to long-range foraging, whereas the one at site II has more characteristics related to short-range foraging.

This is the first report to describe quantitatively an extensive fungal network in a natural soil. The biological properties of the rhizomorph system will be explored further by analysis of the cycles (Figure 1, red lines) using graph-theoretic concepts (Wilson, 1979) in Chapter 7. Analysis of the cyclic paths, the extent of connectivity, and a network representation in which weights, representing length, are assigned to the edges, may provide more insight into ecological significance of rhizomorph systems.

5. ACKNOWLEDGEMENTS

We thank A. Pérez-Sierra (Royal Horticultural Society, Wisley, UK) for identification of the *Armillaria* isolates.

Chapter 7

Quantification of rhizomorph networks

Abstract

The complete mapping of a rhizomorph network of *Armillaria lutea* in a tree plantation (Chapter 6, Figure 1a) has been restricted to the cyclic paths only. The resulting graph is then drawn in the plane such that unconnected rhizomorphs do not cross each other. The graph consists of 169 rhizomorphs, termed edges, and 107 rhizomorph nodes, termed vertices. The connectivity of the rhizomorph network has been explored by focusing on each bridge, i.e. an edge whose removal disconnects the graph into two components. Disruption of two of the bridges would disconnect a large part of the network (13 and 11%), but disruption of one of the other 7 bridges would disconnect only 1-4%, perhaps indicating the ecological relevance for *A. lutea* to maintain a persistent and connected rhizomorph network. Bridges that connect only a minor part of the rhizomorph system may indicate an explorative region of the network. Spanning trees have been defined, where the high number of possibilities indicates the low probability that disruption of a randomly chosen edge disconnects the network into two components. In addition, it has been shown that in only two instances a nutrient source was connected to the cycles, and that disruption of these two rhizomorphs would remove the whole network from the sources. A shortest path from some vertex to a nutrient source has been defined in terms of number of edges, and also in length (m). The edges in the plane drawing defined two-dimensional regions, termed faces, of which a few were very large. The length of the edges enclosing the faces showed that the fungus exhibited both exploitative and explorative foraging strategies, and we speculate about the underlying reasons. The introduction of graph-theoretic concepts to fungal growth may lead to an improved ecological understanding of fungal networks in general, when relevant biological interpretations can be drawn.

1. Introduction

The term *network* is used in its everyday meaning in expressions such as *telephone network* or *railway network*. In addition, the term *network* is used in a more specialised sense to mean a type of diagram, called a *graph*, to which the numerical values of some quantity are added. For example, we can represent part of a railway network in which the stations are represented by points or nodes, called *vertices*, and the connections between them by lines, called *edges* (Figure 1). If the distances or travelling times between the stations are indicated on the graph by inserting their numerical values beside the corresponding edges, the diagram becomes a network in the mathematical sense of the word. The numbers associated with each edge are called *weights* (Wilson, 1996), which can also be associated with vertices, for example as a presentation of the number of platforms at a station.

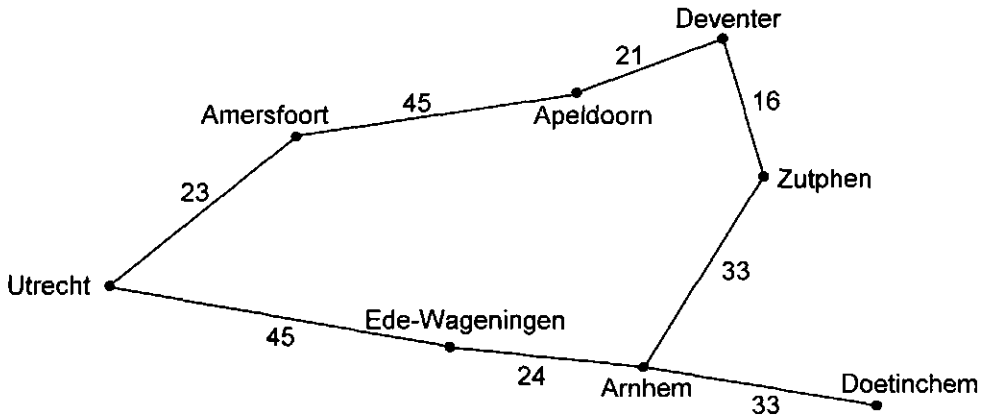


Figure 1. An example of a railway network in which the nodes represent railway stations of the indicated cities, where the numbers associated with each railway indicate the distance (km) between the railway stations.

For many soil-borne fungi the predominant strategy for dispersal is mycelial growth. Mycelial fungi frequently, if not always, form networks which can be easily observed at the growing edge of colonies on an agar medium (Bolton & Boddy, 1993). In addition, mycelial networks of ectomycorrhizal fungi formed between plants have been observed (e.g. Duddridge et al., 1988; Finlay & Read, 1986). A few fungi, notably *Armillaria* spp., assemble hyphae into macroscopic rhizomorphs (Fox, 2000). However, the ecological relevance of these networks has only rarely been investigated, which may be closely linked to the inherent problems of describing or quantifying a fungal network. In Chapter 6, two naturally occurring rhizomorph

networks of *Armillaria lutea* in soil were described. This Chapter focuses on the architecture of one of these rhizomorph networks (at site I) by making use of graph-theoretic concepts (Wilson, 1996; Balakrishkan, 1991; Harary, 1969), and examines the utility of these concepts in ecological interpretation of the networks.

Branching or fusion of rhizomorphs gives rise to a vertex. A rhizomorph connecting two vertices is termed an edge. The network at site I (Chapter 6) is restricted to the cyclic paths only, i.e. regions of the system that start and end at the same vertex. Transport of, for example, nutrients from one vertex to another is determined by the presence or absence of edges, rather than their length, since nutrients flow easily through the medulla of rhizomorphs (Granlund et al., 1984). If a rhizomorph breaks, transport of nutrients between two vertices is not prevented if these vertices are connected by more than one rhizomorph. In this sense a vertex resembles a distribution centre from which nutrients can follow different routes. The significance of vertices is that they bring flexibility to the rhizomorph system, since multiple edges result in more ways to transport nutrients.

Although the mathematical concepts of graph-theory have been widely used (e.g. Beezer et al., 2001; Wu et al., 2000; Zhang et al., 2000), there have been few examples of applications in biology. In this Chapter we explore the potential applications in fungal ecology by analysing the rhizomorph network in terms of graph-theory. Firstly, we outline some key graph-theoretic concepts, translate graph properties into algebraic properties, and deduce possible biological interpretations. Finally, we discuss the contribution of graph theory to an ecological understanding of rhizomorph networks.

2. The graph

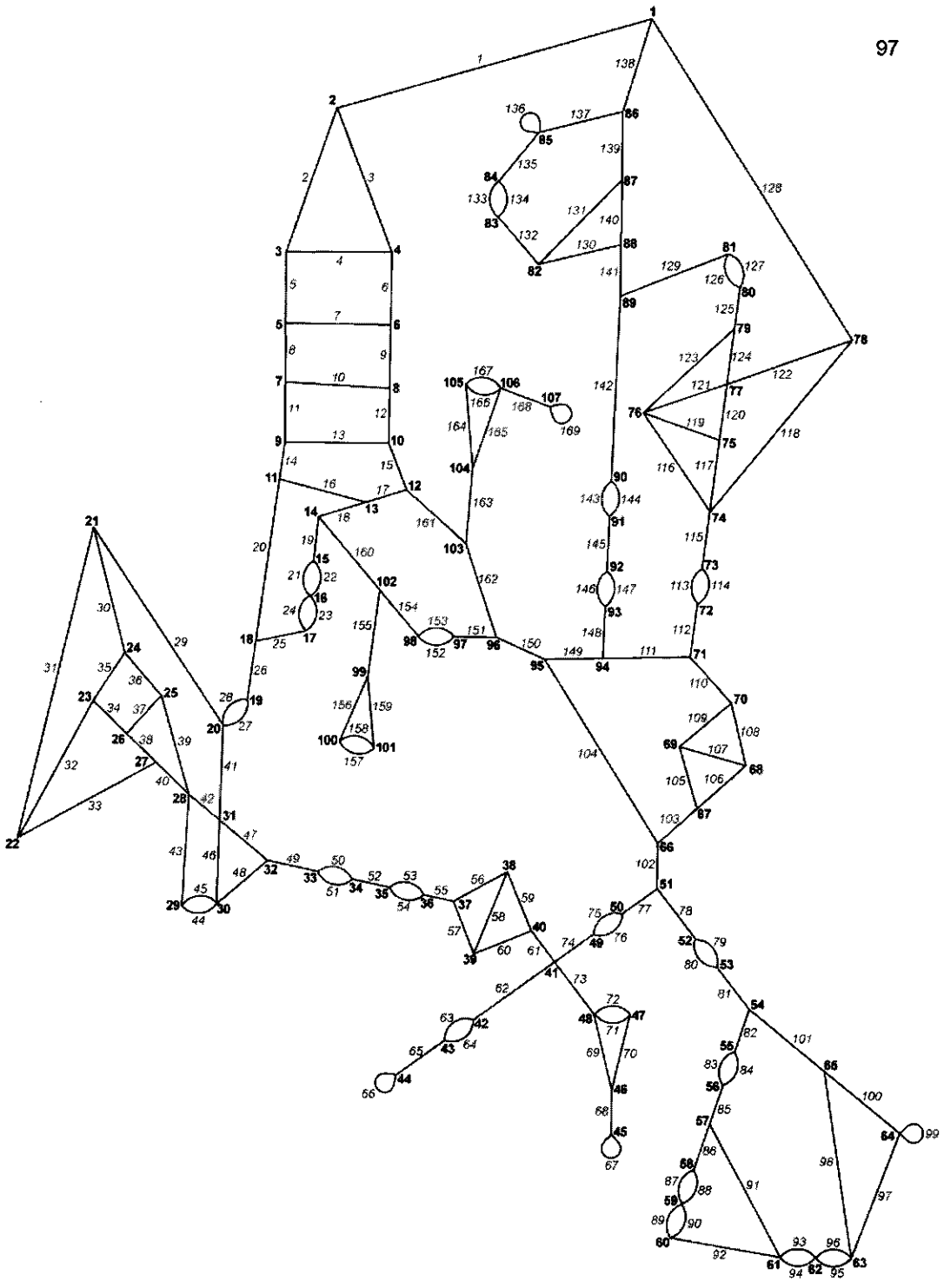
The complete mapping of the rhizomorph network obtained in 1997 (Chapter 6, site I in Figure 1a) is in this chapter termed the graph G_1 . We are going to consider the sequence $G_1 \rightarrow G_2 \rightarrow G_3 \rightarrow G_4$ for different graphs. Most probably the graph G_1 is a *directed graph* in which arrows or directions can be assigned to the edges. However, we do not know the directions of the flows (of for example nutrients), therefore we can only analyse the *underlying graph*. Flow of nutrients through rhizomorphs can be bi-directional (Granlund et al., 1985; Gray et al., 1996), however, at one time the flow through a given rhizomorph is one-directional. G_1 is a *disconnected* graph since it can be expressed as the union of connected graphs, each of which is a *component* of G_1 . In G_1 (Chapter 6, Figure 1a) the blue lines are not connected to the red or black lines. A graph is *connected* if there is a sequence

of edges between any given pair of vertices. The largest connected component of this disconnected graph forms 84% of the total graph in terms of rhizomorph length. This is only a minimum estimate since some of the apparently disconnected rhizomorphs may actually be connected outside the mapped area. We will now focus only on this largest connected component, and delete all edges that go beyond the mapped area. Thus, the new graph G_2 is restricted to the cycles of G_1 (Chapter 6, red lines in Figure 1a).

A more schematic way of depicting the graph G_2 is by manipulating the graph such that the number of crossing but unconnected rhizomorphs is minimised. A graph that can be completely drawn in the plane without crossings - that is, so that no two edges intersect geometrically except at a vertex to which both are incident - is called a *planar* graph, and its plane drawing is a *plane graph*. Indeed the graph G_2 appears to be planar, presented as G_3 (Figure 2), although examples exist of non-planar graphs (Figure 3). In a plane graph, irrelevant 'metrical' properties such as length and straightness of the rhizomorphs have been lost, resulting in an abstract topological presentation of a set of vertices and corresponding edges. The graphs G_2 and G_3 are isomorphic since there is a one-one correspondence between the vertices of G_2 and those of G_3 such that the number of edges joining any two vertices of G_2 is equal to the number of edges joining the corresponding vertices of G_3 .

3. The cycles

The graph G_3 (Figure 2) consists of 107 vertices ($n=107$) and 169 edges ($m=169$). The degree of a vertex, $d(v)$, is the number of edges incident with this vertex. In the rhizomorph network the minimum degree of any vertex equals 3. From G_3 it can be deduced that most of the 107 rhizomorph nodes have degree 3, but that 17 (16%) have degree 4 (vertex 16, 20, 28, 30, 31, 41, 48, 59, 61-64, 74, 76, 77, 85, and 106). The sum of all the vertex degrees is $17 \times 4 + (107-17) \times 3 = 338$, which for every graph is an even number equal to the number of edges. If it were the case that each vertex is of degree 3, then the graph would be *regular of degree 3* or *3-regular*. However, for a graph consisting of 107 vertices it is not possible to have nodes of degree 3 only, since $\sum d(v)$ is not an even number. The network structure that is closest to a 3-regular one has one node of degree 4, and the others of degree 3, giving 161 edges, which is 8 less than in G_3 . Degree-3 vertices likely have resulted from simple branching. Although degree-4 vertices may be the result of multiple branching at one position, our observations point to anastomosis of two crossing rhizomorphs.



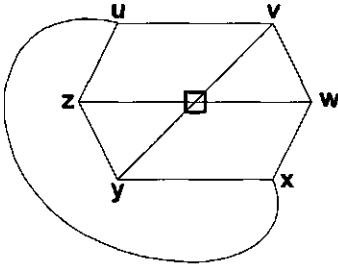


Figure 3. An arbitrary example of a non-planar graph consisting of 6 vertices (u, v, w, x, y, z) and 9 edges. \square : crossing of not-connected edges.

A *simple* graph is a graph without loops or multiple edges. A *loop* is an edge from a single vertex to itself. If more than one edge joins two vertices, these edges are referred to as *multiple edges*. The graph G_3 is not a simple graph, since it has 5 loops, for example at vertex 107, and 23 double edges, for example between vertices 83 and 84. While the function of a multiple edge is easy to understand, namely transport from one vertex to the other is secured in multiple ways, it is more difficult to interpret the functions of loops in a rhizomorph network.

4. Graph connectivity

The basic characteristic of a network is the fact that there are connections. Consequently a basic question is how connected the network is, or, more formally, how connected is a connected graph? One way to deal with this question is to calculate the number of edges that must be removed in order to disconnect the graph. The simplest way to obtain a disconnected graph is to remove one edge, if this is possible. Such an edge is called a *bridge* and occurs in the graph G_3 9 times, namely edges 62, 65, 68, 73, 78, 81, 155, 163, and 168. Bridges connecting two large parts of the network are quite important for the whole network. So, disruption of rhizomorph 78 would disconnect 13% of the rhizomorph system, based on number of vertices. For rhizomorph 81 this percentage is almost similar (11%), but disruption of one of the other 7 bridges would disconnect only 1-4% of the network, perhaps indicating the ecological relevance for *A. lutea* to maintain a persistent and connected rhizomorph network. Bridges that connect only a minor part of the rhizomorph system may indicate an explorative region of the network. Note that the number of bridges is a maximum estimate since parts of the rhizomorph network may be connected outside the observation

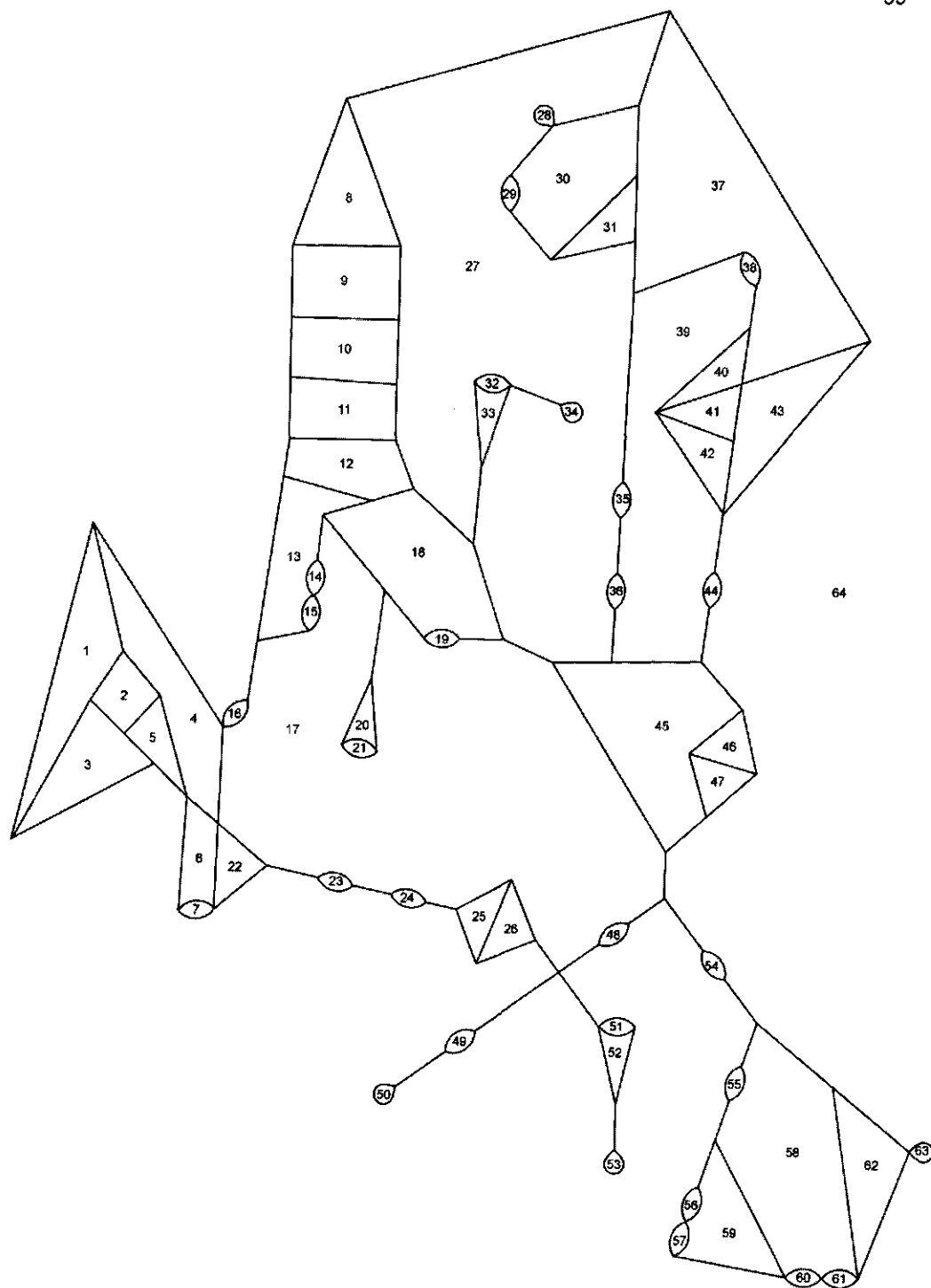


Figure 4. The number of faces of the graph G_3 (Figure 2) equals 64.

plot. A bridge is a special type of *cutset*, which is defined as a set of edges that all must be removed in order to obtain a disconnected graph. For example, the cutset consisting of edges 61 and 102 disconnects edges 62-101. If a cutset disconnects the graph, the network may be favoured if it is cut into two components of the same size, in terms of vertices, since small components with minor benefits of nutrient redistribution have little chance to persist. In G_3 the cutset consisting of edges 26, 150, 148 and 112 disconnects the graph into two components containing 52 and 55 vertices.

If G is a planar graph, then any plane drawing of G divides the set of points of the plane not lying on G into regions. These two-dimensional regions defined by the edges in a plane graph are called *faces*. The unbounded face is called the *infinite face*. Euler's formula (Wilson, 1996) states that for a connected graph $n-m+f=2$, where f is the number of faces. In G_3 the number of faces equals $m-n+2=169-107+2=64$ (Figure 4). The degree of a face, $d(F)$, is defined as the number of edges on the boundary of that face, so bridges are counted twice. The sum of the degrees of all faces, $\sum d(F)$, is equal to the sum of all the vertex degrees, $\sum d(v)$. A few faces have a very large degree, for example face 17 (Figure 4), but the median value equals 3 (Figure 5).

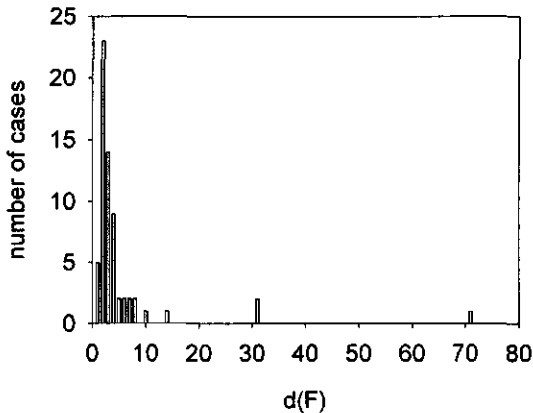


Figure 5. Frequency distribution of the degrees of faces, $d(F)$, occurring in the graph G_3 (Figure 2).

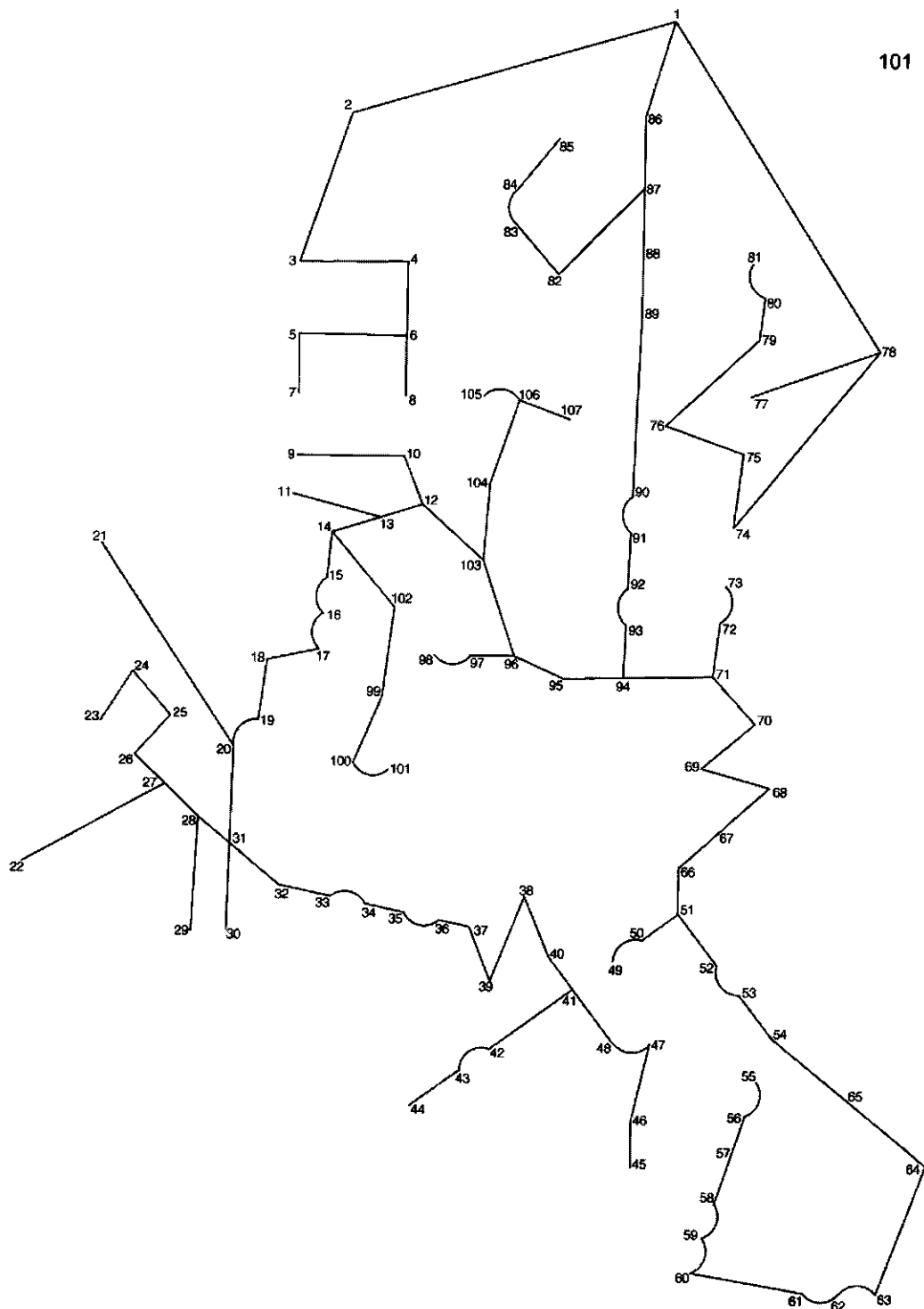


Figure 6. The graph G_4 is one of the spanning trees of G_3 (Figure 2), namely the one with minimum weight.

5. Spanning trees

Given any connected graph G , we can choose a cycle and remove any one of its edges, and the resulting graph remains connected. We repeat this procedure with one of the remaining cycles, continuing until there are no cycles left. The graph that remains is a tree that connects all the vertices of G , called a *spanning tree*. Following this procedure for the graph G_3 , 63 edges must be removed to obtain a spanning tree, namely 5 loops, in 23 occasions one of the double edges, and 35 other edges. The removed edges are called *chords*. One of the spanning trees of the graph G_3 is G_4 (Figure 6).

The *matrix-tree theorem* (Harary, 1969) can be used to calculate the number of spanning trees in any connected simple graph G . Let G have vertex set $\{v_1, \dots, v_n\}$, then we define matrix M to be the $n \times n$ matrix whose ii -th entry is the degree of vertex v_i , and whose ij -th entry equals -1 if v_i and v_j are adjacent, and 0 otherwise. The number of spanning trees of G is equal to the cofactor of any element of M . Firstly, we reduce G_3 to a simple graph by deleting the double edges and loops. Then we construct the resulting 107×107 matrix M as defined above (not shown). According to the matrix-tree theorem, the number of spanning trees equals 5.6×10^{21} . Since the graph G_3 has 23 double edges, the number of spanning trees in G_3 is 2^{23} times as high, giving 4.7×10^{28} possibilities. The fact that G_3 also has loops does not effect the amount of possibilities. Due to this high number of possible spanning trees, the probability is low that disruption of a randomly chosen edge disconnects the network into two components.

If G is an arbitrary graph with n vertices, m edges and k components, the procedure to obtain a spanning tree can be carried out on each component of G . The result is called a *spanning forest*. The total number of edges removed in this process is the *cycle rank* of G , denoted by $\gamma(G)$, where $\gamma(G) = m - n + k$. The cycle rank is also called *circuit rank*, or *cyclomatic number*, and equals the numbers of cycles. For a planar graph with only one component, the number of edges removed to obtain a spanning tree is one less than the number of faces, calculated by Euler's formula ($f = m - n + 2$). In the graph G_3 (Figure 2) we have only one component, giving $\gamma(G) = 169 - 107 + 1 = 63$. The *cutset rank* of G is defined to be the number of edges in a spanning forest, denoted by $\xi(G)$, where $\xi(G) = n - k$. In the graph G_3 we have $\xi(G) = 107 - 1 = 106$.

6. The graph related to nutrient sources

In the complete rhizomorph mapping (Chapter 6, Figure 1a) a rhizomorph was connected in only two instances to a root or stump, probably serving as a single nutrient source. The first

source (S_1) is connected to vertex 81 (by an unnumbered rhizomorph not being part of one of the cycles), the second source (S_2) is connected to edge 44 (also by an unnumbered rhizomorph). Thus, both nutrient sources are connected to the largest component of the rhizomorph network, but disruption of these two rhizomorphs is sufficient to remove the whole network from the sources. Vertex 62 is furthest away from both nutrient sources. The geographic distance measures 4.19 m from S_1 and 4.56 m from S_2 .

Assuming that all parts of the rhizomorph network need access to nutrients and that they mainly originate from sources S_1 and S_2 , the distance over which the nutrients and water have to be transported is relevant. In a connected graph, the *distance* $d(v_i, v_j)$ from vertex i to vertex j is the length of a *shortest path* from vertex i to vertex j . A *path* is a trail in which all the vertices are distinct (except, possibly, $v_0=v_{end}$). Here, length is not expressed in e.g. meters, but in number of edges traversed. To calculate the distance, we create the *adjacency matrix* A , which is for the graph G_3 , consisting of 107 vertices, a 107×107 matrix whose ij -th entry is the number of edges joining vertex i and vertex j . The number of walks of length P from vertex i to vertex j is the ij -th entry of the matrix A^P . In the cases of vertex 81, which is connected to source S_1 in the graph G_3 (Figure 2), and vertex 62, which is furthest away from both sources, the following holds:

$$A^P(81, 62)=0 \text{ for } P \leq 14$$

$$A^P(81, 62) \neq 0 \text{ for } P=15$$

Thus, the number of edges traversed in a shortest path from vertex 81 to vertex 62 equals 15. Since $A^{15}(81, 62)=16$, there are 16 possible shortest paths of length 15. These 16 possibilities arise from the fact that 4 times 2 vertices are connected by double edges, giving 2^4 possibilities. One possible shortest path is (vertex sequence): 81 → 89 → 90 → 91 → 92 → 93 → 94 → 95 → 66 → 51 → 52 → 53 → 54 → 65 → 63 → 62.

The length of each rhizomorph can also be measured, using the line intersection method (Newman, 1966; Marsh, 1971), and this number can be assigned to each edge (Figure 7). Such a graph is called a *weighted graph* or *network*, and the number assigned to each edge e is the *weight* of e , denoted by $w(e)$. Instead of finding the number of edges in a shortest path from vertex i to vertex j , the problem is to find a path from vertex i to vertex j with minimum total weight. A frequently used algorithm is the one from Dijkstra (1959), explained shortly in Appendix 1. In the cases of vertex 81 and vertex 62, the path with minimum total weight measures 7.29 m and is (edge sequence): 126 (or 127) → 125 → 124 → 120 → 117 → 115 → 114 → 112 → 110 → 109 → 105 → 103 → 102 → 78 → 80 → 81 → 101 → 98 → 96.

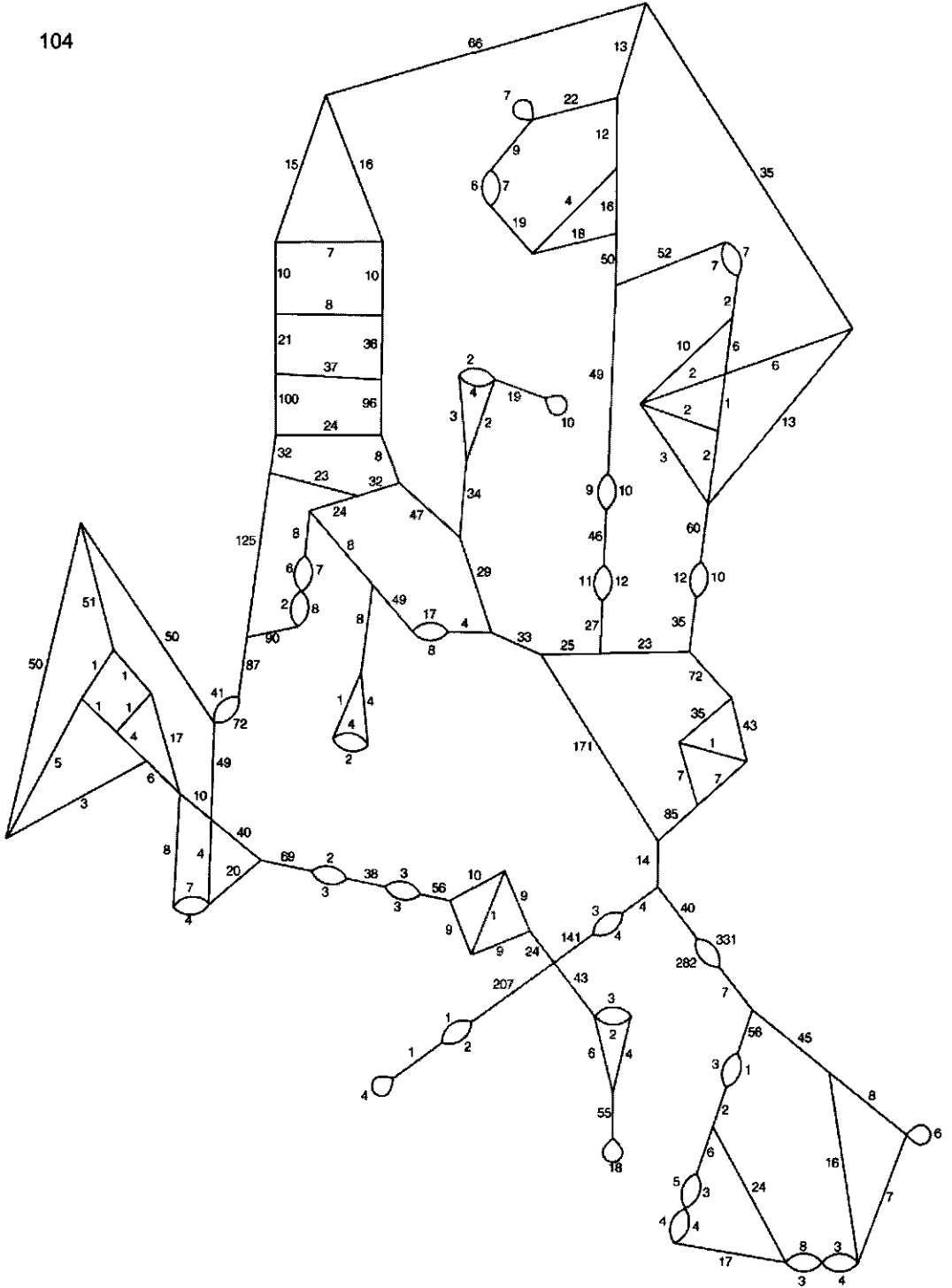


Figure 7. The length of each rhizomorph segment, rounded to the nearest integer (cm), is assigned to each edge of the graph G_3 (Figure 2).

7. Minimum spanning tree

To construct a spanning tree with minimum total weight among all spanning trees, the algorithm of Prim (1957) may be used, or the one of Kruskal (1956). The execution time of Prim's algorithm depends only on the number of vertices, but the time for Kruskal's algorithm increases as the number of edges is increased for a network with the same number of vertices. The efficiency of the algorithm depends in part on the network structure and the distribution of weights. We used Prim's algorithm where an arbitrary vertex is put into spanning tree T , and edges of minimum weight are added successively joining a vertex already in T to a vertex not in T . A worked simple problem is illustrated in Appendix 2. To apply Prim's algorithm to the graph G_3 (Figure 2), we firstly remove the loops (5), and thereafter one of the double edges (23 times), namely the one with highest weight. Prim's algorithm gives a minimal spanning tree (Figure 6) of 24.98 m, which is 58% of the total length of G_3 . The significance of the remaining 42% is the redistribution of nutrients.

8. Discussion

In this Chapter we have explored several graph-theoretic concepts in an attempt to interpret the ecological significance of a rhizomorph network of *A. lutea*. We focused on the cycles of the network, and analysed graph connectivity. To express how strongly parts of a graph are linked, *connectivity* and also *toughness* are needed (Van den Heuvel, 1993). A graph has high connectivity if we need to remove many edges in order that the remainder of the graph falls apart into separate pieces. A graph has high toughness means that we not only need to remove many edges in order to disconnect the graph, but also that the number of components obtained is small, relative to the number of edges removed. However, in this Chapter we focused on connectivity only, and did not use toughness in the analysis.

The rhizomorph network was mapped at only one point in time, and the mapping was analysed as a fixed topology network. However, in fact it is a continuously growing network, as are networks based on transportation systems, electrical distribution systems, and the Internet. Krapivsky et al. (2000) presented a model for the time evolution of the connectivity distribution of growing random networks. In these networks, a new vertex is added to an existing network at each time step, and a directed link to one of the earlier vertices is created. For example, in terms of citations, vertices may be interpreted as publications, and the directed link from one paper to another as a citation to the earlier publication. This is different from a rhizomorph network, where new edges are continuously produced and extended, and vertices arise from fusion of edges.

The formation of rhizomorph networks is likely to be a successful strategy of *Armillaria* to increase its persistence (Reaves et al., 1993; Chapter 6). In a relatively stable ecosystem as a forest, it may be advantageous not only to spread to new areas, but also to remain quiescent until weakened host material becomes available. In the case of *A. lutea*, which is a weak pathogen (Luisi et al., 1996; Rishbeth, 1982), the substrate probably consists of coarse pieces of weakened woody root material. The likelihood of achieving new nutrients may be as large as in surrounding sites that are not colonised, since the influx of decomposable material is irregular and forest soil remains largely undisturbed. The maintenance costs for the network are probably lower than the costs for production of rhizomorphs that have to colonise a new site. Indeed we often observed rhizomorphic growth against woody roots without any sign of infection. This behaviour may be very similar to the behaviour of *Armillaria* reported in tropical Africa (Swift, 1972; Leach, 1939), where rhizomorphs are usually absent due to the prevailing high temperatures, but where quiescent lesions on woody host roots are common, 'waiting' until circumstances are suitable for infection. Although *Armillaria* is able to form basidiocarps, the success rate of basidiospores in colonising new substrate, e.g. freshly cut stumps, is extremely low (Rishbeth, 1970), and therefore basidiospores hardly contribute to persistence.

A persistent network is a network that is not substantially weakened when disruption of one edge disconnects part of the network. The graph G_3 (Figure 2) consists of 9 bridges, of which disruption of only two of them (edge 78 or 81) would disconnect a considerable part of the rhizomorph system (based on the number of vertices), indicating the strategy of the fungus to invest in networks. Disruption of one of the other 7 bridges would disconnect only 1-4% of the network, illustrating explorative parts of the network that may not persist if they do not contribute to the network. The impact of disruption is lower on a densely connected network, for which the number of possible spanning trees is high (4.7×10^{28} in the graph G_3), than on a sparsely connected one.

It was shown that many spanning trees were possible for the observed rhizomorph network, and we could calculate the weight of one of the possible minimum spanning trees. The importance of finding a spanning tree with minimum total weight has been shown for planning large-scale communication and distribution networks when the most important consideration usually is to provide paths between every pair of vertices in the most economical way. The vertices would be cities, terminals, or retail outlets, and the edges

would be highways or pipelines. The weights corresponding to these edges could be distances or costs or time involved in these processes.

Once susceptibility of roots has surpassed the threshold for infection by *A. lutea*, the fungus grows acropetally and infects also above-ground parts (Fox, 2000). During exploitative growth intensive branching occurs, and random encounters result frequently in anastomosis. *Armillaria* forms white mycelial mats on infected host tissue (Mallett et al., 1989; Rizzo & Harrington, 1992), but also rhizomorphic heavily branched 'mats' can be observed frequently (Fox, 2000), especially for *A. lutea* (pers. obs. Termorshuizen). Although rhizomorphic 'mats' were absent in our site, intensive branching of rhizomorphs can be observed (Chapter 6, Figure 1a & 2a). Exploitative rhizomorphic growth may occur at sites where wood is or has been present resulting in anastomosis by random encounters. However, the rhizomorph network observed is not restricted to this type of exploitative formation of cycles, since the length of the edges enclosing the faces is in quite a number of instances larger than the dimensions of host material, i.e. coarse woody roots. If we arbitrarily exclude faces of which the length of the enclosing edges is shorter than 100 cm, then 25% is not ascribable to this type of growth strategy. Although setting the border for exploitative growth is rather arbitrary, it is clear that a cycle of 1030 cm (Figure 4, face 17), which measures at some points more than 2 m in diameter, could not be the result of colonisation of one wood source. Therefore, this cycle is certainly not the result of heavily branching due to the presence of nutrients.

Transportation networks are characterised by a minimum overall cost. Banavar et al. (2000) proved that the shape (convexity or concavity) of the cost function for local transportation of material impacts directly on the topology (the presence or absence of loops) of the emergent networks that minimise the total cost of transportation. In the case where the cost function is concave, it is most efficient to use all possible transportation pathways and loops emerge. If we relate this to fungi, a concave cost function corresponds with dichotomous fungal growth, and an exploitation strategy. For a convex cost function, Banavar et al. (2000) shows that it is more economical to send all the material from a given site to one neighbouring site rather than to multiple neighbouring sites, which leads, globally, to a network with a tree topology. A convex cost function will therefore result in a monopodial fungal growth form or herringbone structure, and an exploration strategy.

We explored different possibilities of graph-theoretic concepts to describe a rhizomorph network, to define foraging strategies of the fungus, and to speculate about the underlying

reasons. The introduction of graph-theoretic properties to fungal growth may lead to an improved ecological understanding of fungal networks in general, when relevant biological interpretations can be drawn.

Appendix 1

Dijkstra's polynomial algorithm (1959) to find the shortest distance and the shortest path from a specified vertex (called vertex 1) to every other vertex.

To each vertex i a label is assigned that is either permanent or tentative. The permanent label $L(i)$ is the shortest distance from vertex 1 to i , whereas the tentative label $L'(i)$ is an upper bound of the shortest distance from vertex 1 to i . At each stage of the procedure, P is the set of vertices with permanent labels and T is its complement. Initially, $P=\{1\}$ with $L(1)=0$ and $L'(i)=w(1,i)$ for each i , where w represents the weight. When P includes all vertices the algorithm halts. Each iteration consists essentially of two steps:

Step 1 (Designation of a permanent label):

Find a vertex k in T for which $L'(k)$ is minimal. Tie-breaking is arbitrary. Declare k to be permanently labeled and adjoin k to the set P . Stop if P includes all vertices.

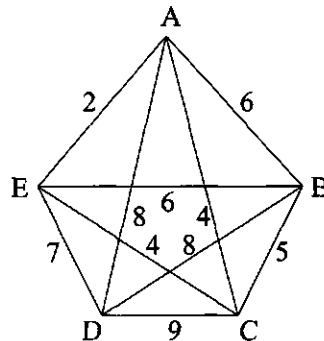
Step 2 (Revision of tentative labels):

If j is a vertex in T , replace $L'(j)$ by the smaller value of $L'(j)$ and $L(k)+w(k,j)$. Go to step 1.

Appendix 2

Worked problem to illustrate Prim's (1957) algorithm to find a spanning tree T with minimum total weight in the following weighted graph:

	A	B	C	D	E
A	-	6	4	8	2
B	6	-	5	8	6
C	4	5	-	9	4
D	8	8	9	-	7
E	2	6	4	7	-



First choice Choose any vertex, say B, and put it into T. Delete row B. Look for the smallest entry in column B; it is 5 in row C.

Second choice BC is the edge of minimum weight joining B to other vertices. Put the edge BC and vertex C into T. The vertex C is now in the tree, so delete row C. Look for the smallest entry in columns B and C; it is 4 in rows A and E.

Third choice CA and CE are the edges of minimum weight joining B and C to other vertices. Choose one of these, say CA, and put edge CA and vertex A into T. Delete row A and look for the smallest entry in columns A, B and C, which is 2 in row E.

Fourth choice AE is the edge of minimum weight joining A, B and C to other vertices, so AE and vertex E are put into T. After deletion of row E, the smallest entry in columns A, B, C and E is 7 in row D.

Fifth choice ED is the edge of minimum weight joining A, B, C and E to D, therefore ED and vertex D are put into T. All the vertices are now in T, which gives a minimum spanning tree of weight $5+4+2+7=18$.

Chapter 8

General conclusions

This thesis has shown that studies on the obtaining and allocation of nutrients provides much insight into fungal growth strategies. In Section I of this thesis, mechanistic fungal growth models were developed to describe fine mycelial networks of microscopic fungi. These models, although simple and not able to reproduce all aspects of the behaviour of complex biological systems, are quite general and may ultimately prove to be of considerable value for understanding and predicting patterns of fungal growth. The principal objective is to use the models as a tool for predicting the qualitative behaviour of the system under consideration: i.e. whether the system will persist in the long-term; the conditions determining whether the fungus will invade; and the relative contribution of model parameters in determining model outcomes. In Section II of this thesis, macroscopic rhizomorph networks of *Armillaria*, as visualised from direct observations in natural soils, are described. The type of mechanistic growth model developed for microscopic fungi in Section I was not appropriate for rhizomorph networks and new approaches using graph-theoretic concepts were developed to quantify and interpret network properties.

The mechanistic fungal growth model proposed in Section I is based on a detailed consideration of the dynamics of carbon and nitrogen, arising from the colonisation and decomposition of substrate, for example soil organic matter. The overall-steady states for the variables were obtained, and analysis of the conditions for existence showed that the 'energy' (in terms of carbon) *invested in* breakdown of substrate should be less than the 'energy' *resulting from* breakdown of substrate, leading to a positive carbon balance. For growth the 'energy' necessary for production of structural fungal biomass and for maintenance should be less than this positive carbon balance in the situation where all substrate is colonised. This fungal growth model predicted the behaviour from initial conditions until the final state. The initial state of the system was not relevant for long-term dynamics as the system settled on a single biologically meaningful attractor determined by the dynamics of the model. Information on the final state is usually relevant, but there are many examples in biochemical and biological systems where the transient behaviour is more interesting than the final state.

If the nutrient dynamics are very fast compared to the dynamics of fungal biomass and substrate, then after a fast transient the system will reach a quasi-steady state. This quasi-steady state approach simplified the fungal growth model, and we derived an explicit fungal invasion criterion: one for systems where carbon is limiting, another for systems where nitrogen is limiting. Knowledge of the factors that determine invasion is essential to an understanding of fungal dynamics. Under the assumption that only carbon is limiting fungal growth, we excluded nitrogen dynamics from the model. This further simplification to the model, exhibiting carbon-limited dynamics, produced a good fit to data of the soil-borne pathogen *Rhizoctonia solani* obtained in Petri plate growth experiments. In further work a similar approach can be taken by excluding the carbon-dynamics and concentrating on nitrogen-limited dynamics, although the parameter estimates will be more difficult to interpret biologically.

Graph-theoretic concepts proposed in Section II were applied to rhizomorph networks of the fungus *A. lutea*, which causes a serious disease in many forests and horticultural tree crops world-wide. Two rhizomorph networks were observed over an area of 25 m² at tree plantations of *Pinus nigra* and *Picea abies*. A large proportion of each network was interconnected (84 and 48%) with many cyclic paths, and the fractal dimensions were very similar. However, there were differences as well as similarities between the two observed networks. One network was connected in only two instances to a nutrient source, where the

other network had many connections to stumps and tree roots. The first network was analysed using graph-theoretic concepts. The connectivity of the rhizomorph network was examined by focusing on cyclic paths (i.e. regions of the system that start and end at the same point), bridges (i.e. edges whose removal disconnects the graph into two components), and spanning trees (i.e. graphs with a minimum amount of edges connecting all the vertices of the graph). Analysis of the network structure showed that the fungus exhibited foraging strategies related to exploitative growth, e.g. the frequency of branching, and also explorative growth, e.g. disruption of a bridge disconnects in many instances only a small part of the network, and we concluded that the formation of rhizomorph networks is a successful strategy for *Armillaria* to ensure its persistence. The high frequency of cyclic paths limits the effects of unsuccessful exploration by enhancing the redistribution of nutrients and reducing the chance of a disconnected system when one rhizomorph breaks. It is advantageous not only to spread to new areas, but also to remain quiescent until weakened host material becomes available.

The results showed that both mechanistic models and graph-theoretic concepts can be applied to improve the ecological understanding of fungal growth. Growth of microscopic fungi is difficult to study experimentally, so there was emphasis on modelling. Conversely, macroscopic networks are relatively easy to study, but modelling approaches using graph-theory were more difficult with new concepts necessary. Petri plate experiments on nitrogen-limited fungal growth can take the research forward, and also replacement of agar as a nutrient source by organic matter, for example straw. The proposed fungal growth model assumes a uniform distribution of nutrient sites, but an adapted version of the model may consider a distribution that is to a small or larger extent clustered. Analysis of the rhizomorph network structure of *Armillaria* can be extended by recording nutrient flows in the form of stable isotopes through the rhizomorph network in natural soils. This would provide insight into the direction of nutrient flows, the importance of the various nutrient sources, and the impact of disruption of each edge.

REFERENCES

- ADAMS, P.B. & AYERS, W.A. 1982 Biological control of *Sclerotinia* lettuce drop in the field by *Sporeidismium sclerotivorum*. *Phytopathology* **72**, 485-488.
- ADAMS, P.B. 1990 The potential of mycoparasites for biological control of plant diseases. *Annu. Rev. Phytopathol.* **28**, 59-72.
- ANDERSON, J.B. & STASOVSKI, E. 1992 Molecular phylogeny of northern hemisphere species of *Armillaria*. *Mycologia* **84**, 505-516.
- ANONYMOUS 2001 3D high resolution X-Ray microtomography of small living animals. In: High resolution imaging in small animals. Book of abstracts, pp. 244-245. Rockville, USA.
- ARCHER, D.B. & WOOD, D.A. 1995 Fungal exoenzymes. In: The growing fungus (N.A.R.Gow & G.M. Gadd, eds.). London: Chapman & Hall.
- BAILEY, D.J., OTTEN, W. & GILLIGAN, C.A. 2000 Saprotrophic invasion by the soil-borne fungal plant pathogen *Rhizoctonia solani* and percolation thresholds. *New Phytol.* **146**, 535-544.
- BALAKRISHNAN, V.K. 1991 Introductory discrete mathematics. Englewood Cliffs, New Jersey: Prentice-Hall.
- BANAVAR, J.R., COLAIORI, F., FLAMMINI, A., MARITAN, A. & RINALDO, A. 2000 Topology of the fittest transportation network. *Phys. Rev. Lett.* **84**, 4745-4748.
- BEEZER, R.A., RIEGSECKER, J.E. & SMITH, B.A. 2001 Using minimum degree to bound average distance. *Discrete Math.* **226**, 365-371.
- BENDING, G.D. & READ, D.J. 1995 The structure and function of the vegetative mycelium of ectomycorrhizal plants. *New Phytol.* **130**, 401-409.
- BOLTON, R.G., MORRIS, C.W. & BODDY, L. 1991 Non-destructive quantification of growth and regression of mycelial cords using image analysis. *Binary* **3**, 127-132.

- BOLTON, R.G. & BODDY, L. 1993 Characterization of the spatial aspects of foraging mycelial cord systems using fractal geometry. *Mycol. Res.* **97**, 762-768.
- BORGHANS, J.A.M., DE BOER, R.J. & SEGEL, L.A. 1996 Extending the quasi-steady state approximation by changing variables. *Bull. Math. Biol.* **58**, 43-63.
- BROWN, T.N., KULASIRI, D. & GAUNT, R.E. 1997 A root-morphology based simulation for plant/soil microbial ecosystem modelling. *Ecological modelling* **99**, 275-287.
- BRUHN, J.N., MIHAIL, J.D. & MEYER, T.R. 1996 Using spatial and temporal patterns of *Armillaria* root disease to formulate management recommendations for Ontario's black spruce (*Picea mariana*) seed orchards. *Can. J. For. Res.* **26**, 298-305.
- BULL, A.T. & TRINCI, A.P.J. 1977 The physiology and metabolic control of fungal growth. *Adv. in microbial physiology* **15**, 1-84.
- BURNETT, J.H. 1979 Aspects of the structure and growth of hyphal walls. In: Fungal walls and hyphal growth (J.H. Burnett & A.P.J. Trinci, eds.). Cambridge: University Press.
- CAIRNEY, J.W.G., JENNINGS, D.H., RATCLIFFE, R.G. & SOUTHON, T.E. 1988 The physiology of basidiomycete linear organs. II. Phosphate uptake by rhizomorphs of *Armillaria mellea*. *New Phytologist* **109**, 327-333.
- CHADOEUF, J., PIERRAT, J.C., NANDRIS, D., GEIGER, J.P. & NICOLE, M. 1993 Modeling rubber tree root disease epidemics with a Markov spatial process. *Forest Science* **39**, 41-54.
- CHILLALI, M., IDDER-IGHILI, H., GUILLAUMIN, J.J., MOHAMMED, C. & BOTTON, B. 1997 Species delimitation in the African *Armillaria* complex by analysis of the ribosomal DNA spacers. *J. General Appl. Microbiology* **43**, 23-29.
- COOKE, R.C. & WHIPPS, J.M. 1993 *Ecophysiology of fungi*. Oxford: Blackwell Scientific Publications.

DATTA, A., BETTERMANN, A. & KIRK, T.K. 1991 Identification of a specific manganese peroxidase among ligninolytic enzymes secreted by *Phanerochaete chrysosporium* during wood decay. *Appl. and Environmental Microbiology* **57**, 1453-1460.

DAVIDSON, F.A., SLEEMAN, B.D., RAYNER, A.D.M., CRAWFORD, J.W. & RITZ, K. 1997 Travelling waves and pattern formation in a model for fungal development. *J. Math. Biol.* **35**, 589-608.

DEACON, J.W. 1980 Introduction to modern mycology. Oxford: Blackwell Scientific Publications.

DIEKMANN, O., HEESTERBEEK, J.A.P. & METZ, J.A.J. 1990 On the definition and the computation of the basic reproduction ratio R_0 in models for infectious diseases in heterogeneous populations. *J. Math. Biol.* **28**, 365-382.

DIGHTON, J. 1997 Nutrient cycling by saprotrophic fungi in terrestrial habitats. In: *The Mycota IV: Environmental and microbial relationships* (D.T. Wicklow & B. Söderström, eds.). Berlin: Springer-Verlag.

DIJKSTRA, E.W. 1959 A note on two problems in connection with graphs. *Numer. Math* **1**, 269-271.

DUDDRIDGE, J.A., FINLAY, R.D., READ, D.J. & SODERSTROM, B. 1988 The structure and function of the vegetative mycelium of ectomycorrhizal plants. III. Ultrastructural and autoradiographic analysis of inter-plant carbon distribution through intact mycelial systems. *New Phytol.* **108**, 183-188.

EAMUS, D. & JENNINGS, D.H. 1984 Determination of water, solute and turgor potentials of mycelium of various basidiomycete fungi causing wood decay. *J. of experimental botany* **35**, 1782-1786.

EDELSTEIN, L. 1982 The propagation of fungal colonies: a model for tissue growth. *J. theor. Biology* **98**, 679-701.

- EDELSTEIN, L. & SEGEL, L.A. 1983 Growth and metabolism in mycelial fungi. *J. theor. Biology* **104**, 187-210.
- EGHBALL, B., SETTIMI, J.R., MARANVILLE, J.W. & PARKHURST, A.M. 1993 Fractal analysis for morphological description of corn roots under nitrogen stress. *Agronomy Journal* **85**, 287-289.
- FINLAY, R.D. & READ, D.J. 1986 The structure and function of the vegetative mycelium of ectomycorrhizal plants. II. The uptake and distribution of phosphorus by mycelial strands interconnecting host plants. *New Phytol.* **103**, 157-165.
- FOX, R.T.V. 2000 Biology and life cycle. In: *Armillaria* root rot: biology and control of honey fungus (R.T.V. Fox, ed.). Andover, Hants: Intercept Ltd.
- FRANKLAND, J.C. 1994 Mechanisms in fungal succession. In: *The fungal community: Its organization and role in the ecosystem.* (G.C. Carroll & D.T. Wicklow, eds.). New York: Marcel Dekker, Inc.
- FRAVEL, D.R. 1997 Use of *Sporidesmium sclerotivorum* for biocontrol of sclerotial plant pathogens. In: *Plant-microbe interactions and biological control* (G.J. Boland & L.D. Kuykendall, eds.). New York: Marcel Dekker, Inc.
- GARRETT, S.D. 1946 Soil as a medium for multiplication and transfer of disease organisms. *Soil Science* **61**, 3-8.
- GIBSON, G.J., GILLIGAN, C.A. & KLECZKOWSKI, A. 1999 Predicting variability in biological control of a plant-pathogen system using stochastic models. *Proc. R. Soc. Lond. B* **266**, 1743-1753.
- GILLIGAN, C.A. & BAILEY, D.J. 1997 Components of pathozone behaviour. *New Phytol.* **136**, 343-358.
- GRANLUND, H.I., JENNINGS, D.H. & VELTKAMP, K. 1984 Scanning electron microscope studies of rhizomorphs of *Armillaria mellea*. *Nova Hedwigia* **39**, 85-100.

GRANLUND, H.I., JENNINGS, D.H. & THOMPSON, W. 1985 Translocation of solutes along rhizomorphs of *Armillaria mellea*. *Trans. Br. Mycol. Soc.* **84**, 111-119.

GRAY, S.N., DIGHTON, J. & JENNINGS, D.H. 1996 The physiology of basidiomycete linear organs. III. Uptake and translocation of radiocaesium within differentiated mycelia of *Armillaria* spp. growing in microcosms and in the field. *New Phytol.* **132**, 471-482.

GUBBINS, S. & GILLIGAN, C.A. 1996 Population dynamics of a parasite and hyperparasite in a closed system: model analysis and parameter estimation. *Proc. R. Soc. Lond. B* **263**, 1071-1078.

HARARY, F. 1969 Graph theory. Reading: Addison-Wesley.

HUGHES, G. & MADDEN, L.V. 1998 Comment - Using spatial and temporal patterns of *Armillaria* root disease to formulate management recommendations for Ontario's black spruce (*Picea mariana*) seed orchards. *Can. J. For. Res.* **28**, 154-158.

HUISMAN, G. & DE BOER, R.J. 1997 A formal derivation of the "Beddington" functional response. *J. Theor. Biol.* **185**, 389-400.

HUNDING, A. & KÆRN, M. 1998 The effect of slow allosteric transitions in a simple biochemical oscillator model. *J. Theor. Biol.* **191**, 309-322.

JACKSON, A.M., WHIPPS, J.M. & LYNCH, J.M. 1991 Nutritional studies of four fungi with disease biocontrol potential. *Enzyme Microb. Technol.* **13**, 456-461.

JEGER, M.J. 1990 Mathematical analysis and modeling of spatial aspects of plant disease epidemics. In: Epidemics of plant diseases: mathematical analysis and modeling (J. Kranz, ed.). Berlin: Springer-Verlag.

JENNINGS, D.H. 1975 Transport and translocation in filamentous fungi. In: The filamentous fungi. Vol. 2: Biosynthesis and metabolism (J.E. Smith & D.R. Berry, eds.). London: Arnold.

KLECZKOWSKI, A., BAILEY, D.J. & GILLIGAN, C.A. 1996 Dynamically generated variability in plant-pathogen systems with biological control. *Proc. R. Soc. Lond. B* **263**, 777-783.

- KLECZKOWSKI, A. 1998 Statistical properties of dynamical systems with disturbances: variation in parameters. *Acta Physica Polonica B* **29**, 1717-1735.
- KLECZKOWSKI, A. & GRENFELL, B.T. 1999 Mean-field-type equations for spread of epidemics: the 'small world' model. *Physica A* **274**, 355-360.
- KLEIN-GEGBINCK, H.W., BLENIS, P.V. & HIRATSUKA, Y. 1991 Spread of *Armillaria ostoyae* in juvenile lodgepole pine stands in west central Alberta. *Can. J. For. Res.* **21**, 20-24.
- KRAPIVSKY, P.L., REDNER, S. & LEYVRAZ, F. 2000 Connectivity of growing random networks. *Phys. Rev. Lett.* **85**, 4629-4632.
- KRUSKAL, J.B. 1956 On the shortest spanning subtree of a graph and the traveling salesman problem. *Proc. Amer. Math. Soc.* **7**, 48-50.
- LAMOUR, A. & JEGER, M.J. 2000 Quantitative aspects of the epidemiology of *Armillaria* in the field. In: *Armillaria* root rot: biology and control of honey fungus (R.T.V. Fox, ed.). Andover, Hants: Intercept Ltd.
- LAMOUR, A., VAN DEN BOSCH, F., TERMORSHUIZEN, A.J. & JEGER, M.J. 2001 Modelling the growth of soil-borne fungi in response to carbon and nitrogen. *IMA J. Math. Appl. Med. Biol.* **17**, 329-346.
- LAMOUR, A., VAN DEN BOSCH, F., TERMORSHUIZEN, A.J. & JEGER, M.J. Quasi-steady state approximation to a fungal growth model. Submitted to *IMA J. Math. Appl. Med. Biol.*
- LEACH, R. 1939 Biological control and ecology of *Armillaria mellea* (Vahl) Fr. *Trans. Br. Mycol. Soc.* **23**, 320-329.
- LENBURY, Y., OUNCHAROEN, R. & TUMRASVIN, N. 2000 Higher-dimensional separation principle for the analysis of relaxation oscillations in nonlinear systems: application to a model of HIV infection. *IMA J. Math. Appl. Med. Biol.* **17**, 243-261.

LOCKWOOD, J.L. 1981 Exploitation competition. In: The fungal community: its organization and role in the ecosystem (D.T. Wicklow & G.C. Carroll, eds.). New York, Marcel Dekker.

LOCKWOOD, J.L. & FILONOW, A.B. 1981 Responses of fungi to nutrient-limiting conditions and to inhibitory substances in natural habitats. *Adv. Microbial Ecol.* **5**, 1-61.

LUIZI, N., SICOLI, G., LARARIO, P., DREYER, E. & AUSSENAC, G. 1996 Proc. Int. Symp. Ecology and physiology of oaks in a changing environment. *Ann. Sci. For.* **53**, 389-394 [in French].

LUNDQUIST, J.E. 1993 Spatial and temporal characteristics of canopy gaps caused by *Armillaria* root disease and their management implications in lowveld forests of South Africa. *Eur. J. For. Path.* **23**, 362-371.

MALLET, K.I., HOPKIN, A.A. & BLENIS, P.V. 1989 Vegetative incompatibility in diploid isolates of *Armillaria* North American biological species I and V. *Can. J. Bot.* **67**, 3083-3089.

MANDELBROT, B.B. 1982 The fractal geometry of nature. San Francisco, California: W.H. Freeman and Co.

MARSDEN, M.A. 1992a Sensitivity of the Western Root Disease Model: inventory of root disease. *USDA Forest Service. Research Paper RM-303*.

MARSDEN, M.A. 1992b Sensitivity analyses of the Western Root Disease Model to user-specified starting parameters. *USDA Forest Service. Research Paper RM-306*.

MARSDEN, M.A., SHAW, C.G. & MORRISON, M. 1993a Simulation of management options for stands of southwestern ponderosa pine attacked by *Armillaria* root disease and dwarf mistletoe. *USDA Forest Service. Research Paper RM-308*.

MARSDEN, M.A., EAV, B.B. & THOMPSON, M.K. 1993b Modeling initial conditions for root rot in forest stands: random proportions. *USDA Forest Service. Research Note RM-524*.

MARSH, R.W. 1951 Field observations on the spread of *Armillaria mellea* in apple orchards and in a blackcurrant plantation. *Trans. Br. Mycol. Soc.* **35**, 201-207.

- MARSH, B. a'B. 1971 Measurement of length in random arrangements of lines. *J. Appl. Ecol.* **8**, 265-267.
- MIHAIL, J.D., OBERT, M., TAYLOR, S.J. & BRUHN, J.N. 1994 The fractal dimension of young colonies of *Macrophomina phaseolina* produced from microsclerotia. *Mycologia* **86**, 350-356.
- MIHAIL, J.D. & BRUHN, J.N. 1995 Using fractal geometry to compare rhizomorph foraging strategies among six *Armillaria* species. (Abstract). *Phytopathology* **85**, 1127.
- MIHAIL, J.D., OBERT, M., BRUHN, J.N. & TAYLOR, S.J. 1995 Fractal geometry of diffuse mycelia and rhizomorphs of *Armillaria* species. *Mycol. Res.* **99**, 81-88.
- MOLIN, P., GERVAIS, P. & LEMIERE, J-P. 1993 A computer model based on reaction-diffusion equations for the growth of filamentous fungi on solid substrate. *Biotechnol. Prog.* **9**, 385-393.
- MORRISON, D.J. 1976 Vertical distribution of *Armillaria mellea* rhizomorphs in soil. *Trans. Br. Mycol. Soc.* **66**, 393-399.
- MORRISON, D.J., WILLIAMS, R.E. & WHITNEY, R.D. 1991 Infection, disease development, diagnosis, and detection. In: *Armillaria root disease* (C.G. Shaw III & G.A. Kile, eds.). Forest Service Handbook No. 691. Washington, D.C.: USDA.
- NÅSELL, I. 1995 The threshold concept in stochastic epidemic and endemic models. In: *Epidemic models: their structure and relation to data* (D. Mollison, ed.). Cambridge: Cambridge University Press.
- NEWMAN, E.I. 1966 A method of estimating the total length of root in a sample. *J. Appl. Ecol.* **3**, 139-145.
- NICOLARDOT, B., GUIRAUD, G., PERROT, C., COUTON, Y. & CATROUX, G. 1989 Consideration of nitrogen immobilization in the estimation of microbial biomass nitrogen with the chloroform fumigation method. *Soil Biol. and Biochem.* **21**, 995-1002.

OBERT, M., PFEIFER, P. & SERNETZ, M. 1990 Microbial growth patterns described by fractal geometry. *J. Bacteriol.* **172**, 1180-1185.

ONO, K. 1965 *Armillaria* root rot in plantations of Hokkaido. Effects of topography and soil conditions on its occurrence. *Bull. Government Forest Experiment Station, Meguro* **179**, 1-62.

ONO, K. 1970 Effect of soil conditions on the occurrence of *Armillaria* root rot of the Japanese Larch. *Bull. Government Forest Experiment Station, Meguro* **229**, 1-219.

ORITSEJAFOR, J.J. 1986 Carbon and nitrogen nutrition in relation to growth and sporulation of *Fusarium oxysporum* f. sp. *elaeidis*. *Trans. Br. Mycol. Soc.* **87**, 519-524.

PALSSON, B.O. 1987 On the dynamics of the reversible Michaelis-Menten reaction mechanisms. *Chem. Eng. Sci.* **42**, 447-458.

PARK, Y., STACK, J.P. & KENERLEY, C.M. 1991 Production of gliotoxin by *Gliocladium virens* as a function of source and concentration of carbon and nitrogen. *Mycol. Res.* **95**, 1242-1248.

PAUSTIAN, K. & SCHNÜRER, J. 1987a Fungal growth response to carbon and nitrogen limitation: a theoretical model. *Soil biol. and biochem.* **19**, 613-620.

PAUSTIAN, K. & SCHNÜRER, J. 1987b Fungal growth response to carbon and nitrogen limitation: application of a model to laboratory and field data. *Soil biol. and biochem.* **19**, 621-629.

PAWSEY, R.G. & RAHMAN, M.A. 1976 Chemical control of infection by honey fungus, *Armillaria mellea*: a review. *Arboricultural J.* **2**, 468-479.

PEBERDY, J.F. 1990 Fungal cell walls-a review. In: *Biochemistry of cell walls and membranes in fungi* (P.J.Kuhn, A.P.J.Trinci, M.J.Jung., M.W.Goosey & L.G. Copping, eds.). Berlin: Springer-Verlag.

PFEIFER, P. & OBERT, M. 1989 Fractals: basic concepts and terminology. In: The fractal approach to heterogeneous chemistry (D. Avnir, ed.). New York: John Wiley and Sons.

PIELOU, E.C. 1961 Segregation and symmetry in two species populations as studied by nearest neighbor relationships. *J. Ecol.* **49**, 255-269.

PRIM, R.C. 1957 Shortest connection networks and some generalizations. *Bell System Tech. J.* **36**, 1389-1401.

PROSSER, J.I. 1979 Mathematical modelling of mycelial growth. In: Fungal walls and hyphal growth (J.H. Burnett & A.P.J. Trinci, eds.). Cambridge: University Press.

PROSSER, J.I. & TRINCI, A.P.J. 1979 A model for hyphal growth and branching. *J. of General Microbiol.* **111**, 153-164.

RAYNER, A.D.M. 1991 The challenge of the individualistic mycelium. *Mycologia* **83**, 48-71.

RAYNER, A.D.M., GRIFFITH, G.S. & AINSWORTH, A.M. 1994 Mycelial interconnectedness. In: The growing fungus (A.R. Gow & G.M. Gadd, eds.). London: Chapman & Hall.

RAYNER, A.D.M., GRIFFITH, G.S. & WILDMAN, H.G. 1994 Differential insulation and the generation of mycelial patterns. In: Shape and form in plants and fungi (D.S. Ingram & A. Hudson, eds.). London: Ac. Press.

REAVES, J.L., SHAW, C.G. & ROTH, L.F. 1993 Infection of ponderosa pine trees by *Armillaria ostoyae*: residual inoculum versus contagion. *Northw. Sci.* **67**, 156-162.

REDFERN, D.B. 1973 Growth and behaviour of *Armillaria mellea* rhizomorphs in soil. *Trans. Br. Mycol. Soc.* **61**, 569-581.

REDFERN, D.B. & FILIP, G.M. 1991 Inoculum and infection. In: *Armillaria* root disease (C.G. Shaw and G.A. Kile, eds.). U.S. Dep. Agric. Handb. 691.

- REGALADO, C.M., CRAWFORD, J.W., RITZ, K. & SLEEMAN, B.D. 1996 The origins of spatial heterogeneity in vegetative mycelia: a reaction-diffusion model. *Mycol. Res.* **100**, 1473-1480.
- RICCIARDI, R.P., HOLLOMON, D.W. & GOTTLIEB, D. 1974 Age dependent changes in fungi: ribosomes and protein synthesis in *Rhizoctonia solani* mycelium. *Archives of Microbiology* **95**, 325-336.
- RICHARDS, B.N. 1987 The microbiology of terrestrial ecosystems. Harlow: Longman.
- RIGHELATO, R.C. 1979 The kinetics of mycelial growth. In: Fungal walls and hyphal growth (J.H. Burnett & A.P.J. Trinci, eds.). Cambridge: University Press.
- RISHBETH, J. 1970 The role of basidiospores in stump infection by *Armillaria mellea*. In: Root diseases and soil borne pathogens (T.A. Tousson, R. Bega & P. Nelson, eds.). Berkeley: Univ. California Press.
- RISHBETH, J. 1972 The production of rhizomorphs by *Armillaria mellea* from stumps. *Eur. J. For. Path.* **2**, 193-205.
- RISHBETH, J. 1978 Effect of soil temperature and atmosphere on growth of *Armillaria* rhizomorphs. *Trans. Br. Mycol. Soc.* **70**, 213-220.
- RISHBETH, J. 1982 Species of *Armillaria* in southern England. *Plant Path.* **31**, 9-17.
- RITZ, K. & CRAWFORD, J. 1990 Quantification of the fractal nature of colonies of *Trichoderma viride*. *Mycol. Res.* **94**, 1138-1152.
- RIZZO, D.M., BLANCHETTE, R.A. & PALMER, M.A. 1992 Biosorption of metal ions by *Armillaria* rhizomorphs. *Canadian J. of Botany* **70**, 1515-1520.
- RIZZO, D.M. & HARRINGTON, T.C. 1992 Nuclear migration in diploid_haploid pairings of *Armillaria ostoyae*. *Mycologia* **84**, 863-869.

SEGEL, L.A. 1988 On the validity of the steady state assumption of enzyme kinetics. *Bull. Math. Biol.* **6**, 579-593.

SEGEL, L.A. & SLEMROD, M. 1989 The quasi-steady state assumption: a case study in perturbation. *SIAM Rev.* **31**, 446-477.

SHAW, C.G., STAGE, A.R. & McNAMEE, P. 1991 Modeling the dynamics, behavior, and impact of *Armillaria* root disease. In: *Armillaria* root disease (C.G. Shaw and G.A. Kile, eds.). U.S. Dep. Agric. Handb. 691.

SIMS, R.A., TOWILL, W.D., BALDWIN, K.A. & WICKWARE, G.M. 1989 Field guide to the forest ecosystem classification for northwestern Ontario. Toronto: Ontario Ministry of Natural Resources.

SINGH, P. 1981 *Armillaria mellea*: growth and distribution of rhizomorphs in the forest soils of Newfoundland. *Eur. J. For. Path.* **11**, 208-220.

SMITH, M.L., BRUHN, J.N. & ANDERSON, J.B. 1992 The fungus *Armillaria bulbosa* is among the largest and oldest living organisms. *Nature* **356**, 428-431.

SNEH, B., JABAJI-HARE, S., NEATE, S. & DIJST, G. 1996 *Rhizoctonia* species: taxonomy, molecular biology, ecology, pathology and disease control. Dordrecht: Kluwer.

STACK, J.P., KENERLEY, C.M. & PETTIT, R.E. 1987 Influence of carbon and nitrogen sources, relative carbon and nitrogen concentrations, and soil moisture on the growth in nonsterile soil of soilborne fungal antagonists. *Can. J. Microbiol.* **33**, 626-631.

STAGE, A.R., SHAW, C.G., MARSDEN, M.A., BYLER, J.W., RENNER, D.L., EAV, B.B., McNAMEE, P.J., SUTHERLAND, G.D. & WEBB, T.M. 1990 User's manual for Western Root Disease Model. *USDA Forest Service. General Technical Report INT-267*.

STANOSZ, G.R. & PATTON, R.F. 1991 Quantification of *Armillaria* rhizomorphs in Wisconsin aspen sucker stands. *Eur. J. For. Path.* **21**, 5-16.

STARK, N. 1972 Nutrient cycling pathways and litter fungi. *Bioscience* **22**, 355-360.

STIEFENHOFER, M. 1998 Quasi-steady state approximation for chemical reaction networks. *J. Math. Biol.* **36**, 593-609.

STOLK, C., VAN DEN BOSCH, F., TERMORSHUIZEN, A.J. & JEGER, M.J. 1998 Modeling the dynamics of a fungal mycoparasite and its host: an energy-based approach. *Phytopathology* **88**, 481-489.

SWIFT, M.J. 1972 The ecology of *Armillaria mellea* Vahl (ex Fries) in the indigenous and exotic woodlands of Rhodesia. *Forestry* **45**, 67-86.

SWIFT, M.J., HEAL, O.W. & ANDERSON, J.M. 1979 Decomposition in terrestrial ecosystems. Oxford: Blackwell Scientific.

TERMORSHUIZEN, A.J. 2000 Ecology and epidemiology of *Armillaria*. In: *Armillaria* root rot: biology and control of honey fungus (R.T.V. Fox, ed.). Andover, Hants: Intercept Ltd.

TERMORSHUIZEN, A.J., LAMOUR, A. & JEGER, M.J. 1998 Networks formed by rhizomorphs of *Armillaria ostoyae*. Proceedings of the sixth International Mycological Congress, Jerusalem, Israel, August 23-28.

THORNLEY, J.H.M. & JOHNSON, I.R. 1990 Plant and crop modelling - A mathematical approach to plant and crop physiology. Oxford: Scientific Publications.

TWERY, M.J., MASON, G.N., WARGO, P.M. & GOTTSCHALK, K.W. 1990 Abundance and distribution of rhizomorphs of *Armillaria* spp. in defoliated mixed oak stands in western Maryland. *Can. J. For. Res.* **20**, 674-678.

VAN DEN HEUVEL, J.P.M. 1993 Degree and toughness conditions for cycles in graphs. PhD Thesis, 169 p.

VAN DER KAMP, B.J. 1995 The spatial distribution of *Armillaria* root disease in an uneven-aged, spatially clumped Douglas-fir stand. *Can. J. For. Res.* **25**, 1008-1016.

- VERCESI, A., LOCCI, R. & PROSSER, J.I. 1997 Growth kinetics of *Botrytis cinerea* on organic acids and sugars in relation to colonization of grape berries. *Mycol. Res.* **101**, 139-142.
- VOLLBRECHT, G. & AGESTAM, E. 1995 Modelling incidence of root rot in *Picea abies* plantations in southern Sweden. *Scand. J. For. Res.* **10**, 74-81.
- VOLLBRECHT, G. & JØRGENSEN, B.B. 1995 Modelling the incidence of butt rot in plantations of *Picea abies* in Denmark. *Can. J. For. Res.* **25**, 1887-1896.
- WARGO, P.M. & HARRINGTON, T.C. 1991 Host stress and susceptibility. In: *Armillaria* root disease (C.G. Shaw and G.A. Kile, eds.). U.S. Dep. Agric. Handb. 691.
- WHITNEY, R.D. 1997 Relationship between decayed roots and aboveground decay in three conifers in Ontario. *Can. J. For. Res.* **27**, 1217-1221.
- WIENSCZYK, A.M., DUMAS, M.T. & IRWIN, R.N. 1997 Predicting *Armillaria ostoyae* infection levels in black spruce plantations as a function of environmental factors. *Can. J. For. Res.* **27**, 1630-1634.
- WILLIAMS, R.E. & LEAPHART, C.D. 1978 A system using aerial photography to estimate area of root disease centres in forests. *Can. J. For. Res.* **8**, 214-219.
- WILLIAMS, R.E. & MARSDEN, M.A. 1982 Modelling probability of root disease centre occurrence in northern Idaho forests. *Can. J. For. Res.* **12**, 876-882.
- WILSON, R.J. 1979 Introduction to graph theory. New York: Academic Press.
- WU, B.Y., CHAO, K.M. & TANG, C.Y. 2000 Approximation algorithms for some optimum communication spanning tree problems. *Discrete Appl. Math.* **102**, 245-266.
- ZHANG, S.G., LI, X. & BROERSMA, H.J. 2000 Heavy paths and cycles in weighted graphs. *Discrete Math.* **223**, 327-336.

Nederlandse samenvatting

Het kwantificeren van schimmelgroei: modellen, experimenten en observaties

Bodemschimmels zijn schimmels die het grootste deel van hun levenscyclus in de grond leven, waar ze kunnen uitgroeien tot grote netwerken. Planten-pathogene bodemschimmels kunnen bij contact met plantenwortels de plant ziek maken door naar binnen te groeien. Er bestaan ook schimmels die geen planten infecteren, maar van dood organisch materiaal leven, de zogenaamde saprotrofe schimmels.

Over de groei van bodemschimmels is lang niet alles bekend. Dit komt hoofdzakelijk omdat bodemschimmels moeilijk in ondoorzichtige grond te observeren zijn. Schimmelgroei is wel bestudeerd in eenvoudige laboratoriumproeven op b.v. kunstmatige voedingsbodems, maar een natuurlijk ecosysteem is veel ingewikkelder. Denk maar aan de vele soorten micro-organismen die voorkomen en moeilijk van elkaar te onderscheiden zijn. Hoewel er al veel toegepast onderzoek gedaan is aan bodemschimmels, is nog weinig bekend van de dynamiek van schimmelpopulaties waardoor het moeilijk is om bestrijdingsmethoden tegen pathogene soorten te ontwikkelen. Het onderzoek dat beschreven is in dit proefschrift is uitgevoerd om meer inzicht te krijgen in die dynamiek. In de eerste sectie (Section I) staan microscopisch kleine schimmels centraal, in de tweede sectie (Section II) zijn dat macroscopisch grote schimmelsoorten die unieke draden bezitten die makkelijk met het blote oog waar te nemen zijn. Beide secties bezitten een theoretische benadering van het systeem, ondersteund door experimentele gegevens dan wel observaties.

In de eerste sectie wordt een schimmelgroeimodel beschreven waarbij wiskundige vergelijkingen de dynamiek van schimmelbiomassa en substraat beschrijven. Nadat de schimmel substraat heeft gekoloniseerd, wordt dit substraat afgebroken door extracellulaire enzymen en ontstaan kleinere substraatcomponenten die de schimmel kan opnemen. Vervolgens kan de schimmel groeien in de vorm van nieuwe schimmeldraden en kan zich zodoende verspreiden naar andere lokaties waar zich mogelijk nieuw substraat bevindt. Omdat schimmels, net als planten en dieren (en dus ook substraat), uit een bepaalde verhouding aan koolstof en stikstof bestaan, is bij het bovenstaande schimmelgroeimodel de dynamiek van koolstof en stikstof in detail gemodelleerd.

Als er evenveel nieuwe schimmeldraden worden geproduceerd als dat er afsterven en als ook alle andere processen met elkaar in evenwicht zijn, kan het systeem in een evenwichtstoestand (steady state) terechtkomen. Dit is met behulp van een wiskundige techniek uitgerekend (Hoofdstuk 2). De voorwaarden voor het bestaan van een evenwicht zijn ook uitgerekend en hoewel deze formules ingewikkeld bleken te zijn, zijn ze in woorden vertaald en werd de biologische betekenis duidelijk. Dat was heel verhelderend. In natuurlijke systemen kunnen ook quasi-evenwichten ontstaan, waarbij een aantal processen met elkaar in evenwicht zijn, maar ook een aantal niet. Bij het uitrekenen daarvan (Hoofdstuk 3) bleek het mogelijk te zijn om ook het invasie criterium uit te rekenen. Dit biologisch interessante criterium geeft aan waaraan moet worden voldaan wil een schimmel in staat zijn een nieuw gebied te betrekken en wanneer de schimmel hierin zal falen met uitsterven tot gevolg. Tot slot van deze sectie (Hoofdstuk 4) zijn laboratoriumexperimenten uitgevoerd waarvan de resultaten gebruikt zijn om de waarden van de parameters van het schimmelgroei model te schatten. Het betreft experimenten waarbij de groei van *Rhizoctonia solani*, een schadelijke schimmel die o.a. in aardappelvelden voorkomt, in een steriel plastic schaalte is gemeten bij het toedienen van diverse suikerconcentraties. Deze experimenten zijn uitgevoerd bij de Universiteit van Cambridge (Engeland).

In de tweede sectie zijn macroscopisch grote schimmeldraden van de honingzwam (*Armillaria sp.*) geobserveerd. Als introductie is een overzicht gepresenteerd van bestaande literatuur (Hoofdstuk 5). De honingzwam produceert niet alleen prachtige paddestoelen met een honingachtige kleur (zie omslag proefschrift), maar ondergronds ook zwarte draden die qua vorm en dikte op schoenveters lijken. Er zijn slechts kleine verschillen waarneembaar met bruine plantenwortels, vandaar dat deze schimmeldraden ook wel 'rhizomorfen' worden genoemd. In twee verschillende dennenbossen werd 25 m² bosgrond voorzichtig omgewoeld en werden de rhizomorfen blootgelegd. Er bleken ingewikkelde netwerken onder de grond voor te komen (Hoofdstuk 6, Figuur 1) als gevolg van vertakkingen van rhizomorfen, maar ook als gevolg van samensmeltingen van twee rhizomorfen die, toevallig of 'bewust', naar elkaar toe gegroeid waren. De in kaart gebrachte netwerken zijn wiskundig geanalyseerd (Hoofdstuk 7) en er is gespeculeerd over de verschillende groeistrategieën: Liever op deze plek energie steken in het vormen van vele, korte draden om zodoende hier uitgebreid te kunnen fourageren (exploitatieve groei)? Of liever slechts enkele, lange draden vormen die een langere afstand kunnen uitgroeien op zoek naar nieuwe voedselbronnen op een nieuwe lokatie (exploratieve groei)?

Curriculum vitae

Angélique Lamour werd op 9 mei 1967 geboren te Sittard. In 1987 slaagde zij voor het gymnasium aan het 'College Sittard' te Sittard. Daarna ging zij Planteziektenkunde studeren aan de Landbouwniversiteit Wageningen. Haar aandacht ging vooral uit naar de populatiedynamiek van insecten en schimmels. Na het behalen van het doctoraalexamen in 1993 verdiepte zij zich in de theoretische biologie bij de leerstoelgroep Wiskundige en Statistische Methoden. Vanaf november 1996 was zij 'Assistent in Opleiding' bij Ecologische Fytopathologie, hetgeen nu onderdeel is van de leerstoelgroep Biologische Bedrijfssystemen van Wageningen Universiteit. Het in dat kader uitgevoerde onderzoek heeft geleid tot het voor u liggende proefschrift.



Vormgeving omslag: Piet Kostense

Fotografie omslag: René Geschiere